UNIVERSITI PUTRA MALAYSIA

UTILIZATION OF RICE HUSK ASH AND SILICONE RUBBER IN THE PRODUCTION OF MOISTURE-FIRE RETARDANT GEOPOLYMER COMPOSITE COATING USING RESPONSE SURFACE METHODOLOGY

TEE HUI YEK

UTILIZATION OF RICE HUSK ASH AND SILICONE RUBBER IN THE PRODUCTION OF MOISTURE-FIRE RETARDANT GEOPOLYMER COMPOSITE COATING USING RESPONSE SURFACE METHODOLOGY

TEE HUI YEK

188060

PROJECT REPORT SUBMITTED IN PARTIALLY FULFILLMENT OF THE REQUIREMENT FOR THE

BACHELOR OF PROCESS AND FOOD ENGINEERING

DEPARTMENT OF PROCESS AND FOOD ENGINEERING

FACULTY OF ENGINEEERING

UNIVERSITI PUTRA MALAYSIA

2020

ACKNOWLEDGEMENT

First and foremost, I would like to express my deepest gratitude to all the people who have given me the patience, strength, determination, and courage to complete this final year project. I would like to express gratitude to my supervisor, Ts. Dr. Mohd Salahuddin bin Mohd Basri for his willingness in the guidance and giving me advice throughout this project. My supervisor also shared his truthful and illuminating views on several issues related to the project. I believe that all his advice, suggestions and opinions are beneficial towards my final year project.

Next, I would like to express my appreciation to the presentation examiners, Prof. Madya Dr. Rosnita A. Talib and Dr. Intan Syafinaz Mohamed Amin Tawakkal, who have given me the constructive comments and advice in completing this project. They also shared their valuable experience with me during the presentation of the project proposal. That is very helpful and beneficial to me.

I feel to acknowledge my deep sense of gratitude to the lab assistants, who are En. Raman Morat and Pn. Siti Hajar binti Zakaria, giving me permission and guidance to use the equipment required for completing this project successfully. I also would like to thank Dr. Ezanee Gires and En. Mohamad Nasir Johari, from the Department of Aerospace Engineering, permitting me to use their laboratory and equipment and guidance to conduct my experiment.

Last but not least, an honorable and special thanks to my loved family members and friends that have contributed faithfully and persistently through the completion of this project. Commitment and cooperation of them have been contributed until the very end of this project. I am most grateful as this final year project is a success from all the hard works and dedication of all of them

ABSTRACT

Rice husk is the major solid waste in rice processing and is usually processed to be rice husk ash (RHA). The utilization of rice husk ash through green technology is vital as a proper disposal method. Geopolymer (Ge) coating is known as a green material and usually made by rice husk ash due to high silica content. It is served as the protective coating to protect the different surface materials, including metal. In this study, the geopolymer coating is applied on the surface of steel plate as the steel plate is one of the materials used in support system of food equipment that cannot withstand high temperature and moisture attack. Silicone rubber (SiR) is added as an additive to extend the shelf life of RHA-based geopolymer coatings since silicone rubber can enhance the moisture and fire retardant properties. The research objectives are to determine the significant effect of different factors and optimum composition of SiR-RHA-Ge coating composite using fractional factorial design (FrFD) and response surface methodology (RSM). Three factors were considered, namely: (i) Molarity of sodium hydroxide (NaOH); (ii) RHA to activated alkaline solution (AA solution) (Ge) ratio; and (iii) SiR to Ge ratio, with AA solution at a constant ratio of 5.5. The result showed that NaOH concentration is the most influential factor on the fire retardant test, while the RHA/AA ratio is the most influential factor on the moisture absorption test. The pair of RHA/AA and SiR/Ge ratio was chosen due to reducing overall material cost. The optimum value for both fire retardant and moisture resistance properties could be achieved when the RHA/AA ratio is 0.85, and the SiR/Ge ratio is 0.70, with 14 M of NaOH. Then, SEM micrographs of SiR-RHA-Ge coating composite were provided as the evidence to prove it can potentially improve the moisture and fire retardant properties when silicone rubber added.

ABSTRAK

Nasi padi adalah sisa pepejal utama dalam pemprosesan padi dan biasanya diproses menjadi abu sekam padi (RHA). Penggunaan abu sekam padi melalui teknologi hijau sangat penting sebagai kaedah pembuangan yang tepat. Lapisan geopolimer (Ge) dikenali sebagai bahan hijau dan biasanya dibuat oleh abu sekam padi kerana kandungan silika yang tinggi. Ini berfungsi sebagai lapisan pelindung untuk melindungi pelbagai bahan permukaan termasuk logam. Dalam kajian ini, lapisan geopolimer digunakan pada permukaan plat keluli kerana plat keluli adalah salah satu bahan binaan untuk sistem sokongan dalam mesin makanan yang tidak tahan terhadap suhu tinggi dan kelembapan yang diserang. Getah silikon (SiR) ditambah sebagai bahan tambahan untuk memanjangkan jangka hayat lapisan geopolimer berasaskan RHA kerana getah silikon dapat meningkatkan sifat kelembapan dan tahan api. Objektif kajian adalah untuk menentukan pengaruh signifikan faktor yang berbeza dan komposisi optimum komposisi lapisan SiR-RHA-Ge menggunakan reka bentuk faktorial pecahan (FrFD) dan metodologi permukaan tindak balas (RSM). Tiga faktor dipertimbangkan, iaitu: (i) Molariti NaOH; (ii) Nisbah RHA ke AA (Ge); dan (iii) Nisbah SiR ke Ge, dengan larutan AA pada nisbah malar 5.5. Hasil kajian menunjukkan kepekatan NaOH adalah faktor yang paling berpengaruh pada ujian tahan api manakala nisbah RHA / AA adalah faktor yang paling berpengaruh pada ujian penyerapan kelembapan. Nisbah pasangan RHA / AA dan SiR / Ge dipilih kerana mengurangkan kos keseluruhan bahan. Nilai optimum untuk sifat tahan api dan tahan kelembapan dapat dicapai apabila nisbah RHA / AA 0,85 dan nisbah SiR / Ge adalah 0,70, dengan NaOH 14 M. Kemudian, mikrograf SEM komposit lapisan SiR-RHA-Ge disediakan sebagai bukti untuk membuktikan ia berpotensi meningkatkan sifat kelembapan dan tahan api ketika getah silikon ditambahkan.

Table of Contents

LIST OF TABLES

CHAPTER 2

CHAPTER 3

CHAPTER 4

LIST OF FIGURES

CHAPTER 2

CHAPTER 3

CHAPTER 4

CHAPTER 1

INTRODUCTION

1.1 Research Background

Wheat is the most important crop globally, followed by rice. Rice is mostly produced in Asia and Asians consume more than 80% of the world's rice. Based on 2015 data, the volume of rice production is estimated to be 156 million tons per year, thus generating a massive amount of solid waste (Rajamoorthy, Rahim, & Munusamy, 2015). Rice husk is the outer cover of the rice grain that is usually discarded as the major solid waste in rice processing. During the de-husking process, the rice husk and rice are separated mechanically by machine and the grains collected separately in silo tanks. For 100 kg of rice, 20 kg of rice husk is produced or 20 % of total rice harvested (A.N & Ravi.S, 2017).

Rice husk ash (RHA) is obtained by burning the rice husks at 600°C for 6 hours and grinding it by using jet mill in order to reduce the particle size (Chuayjuljit, Eiumnoh, & Potiyaraj, 2001). The rice husk ash has silica content as high as 90 %. RHA can be used as a partial replacement of cement in construction material for buildings and also as a source for geopolymer. RHA is suitable as a pozzolanic material because of its high silica content that can improve the compressive and tensile strength of concrete or in protective geopolymer coating. It is simultaneously environment friendly and low cost compared to conventional materials (Muthadhi & Kothandaraman, 2013).

Geopolymer is an inorganic material with superior mechanical, chemical and thermal resistance properties. Geopolymer is also known as a green material that is environmentally friendly due to its low carbon emission. It is thus highly recommended as a protective coating due to its high compressive strength, low shrinkage, acid and fire resistance and ability to immobilize toxic and radioactive materials ("Review on Current Geopolymer as a Coating Material," 2013). In addition, geopolymer can be manufactured from sustainable and cheap raw materials such as rice husk ash, which has suitable chemical properties and are abundantly available. Mass production of geopolymer thus helps in reducing environmental pollution from this material. The primary function of geopolymer is to serve as a protective coating on the concrete surface of buildings from weather corrosion, fire and chemicals.

Coating can be defined as a single or multiple layers applied to a substrate such as steel as a protection from harsh conditions such as fire, corrosion, chemical etc. Since the thickness of coating depends on the application, think coating is normally applied as fire retardant layer with typically ranges from 30 to 500 mils (0.8 to 13 mm). Therefore, the geopolymer composite coating is more precise in describing the material.

In food industry, the material mostly used in fabrication of food equipment is stainless steel rather than mild steel. However, the development of food processing machinery using materials that are not stainless steel in undeveloped areas was increasing due to budget constraints. In the fabrication of food equipment, various metallic materials have been chosen ranging from mild steel (coated and uncoated), galvanized steel to different grades of stainless steel, which reduce the overall fabrication cost (Ofoegbu, Ofoegbu, Neife, & Okorie, 2011). Owing to hygiene issues, mild steel may be used as a

food-free support system to minimize costs. However, the strength and structural properties of steel materials decrease if they remain exposed continuously to high temperatures through heat absorption. The coating layer on the steel surface is therefore important for protection against fire, acid, moisture and external corrosion, thus extending the age of the building. The geopolymer coating is thus developed and contributed to prolonger the shelf life of steel.

Silicon rubber can be mixed with geopolymer coating before applying to the surface of steel, resulting in high fire and water resistance. Although the RHA-based geopolymer coating has lesser ability to withstand corrosion from moisture, its mechanical strength is stronger. The silicon rubber component is able to withstand temperature as high as 300°C without changing its structure while its high-water resistance is due to its hydrophobicity. Identifying the optimum ratio of silicone rubber and RHA-based geopolymer is, therefore, crucial in providing for maximum moisture resistance and fire retardant in building construction while simultaneously contributing significant advancement in the construction sector.

1.2 Problem Statement

RHA is an agricultural waste product produced in huge quantities by the rice-growing industry. Traditionally it is disposed through open burning or dumped in landfills. This removal method has become a growing hazard over the years due to its negative impacts on the environment and public health. The rice-growing industry has resorted to its mitigation through the application of green technology by maximizing the utilization of RHA as a source of manufacturing geopolymer due to high aluminosilicate content.

The steel used in application as a support system could not bear high temperatures without adverse alteration of its properties, such as yield strength. In addition, steel is also easily corroded in the presence of moisture due to oxidization. It is thus necessary for steel surfaces to have a protective coating layer such as geopolymer coating against corrosion and to withstand fire when used as support system in fabrication of food equipment without contact the food.

Several geopolymer materials were investigated and formulated in Malaysia to achieve sustainable development in the field of construction. These include fly ash, palm oil fuel ash (POFA), kaolin, metakaolin and dolomite. Among the geopolymer materials, the fly ash showed good performance because of its high aluminosilicate content, also being more environmentally friendly. Nevertheless, the material has low negative impacts on the environment, such as human toxicity and freshwater ecotoxicity (Zain, Abdullah, Hussin, Ariffin, & Bayuaji, 2017). Furthermore, its mechanical strength is very weak despite its high-water resistance. In its place, the RHA shows higher potential and depicted as better alternatives to other extant geopolymer materials. The component greatly

enhanced the mechanical strength of the geopolymer. For greater efficiency of the RHA-based geopolymer coatings, the optimal ratio between RHA and activated alkaline solution (AA) need to be investigated.

In order to extend the shelf life of RHA-based geopolymer coatings, silicon rubber is added since it is highly hydrophobic and can confer improved moisture resistance properties to the composite product. Further, silicone rubber can also improve fire resistance. For the product to be successful, the mixture of the two components needs to be suitably homogenized. In this study, silicone rubber used as an additive in geopolymer has potential to improve the moisture-fire resistance properties of geopolymer coating.

1.3 Research Objectives

The objectives of this research are:

a) To identify the significant effect of different factors on the moisture resistance and fire retardant properties of silicone rubber-rice husk ash-based geopolymer (SiR-RHA-Ge) coating composite using factorial design.

b) To determine the optimum composition of SiR-RHA-Ge coating composite, which produces the best moisture resistance and fire retardant properties using response surface methodology.

c) To study the microstructure of SiR-RHA-Ge coating composite.

1.4 Scope of the Study

The research scope is divided into two main parts. Firstly, an investigation was focused on the effect of silicone-rubber-RHA-based geopolymer coating composite on moisture resistance and fire retardant properties rather than on the mechanical strength of the composite coating. The mechanical strength of RHA-Ge coating has already been investigated in past studies. Since the strength of geopolymer coating is decreased if moisture is adsorbed, this study investigated the moisture resistance and fire retardant of RHA-Ge coatings when composited with silicone rubber. Accordingly, three factors were considered, namely; (i) Molarity of NaOH; (ii) ratio of RHA and AA (Ge); and (iii) SiR and Ge. An AA solution comprising a mixture of sodium silicate and sodium hydroxide, at a constant ratio of 5.5, is used. Prior to testing, the samples were cured at a temperature of 70°C for 24 hours and subsequently left in ambient room temperature for 6 days. The mild steel plate was used as a substrate throughout the study.

The response surface methodology (RSM) was employed in the study. The RSM is a statistical method used in experimental design and analysis to obtain the optimum composition of SiR-RHA-Ge coating composite, which showed the best performance in moisture and fire resistance. Analyses were conducted to evaluate the moisture and fire resistance properties of SiR-RHA-Ge coating composite, which included microstructural analysis by using scanning electron microscopy (SEM).

CHAPTER 2

LITERATURE REVIEW

2.1 Rice husk

Rice husk is produced in large quantities as a major solid waste in the rice-growing industry. It is an organic waste with cellulose-based fibre containing approximately 20% silica when burnt to produce RHA. Rice husk can absorb water up to 16% its unit weight, and its density is 83-125 kg/m^3 (Phonphuak & Chindaprasirt, 2014).

Rice husk has a hard-protective cover that protects the rice grain against insect infestation. It separates from the rice grain during the de-husking process due to friction. The rice husk constitutes about 20% of the weight of whole rice. About 20 kg of rice husk can, for example, be obtained from 100 kg of whole rice. The rice husk comprises 50% of cellulose, 25-30% of lignin, 15-20% of silicate and 10-15% moisture content (Givi, Rashid, Aziz, & Salleh, 2010).

2.1.1 Properties of rice husk ash

According to Phonphuak and Chindaprasirt, the RHA has a highly porous structure and is lightweight with a high specific surface area. The material is highly recommended as an additive in many applications, such as a replacement for cement and manufacturing of insulation. It is also highly suitable as flame retardants because of its highly porous structure and excellent insulating properties (Phonphuak & Chindaprasirt, 2014).

RHA is the product of the incineration of rice husk. Its characteristic varies according to several factors, namely, the composition of the rice husks, the temperature

and duration of the burn. In order to achieve the maximum silicate content in RHA, the burning temperature should range between 500°C - 700°C for about 1 hour under controlled combustion to reduce air pollution. Additionally, the RHA has high pozzolanic activity and can contribute to improving the strength of concrete (Singh, 2018).

RHA is obtained from rice husk through controlled incineration that yields about 20% of the material. RHA contains high silica content, which can be used as supplementary cementing material (SCM) for building. Many of the studies that have been conducted to analyze the chemical composition of RHA found it be rich in silica content (Gupta & Wayal, 2015). The summary of the chemical composition in RHA is shown in Table 2.1.

Table 2. 1: The chemical composition of RHA

SiO_2	Al_2O_3	Fe_2O_3	CaO	MgO	SO_3	Na_2O	K_2O	LOI*	Reference
86.81	0.50	0.87	1.04	0.85	-	0.69	3.16	4.60	Thanh Le et.al (2014)
91.00	0.35	0.41	-	0.81	1.21	0.08	3.21	8.50	Chao-Lung et.al. (2011)
95.04	0.30	0.44	1.25	0.45	0.01	0.09	1.40	0.51	Zerbino et.al. (2011)
90.90	0.83	0.60	0.80	0.56	-	1.55	-	-	Madandoust et.al. (2014)
87.40	0.40	0.30	0.90	0.60	0.40	0.04	-	3.39	Van et.al. (2014)
87.32	0.22	0.28	0.48	0.28	---	1.02	3.14	4.60	Ganesan et.al. (2008)

*Notes: LOI-Loss on Ignition

RHA was reported to comprise of very fine porous material with particle size within 5-75 micron. Table 2.2 shows the physical properties of RHA recorded in two studies.

Table 2. 2: The physical properties of RHA

Physical Properties	**Mehta et.al (2002)**	**Nagrale et.al (2012)**
Mean particle size (μm)	---	63.8
Specific gravity	2.06	2.11
Fineness passing 45 μm (%)	99	98

The physical properties of RHA may, however, vary according to the burning treatments, as shown in Table 2. 3. It was concluded that the burning temperature for rice husk should be below 700°C to produce the amorphous silica with high surface area (Shaswat Kumar Das, Jyotirmoy Mishra, 2018).

Table 2. 3: The physical properties of RHA in different burning conditions

Burning Temperature	**Hold time**	**Furnace Environment**	**Properties of RHA**	
			Silica Form	**SurfaceArea (m^2/g)**
500 – 600 °C	1 min	Moderately oxidizing	Amorphous	122
	30 mins			97
	2 hours			76
700 – 800 °C	15 mins			100
	>1 hour	Highly oxidizing	Partially crystalline	6 - 10
> 800 °C	>1 hour		Crystalline	<5

2.1.2 Use of rice husk ash

RHA is used as a partial replacement for cement in concrete. In order to assess the relevant properties, a study was conducted to gauge the effects of RHA particle size on strength, water permeability and workability of binary blended concrete. In the study, the cement of 5, 10, 15 and 20% by weight was replaced by RHA with a particle size of 95 and 5 μm. The strength of concrete improved by 15% and 20% when RHA with a particle size of 95 and 5 μm was used, respectively. At the same time, the water permeability of concrete is reduced by decreasing the average particle size of RHA (Givi *et al.*, 2010).

The RHA treated concrete is increased in hardness, mechanical and physical properties and moisture absorption. The RHA was produced under controlled combustion of below 700°C to ensure minimal carbon emission and negative impact on the environment. The compressive strength, water absorption and slump retention were subsequently evaluated on different percentages of RHA with different w/c ratios and for durations of 7, 14, 21 and 28 days. Results showed an increase in the compressive strength of concrete, but the slump values decreased with the addition of RHA. In the water absorption tests, the quantity of water absorbed decreased with greater substitution of RHA, since its particle size is smaller than cement. Without RHA (0%), however, the strength of concrete is rapidly decreased compared to the concrete with 15% of RHA over 7 days to 28 days (Nagrale, Hajare, & Modak, 2012).

RHA can also be used for other applications, such as in steel industries as a source of silica, as an adsorbent for heavy metals, in flame retardants for fire safety and vulcanizing rubber. RHA is suitably used as a coating over molten metal in the tundish or

ladles due mainly to its low thermal conductivity, high melting point, low bulk density and as a good insulator. With its high silica content, it can also serve as reinforcing filler in natural rubber to improve on its mechanical properties, such as tensile strength and compression set. Its performance is better compared to the addition of commercial silica. RHA is also effective as an absorbent for heavy metals, especially in removing mercury from wastewater (Kumar, Sangwan, V, & Bidra, 2013).

The pozzolanic reaction is vital in turning RHA into compounds exhibiting cementitious properties. It occurs when a siliceous or aluminous material reacts with calcium hydroxide in the presence of humidity. The reactions are shown in Equation 1 and 2.

$$2(3CaO.SiO_2) + 6H_2O \rightarrow 3CaO.2SiO_2.3H_2O + 3Ca(OH)_2 \quad \text{(Eq. 1)}$$

$$2(2CaO.SiO_2) + 4H_2O \rightarrow 3CaO.2SiO_2.3H_2O + Ca(OH)_2 \quad \text{(Eq. 2)}$$

However, any excess calcium hydroxide tends to create crystalline growth, which may weaken concrete strength. The addition of RHA can mitigate the problem by reducing the CH formed in the pozzolanic reaction. RHA may also simultaneously produce more C-S-H gel that can enhance the strength and durability of concrete relative to concrete without the material. The reaction occurs, as shown in Equation 3.

$$SiO_2 + Ca(OH)_2 + H_2O \rightarrow CaO.SiO_2H_2O \quad \text{(Eq. 3)}$$

RHA is an extremely reactive pozzolanic substance that contains high amorphous silica (85 – 95%) following the combustion of the rice husk. The partial replacement of cement with RHA not only enhances the compressive strength of concrete it also reduces its moisture penetration through capillary action (Givi, A. N., Abdul Rashid, S., Abdul Aziz, F. N. & Mohd Salleh, 2010).

2.2 Silicone rubber

Silicone rubber (SiR) is popular because it can be sustained in a stable structure over a wide range of temperatures due to its unique molecular structure (Ryan & Chemist, n.d.). Silicone rubber can be categorized as an organo-silicon compound because it contains both inorganic and organic components. Its extraordinary properties, relative to other organic rubbers, are due to the Si-O silicone bond and its inorganic properties (Shit & Shah, 2013).

2.2.1 Hydrophobicity

Hydrophobicity is defined as the ability to resist the flow of water on the surface of a material. The materials can be considered as least hydrophobic, if water drops flow in the form of tracks on its surface, or even penetrate throughout its exterior. Hydrophobicity is contrasted to hydrophilicity since the former is related to water repellence while the latter to surface wetting.

Hydrophobicity can be measured by the contact angle between a drop of water and the surface of the material (θ_c), as shown in Figure 2. 1. A contact angle of less than 90° indicates that the material allows water to cover a large surface area, thus displaying high wettability. Conversely, a highly hydrophobic material allows less water surface contact area and the contact angle is larger than 90° (Amin, Akbar, & Amin, 2007).

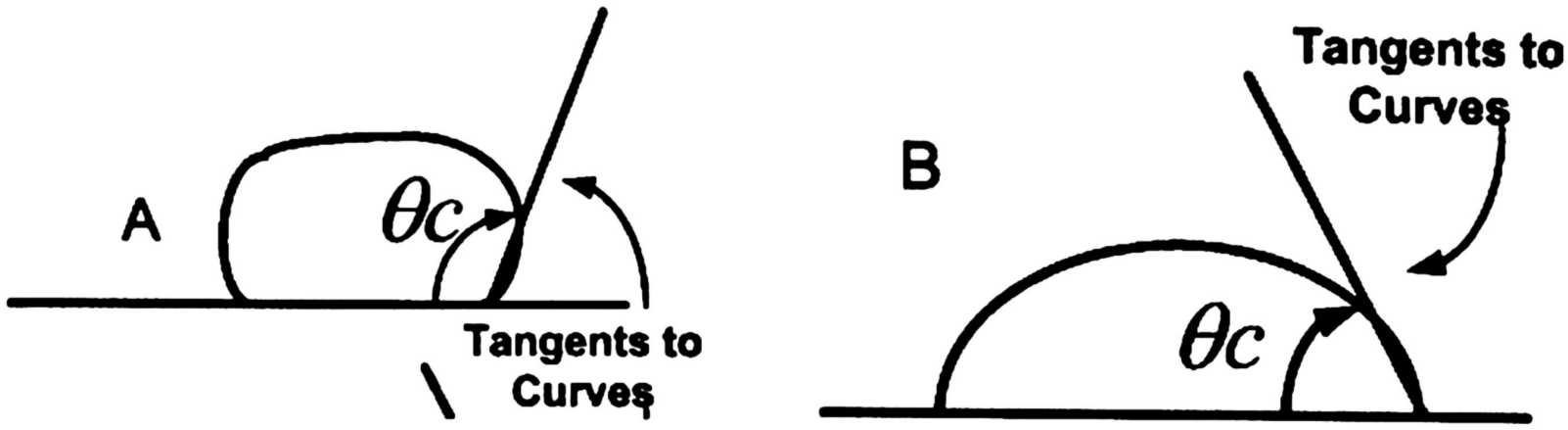

Figure 2. 1: Contact angle between hydrophobic (left) and less hydrophobic (right) materials

However, the decrease in hydrophobicity of polymeric or non-ceramic insulators, including silicone rubber, influences other factors. Firstly, is the reduction in insulation capability of silicone rubber materials, thus reducing its performance under electrical and pollution conditions. Secondly, the aging process of silicone rubber insulator is also greatly influenced by the reduction in hydrophobicity (Chaipanit, Rattanakhongviput, & Sundararajan, 2001). Regardless of these shortcomings, silicone rubber still possesses adequate hydrophobicity properties even after ten years of application in some heavily polluted environments.

Several methods, direct or indirect, can be used to measure contact angles between water droplets and the material surface to evaluate its hydrophobicity. The direct method employs sessile-drop goniometry with a tilting plate, while Wilhelmy plate is used in the indirect method. The most common method used is the former due to its simplicity. It can be applied to a wide variety of materials, such as polymer, metals and biological surfaces (Huhtamäki, Tian, Korhonen, & Ras, 2018).

2.2.2 Water resistant properties

Silicone molecules are helical and with weak intermolecular forces. They possess high elasticity and compressibility and excellent resistance to cold temperatures. The molecules also display high water repellence and good releasability since the methyl groups attached externally to the coil structure can rotate freely. The water absorption of silicone rubber, for example, is about 1% when immersed in water (cold, warm or boiling water) over long periods (Shin Etsu Company, 2013).

The relationship between moisture absorption and dielectric loss factor of the new and operational silicone rubber has been studied. Both types were examined under a high humidity environment (90%) with a temperature of 20°C. Moisture absorption and dielectric loss factor were found to be higher for operated silicone rubber compared to the new product due mainly to its reduced hydrophobicity. It would cause the former material to deteriorate faster. The maximum moisture content for the new and operated silicone rubber was approximately 0.11% and 0.23%, respectively (Gong *et al.*, 2013).

2.2.3 Fire retardant properties

As shown in Figure 2. 2, Silicone has high binding energy due to its siloxane bonds (-Si-O-Si-), which form the backbone of silicone (dimethylpolysiloxane), making it highly stable. The binding energy of the siloxane bonds at 433 kJ / mol is much higher than that of the carbon bonds at 355 kJ / mol. Due to its high binding energy, silicone rubber is able to withstand high temperatures. Even near the flame, silicone rubber is not ignited easily. It will, however, continue to burn once it has ignited. This problem can quickly be resolved by adding a small amount of fire retardant. Silicone rubber on ignition does not emit black

smoke or harmful gas pollutants as it does not contain organic halogens typically found in organic polymer rubbers (Shin Etsu Company, 2013).

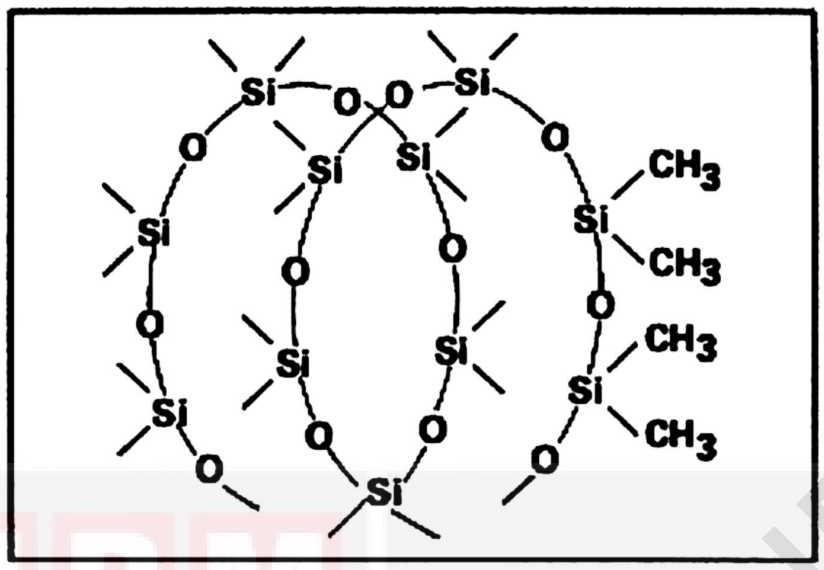

Figure 2. 2: The structure of silicone molecules

Silicone can be used in rail transport, such as gantry bellows used for interconnecting train carriages. With lower smoke and contamination compared to organic rubber and lower burn rate, silicone rubber has a distinct advantage in case of fire that satisfies fire safety requirements (Hallett & Turner, n.d.).

The flame resistance and heat resistance properties of silicone rubber can be increased effectively by adding acetyl acetonates or oxalates of Ce, Zn, Fe and Cr together with compounds of platinum, rhodium, and ruthenium (Kopylov, Kovyazin, Kostyleva, Fedorov, & Kovyazin, 2016).

2.3 Silicone rubber-based composite

2.3.1 Use of the silicone rubber-based composite

Ceramic silicone composites serve as elastic technical materials, which can increase the flame retardance of electrical cables and prevent them from burning because of their ability to create a continuous ceramic structure (Imiela *et al.*, 2016).

Silicone rubber composites have excellent antipollution flashover capability and act as an insulator. Its high hydrophobicity leads to a low energy surface affecting any pollution layer. The water thus absorbed by this layer surface remains as small water droplets instead of a continuous water film covering the surface (Hu & Liu, 2017).

The power sector is one of the most important infrastructures. Nevertheless, the interruption of power generation, transmission and distribution are affected by natural disasters. It is due to the formation of contaminants in the insulators during the foggy weather. According to Parthak et al., the use of a silicone rubber insulator solved flashover problems due to its unique hydrophobic properties. It can, therefore, remove moisture condensation on the surface of the insulator and work well in the contaminated environment (Pathak, Satwani, Patel, & Patel, 2009).

2.3.2 Water resistance properties

Recent developments have led to the alteration of silicone rubber (SiR) to improve its resistance to water absorption and hardness. Silicone rubber materials can replace the traditional ceramic-based insulators in high voltage outdoor applications, due to its hydrophobic property. Silicone rubber filled with various mineral fillers such as calcium

carbonate, silica and wollastonite minerals ($CaCO_3$, SiO_2 and $CaSiO_3$) was compared for hardness and water absorption. Silicone rubber-based composites showed a higher hardness value than the filler-free control sample. They also showed good water absorption due to their good binding interaction between silicone rubber and mineral fillers. The SiR/CaSiO3 was most significant in improving hardness as well as water resistance properties (Kamarudin *et al.*, 2020).

The hydrophobicity of silicone rubber composite can be maintained by the introduction of TiO_2, even if the materials have aged considerably. Hydrophobicity can be determined by measurement of the contact angle of unmodified silicone rubber composite, which at 43.1° is smaller than the modified silicone rubber at 82.8° after aging. It is because of TiO_2 act as an additive that can reduce the surface energy to improve hydrophobicity (Bleszynski & Kumosa, 2018).

2.3.3 Fire retardant properties

The flammability test for silicone rubber compounds containing fillers, such as cenospheres, iron-coated cenospheres, attapulgite, wollastonite, aluminum hydroxide and silica, was conducted. The cone calorimeter has been used to measure flammability. The fillers were used as flame retardants when exposed to high temperatures due to their thermal decomposition and the release of water. Besides, boron trioxide as ceramic additives incorporated in silicone rubber composites may significantly reduce the fire hazard and flammability due to their low melting points, resulting in a decrease in temperature due to the formation of a eutectic filler silica phase (Rybiński, Żukowski, & Bradło, 2016).

Basalt filler silicone composites can reduce flammability to a sufficient degree. The basalt filler was able to reduce the mass and energy flow between the silicone composite sample and the flame because it can absorb a significant amount of heat and form an insulating boundary layer (Rybiński *et al.*, 2019). The introduction of platinum compounds as additive or vulcanizing catalysts into silicone rubber compounds results in increased flame resistance and retention of electrical insulation properties (Hayashida, Tsuge, & Ohtani, 2003).

2.3.4 Microstructure

Pedzich et al. conducted a study on the microstructure evolution of SiR-based composites during ceramization in different conditions. The three conditions applied to the composites were; (i) slow temperature increase from 20°C up to 1000°C followed with 20 minutes of soaking in the water at maximum temperature, (ii) temperature was rapidly heated up to 1000°C and soaking for 20 minutes, and (iii) similar with the second condition but with maximum temperature up to 800°C. The resulting microstructures were observed using SEM, as shown in Figure 2.3.

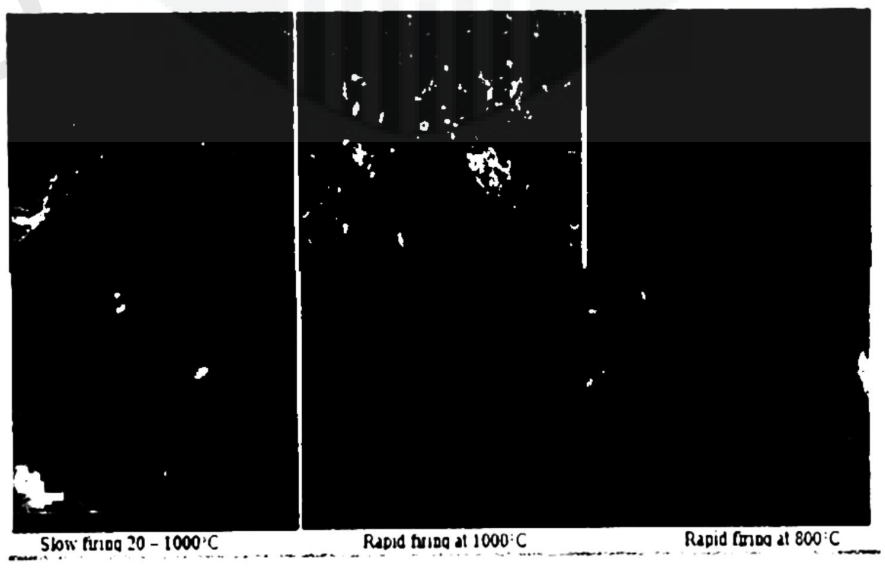

Figure 2. 3: SEM images of silicone rubber-based composites ceramized at different conditions

The samples in condition (i) have a compact microstructure. On the other hand, the samples that were rapidly fired are more porous, with a significant amount of nanometric silica present during polymer degradation. The sample heated to 800°C has a loose microstructure, and nanometric silica particles have also been produced. It was concluded that the final microstructure of the samples did not depend solely on the maximum temperature, but also the kinetics of the firing kinetics (Pędzich *et al.*, 2012).

Additives such as bentonite, kaolinite and wollastonite have been added to provide stable SiR-based composites. Napiera (2011) compared the pore size of composites formed with these additives. Results show in Figure 2.4 indicated that bentonite and kaolinite additives formed an almost non-porous microstructure following ceramization. Wollastonite conversely showed a relatively slow change in microstructure with firing temperature and crystalline phase content. These additives nevertheless show a potential increase in fracture resistance in the ceramic composites and a decrease in their thermal conductivity.

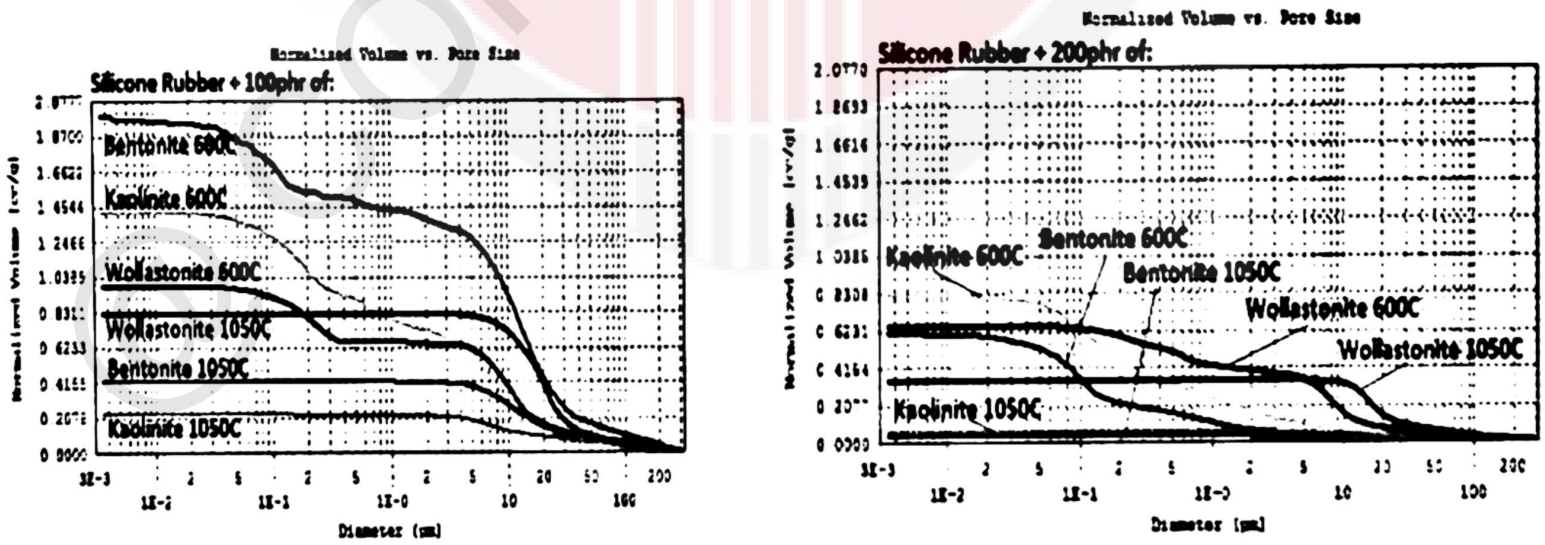

Figure 2. 4: Cumulative curves of the pore size distribution for composites of crystalline phase ceramized at 600 and 1050°C, with 100 phr (left) and 200 phr (right)

2.4 Geopolymer

Geopolymer is made from alkali or silicate-activated aluminosilicate and known as geopolymer binder. Typically, the main source for aluminosilicate is fly ash and ground granulated blast furnace slab (GGBS). The chemical reaction that forms the geopolymer binder is called the polymerization process. Geopolymer composites are more environmentally friendly compared to traditional cement composites due to low carbon emission during production. They are also stronger with excellent strength or mechanical properties, including higher resistance to fire and acid (*Eco-Efficient Mason. Bricks Blocks*, 2015).

The structure of a geopolymer is generally in the form of –Si-O-Al-O- or –Si-O-Al-O-Si-O- or –Si-O-Al-O-SiO-Si-O-. The first model, as shown in Figure 2.5(a) was created by Joseph Davidovits, where the structure is a poly-sialatesilox type. Based on his research, however, the structure was modified to the second model, which is similar to that of vitreous bodies, as shown in Figure 2.5(b). In this model, the porous body of the geopolymer contains water, which acts as an alkali activator transport in the geopolymerization process (Błaszczyński & Król, 2017).

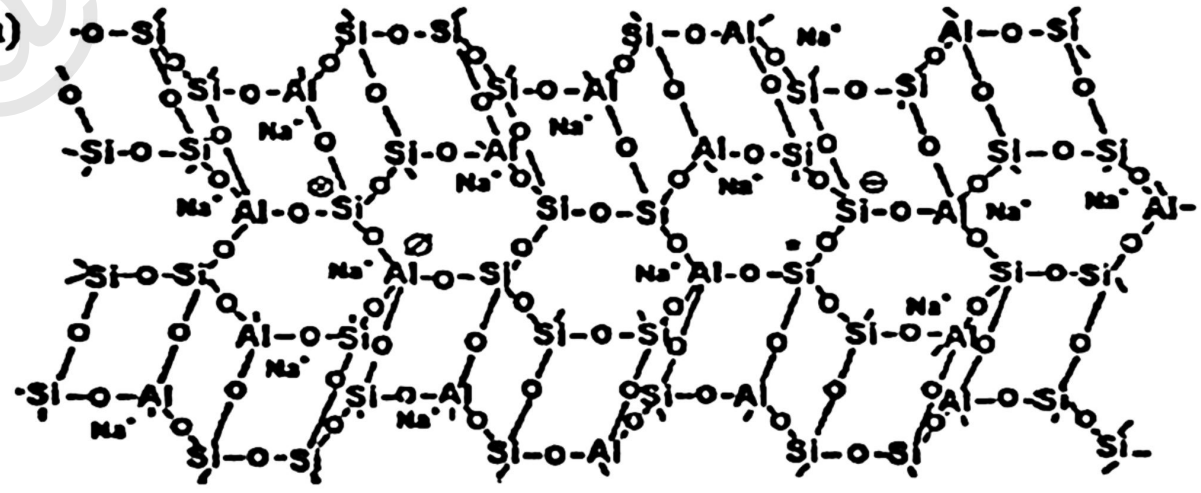

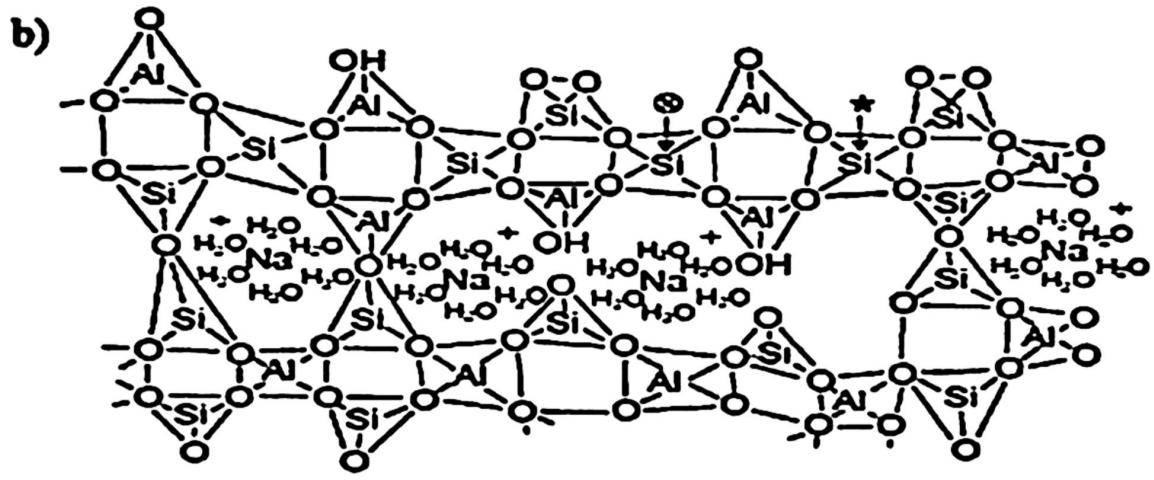

Figure 2. 5: Model of geopolymer structure: (a) proposed by Davidovits, (b) proposed by Barbosa

Except for fly ash and GGBS, RHA was developed as a substitute for one of the alkali-activated geopolymers. A study was conducted to develop the concrete-based geopolymer on alkali-activated RHA (Kim, Lee, Saraswathy, & Kwon, 2014). Its objective was to investigate the effect of the curing method and NaOH concentration on compressive strength and optimum mix proportion of geopolymer mortar. The mortar samples were prepared with RHA to sand ratio of 1:2. NaOH concentrations of 7, 8, 9 and 10 molars were used and mixed with sodium silicate at 2.5 % mass. The study showed that; (i) the alkali-activated RHA geopolymer mortars displayed superior performance in compressive strength, (ii) the geopolymer mortars were compact and denser, and homogenous, as seen from the 3D images of fluorescence micrographs, (iii) geopolymer mortars were more resistant to temperatures of up to 900°C before internal cracking occurred, (iv) compressive strength decreased with increase in temperature from 300 to 900°C due to accelerated drying, and (v) geopolymer mortars showed better acid-resistant properties in acid immersion test. Additionally, any geopolymer properties can be increased when the concentration of alkali-activated was increased.

Prabu, Shalini & Kishore Kumar (2014) compared different waste by-products such as fly ash, ground granulated blast furnace slag and RHA used in geopolymer concrete production. They were gauged for compressive strength, acid resistance, water absorption, sulfate attack, pull out test, carbonation test and corrosion test. RHA showed the most excellent performance relative to the other materials studied.

2.4.1 Water resistant properties

The surface waterproof geopolymer is essential for improving the material strength and durability when exposed to weathering. Alkali activation of metakaolin and hydrophobicity modification was proposed as a method to improve on surface waterproofing of geopolymer. Surface waterproofing was enhanced as measured through contact angle analysis, where the angle was increased from 36°C to 132°. It was further verified by the floating of the specimen at the water level. Fgure 2.6 illustrates the process of surface hydrophobic modification of geopolymer (Duan, Yan, Luo, & Zhou, 2016).

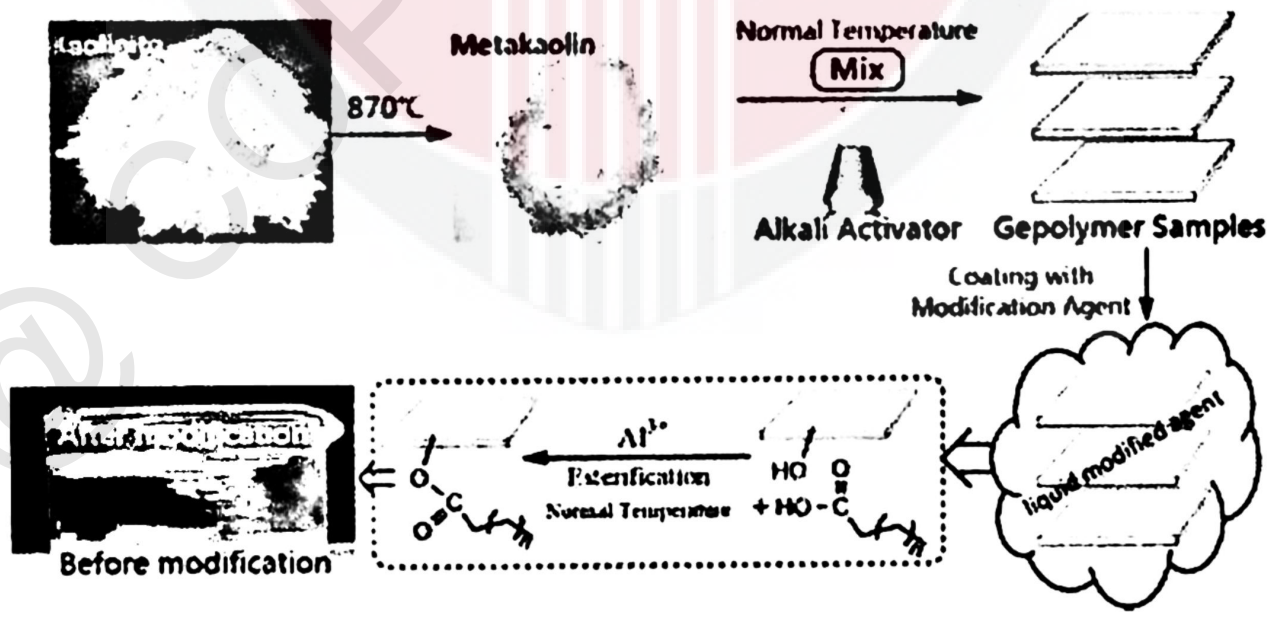

Figure 2. 6: The procedure of surface hydrophobic modification of geopolymer

According to Reffa et al., the water absorption capability can be varied by using different molarity of RHA-based pozzolan binder. The molarity of sodium hydroxide (NaOH) solutions was varied from 4 to 16M and the RHA:AA ratio, varied from 1.0 to 1.5 for each molar. The AA mixture ratios (Na_2SiO_3:NaOH) of 0.5 and 2.5 were used. The geopolymer samples were immersed in a water bath at room temperature, taken out for weighting and then re-immersed in the bath. The steps were repeated at intervals. The percentage of water content in the samples was calculated as: $M_t(\%) = (\frac{W_t - W_o}{W_o}) \times 100$. Water absorption was increased with increase in NaOH concentration for all geopolymer samples due to the geopolymerization (Nurul Reffa, Norkhairunnisa, Azmah Hanim, & Nasir, 2018).

Azrem Azmi *et al.*, (2019) examined the mechanical and water transport performance of geopolymer composite made in two blends, namely, fly ash-bottom ash (FA-BA) and fly ash-rice husk ash (FA-RHA). The mass replacement of both BA and RHA was kept at 40%, 30% and 20% of total solid proportions in geopolymer composite. Results indicated that the FA-BA blend was 15-20% more resistant to the percolation of water compared to the FA-RHA blend for water transport performance due to its denser pore structure. The mechanical properties of the FA-BA blend were also stronger than that for the FA-RHA blend. The risk of damages to the FA-BA structure is thus lower than that for FA-RHA due to the presence of the amount of voids in the bricks, which decreased the density, and the high water absorption capacity (K. A. Khan, Raut, Chandrudu, & Sashidhar, 2019).

A case study examined the properties of rubberized geopolymer interlocking bricks, which included compressive strength, water absorption and initial rate of absorption (Mohammed *et al.*, 2018). The samples were made from fly ash and crumb rubber (ratio 1:1), including the activator solution, NaOH and Na_2SiO_3 (ratio 1:3). The compressive and flexural strengths were shown to be weak, and the water absorption capacity quite high. Additionally, the initial rate of absorption (IRA) was considered low, thus producing negative effects on the bricks and the ability to create strong bonds.

2.4.2 Fire retardant properties

A study was conducted on the utilization of two industrial wastes, namely red mud (RM) and rice husk ash (RHA), for synthesizing lightweight heat resistant geopolymer–based materials. Figure 2.7 shows the experimental procedure to produce geopolymer-based materials from RM and RHA.

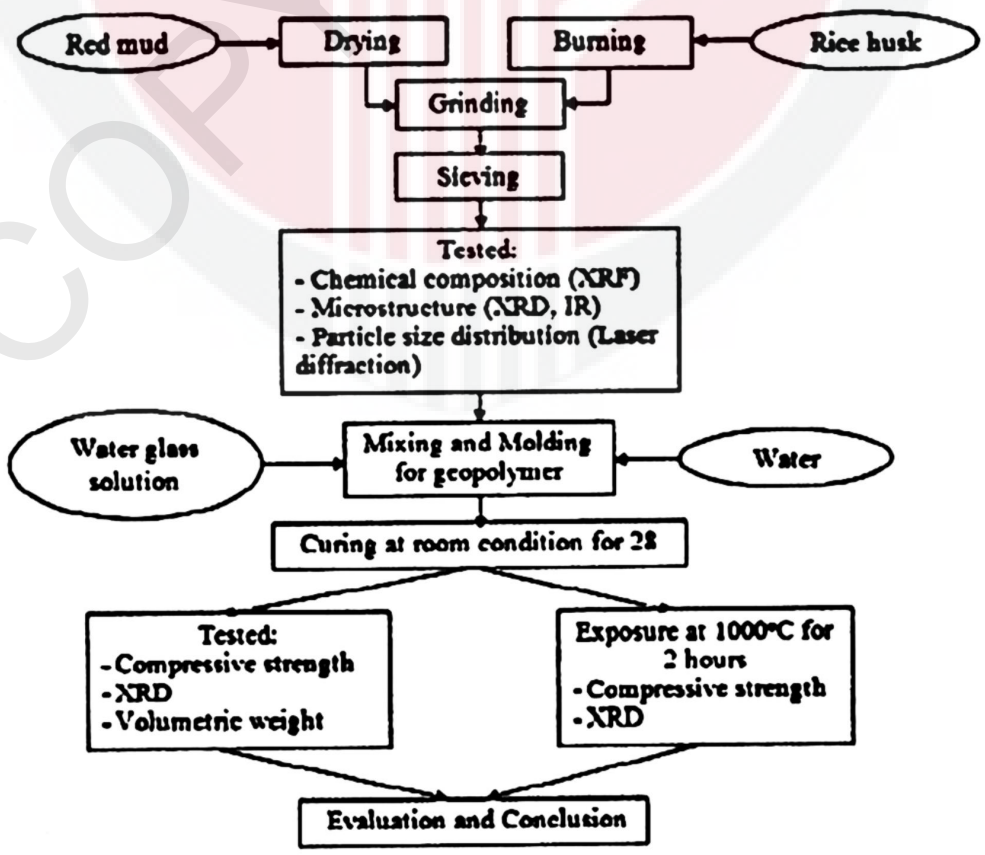

Figure 2. 7: Procedures to produce geopolymer-based materials from RM and RHA

The compressive strength was increased to between 5.86 and 25.45 MPa at 28 days, an improvement from 36 percent to 160 percent, despite being subjected to an extreme temperature of 1,000°C for 2 hours. The materials thus produced displayed good engineering properties that can withstand high temperatures with high heat resistance compressive strength (Hoc Thang, Kien, & Abdullah, 2017).

The fire resistance of a hybrid composite RHA-based geopolymer was also investigated. Several geopolymer samples were prepared with ratios of SiO_2:Al_2O_3 (3.0), Na_2O:SiO_2 (0.2) and H_2O:Na_2O (10.0) through the alkali activation method at 60°C and for 1 hour. RHA was added to the samples at 5%, 10% and 15% respectively by weight. Maulana et al. (2017) observed that the samples released smoke and showed significant physical damage but were, however, not burnt, following exposure to the fire of up to 1540°C for 30 minutes. They concluded that the addition of 10% RHA in the geopolymer showed excellent performance for compressive strength, thermal properties and also acid resistance (Maulana *et al.*, 2017).

RHA-based geopolymer binder for fire resistance coating was developed in a study. Five factors were considered, namely, the ratio of AA solution, RHA:AA ratio, curing temperature, curing time and concentration of NaOH. The RHA:AA ratio was found most influential in all properties of geopolymer. RHA provided the best performance on fire resistance, which is augmented with good adhesion and flexural properties (Mohd Basri, Mustapha, Mazlan, & Ishak, 2016).

Metakaolin and RHA in the coating material have also been investigated for their properties as geopolymer paste. The paste was developed using the alkaline activation method by adding up to 15 percent RHA based on the metakaolin mass. A substrate sample was then coated with the geopolymer paste and cured at 60°C for 3 hours. After seven days, some tests were carried out, including fire and chemical resistance. The result confirmed that the geopolymer paste thus formulated was resistant to fire and chemical attacks and hence make excellent coating material (Kaloari, Syamsidar, Sulfiana, Haris, & Subaer, 2016).

2.5 Fractional factorial design (FrFD)

Fractional factorial design (FrFD) was used to identify the most influential factors or design factors that affected experimental results. FrFD graphs were later generated using the Minitab software system typically applied in real-world examples in the manufacturing industry (Antoy, 2014). In addition, the Plackett-Burman Design (PBD), FrFD, was also used for calculating the main effects, with reduced the number of experiments, and with the assumption of obviating completely any interaction. PBD is commonly used to investigate experiments with more than seven factors (Das & Dewanjee, 2018). Typically, the FrFD can be used together with the RSM. The FrfFD is, however, used first since it can determine the factors which most affect experimental results.

2.6 Response surface methodology (RSM)

RSM is an effective statistical technique used to collect mathematical data on the effects of multiple factors related to the process. These are then analyzed to produce an empirical model (Ba & Boyaci, 2007). The major benefits of RSM are the number of experimental trials that can be reduced, the complex interactions between the independent variables that can be calculated, analyzed and optimized, all leading towards improving on the existing design. In addition, RSM can also reduce the expensive cost of analyses by reducing the number of experimental trials. It is, therefore, a more practical approach relative to conventional ones since it includes interactive effects between factors and indicates their overall effects on the process (Pike, Box, & Draper, 1988). Furthermore, several classes of response surface designs can be displayed in practice, including the Central Composite Design, Box-Behnken design, Hydrid design and Three-level Factorial design (Moradi *et al.*, 2016).

CHAPTER 3

METHODOLOGY

3.1 Overview

The mild steel plate was used as a substrate for geopolymer coating samples. The coatings were made from rice husk ash (RHA), alkaline activator (AA) and silicone rubber (SiR). Three factors related to the coatings investigated in this study included the molarity of sodium hydroxide (NaOH), the ratio of RHA to AA solution (Ge) and the ratio of Ge to silicon rubber. MINITAB software has been used to design the experiments. The fractional factorial design (FrFD) was used to determine the significance of each factor, and the surface response methodology (RSM) was used to optimize the factors and perform validation. Samples were tested for fire retardant and moisture absorption. In the study, the optimum composition of the geopolymer (SiR-RHA-Ge) composite coating was clarified. Flow chart for the fabrication of the coating composite and overall study are shown in Figure 3.1 and Figure 3.2, respectively.

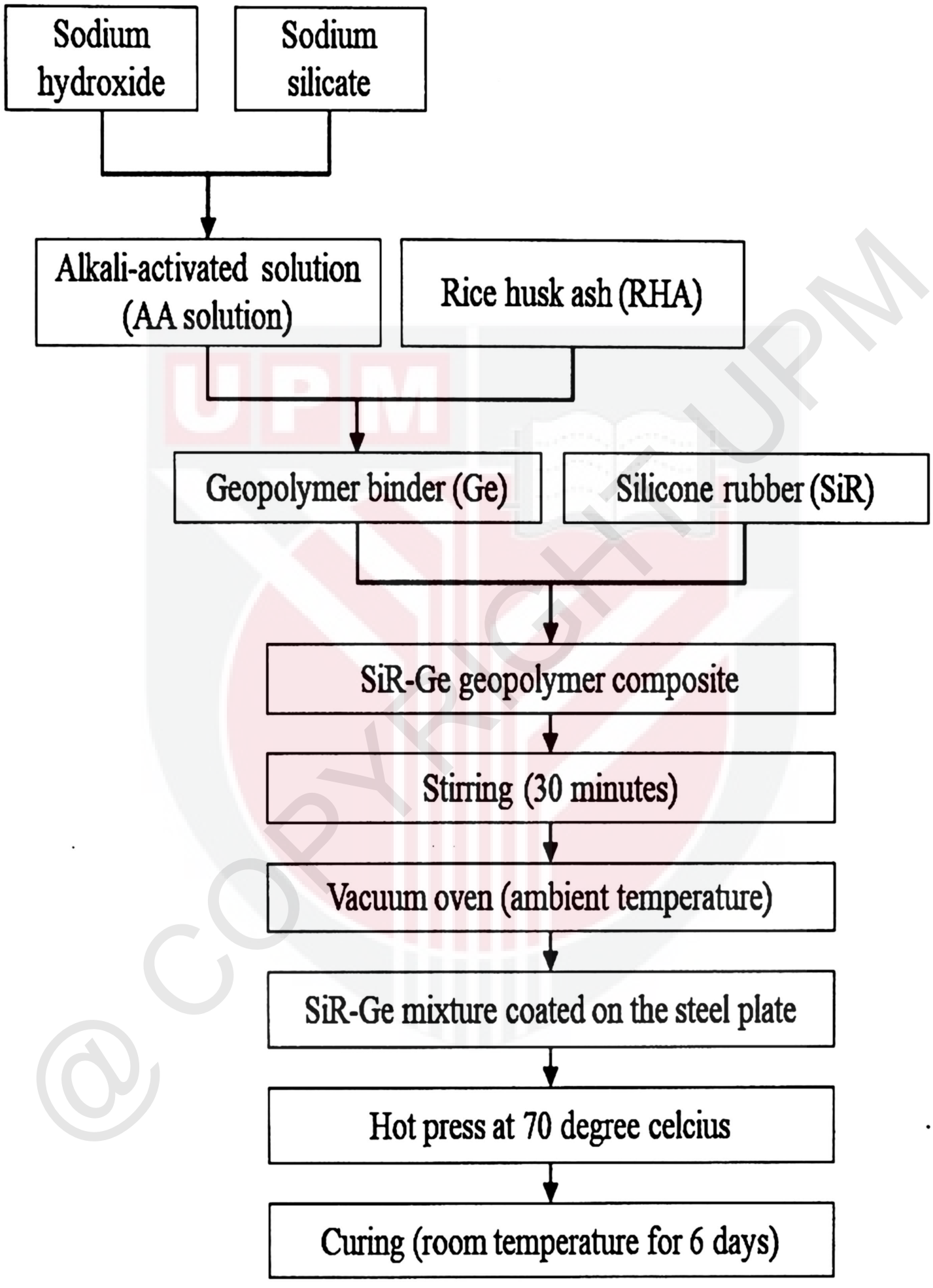

Figure 3. 1: Flow chart for the fabrication of SiR-RHA-Ge coating composite

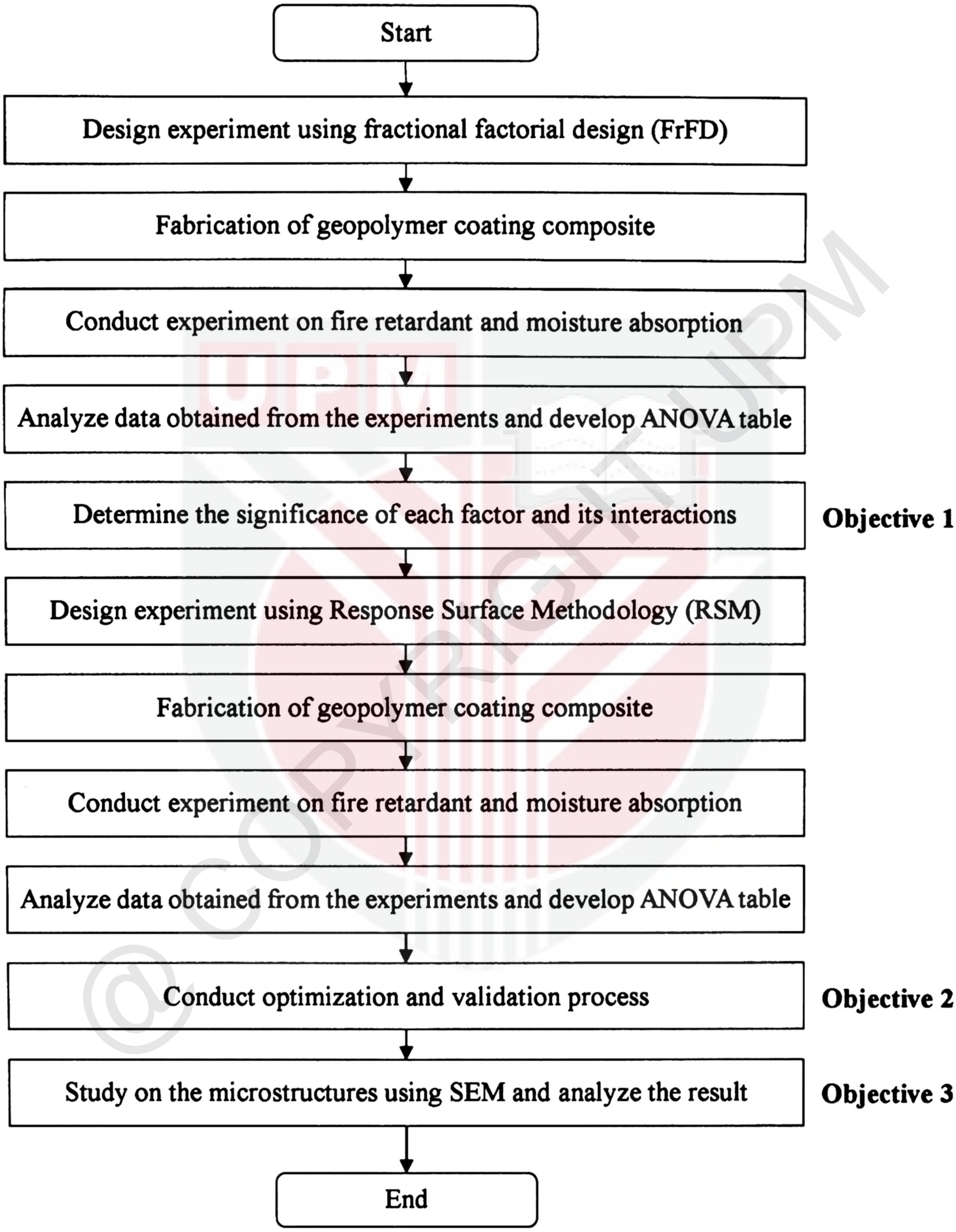

Figure 3. 2: Flowchart of the study

3.2 Materials

3.2.1 Rice husk ash

Rice husk ash (RHA) has been obtained from Maero Tech Sdn. Bhd, located at Nilai 3, Negeri Sembilan. It was ground with a blender (MX-SM1031SSL, Panasonic, Malaysia) in finer particle sizes. It was then sieved (using AS200 Digit, Retsch, Germany) to obtain a particle size of smaller than 125 microns. Figure 3.3 shows images of RHA before and after grinding. The physical properties of the RHA after ground is given in Table 3.1

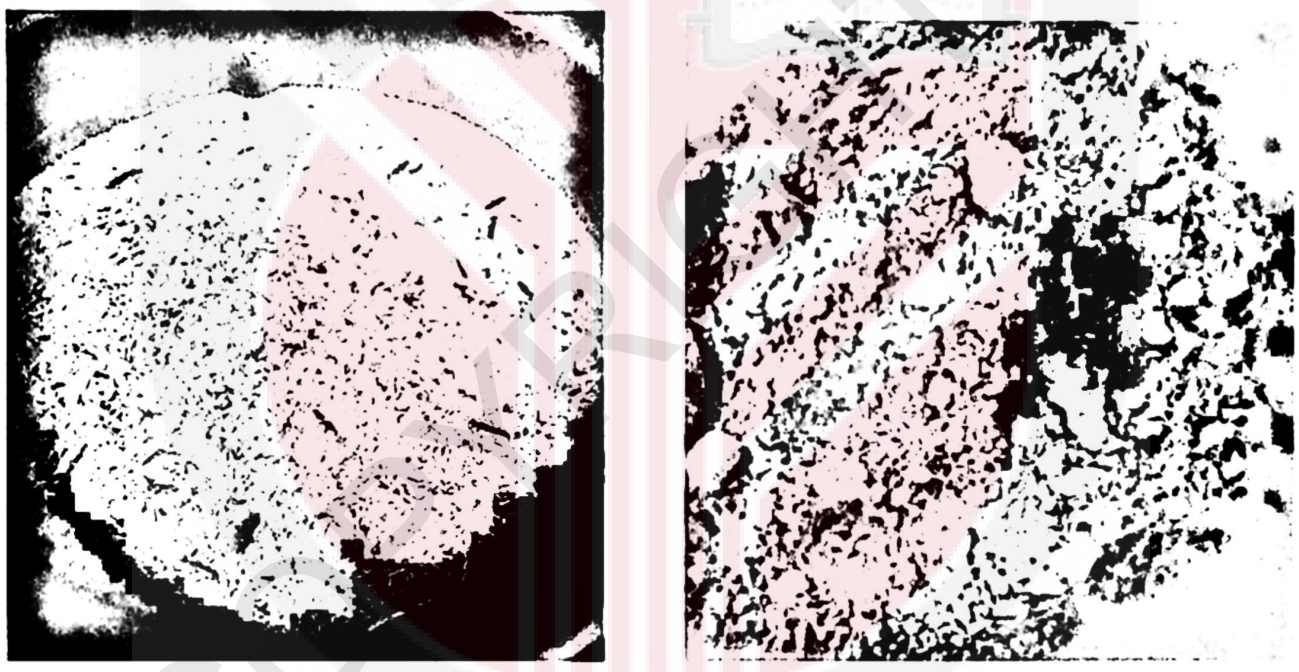

Figure 3. 3: Images of RHA before (left) and after (right) grinding

Table 3. 1: Physical properties of RHA after ground

Particles Size	**< 125 mircon**
Colour	Light grey
Structure	Power form
Odour	Non

The fine structure of RHA before and after ground under a scanning electron microscope (SEM) is shown in Figure 3.4. The RHA particle size before grinding ranges from 1μm to 100μm. Particles appear as plates and thin shell-like structures with rectangular indents on the surface. Such forms are the initial structure of the RH. Besides, RHA has porous, cellular surfaces due to its sponge-like particles (Mohd Basri, 2016).

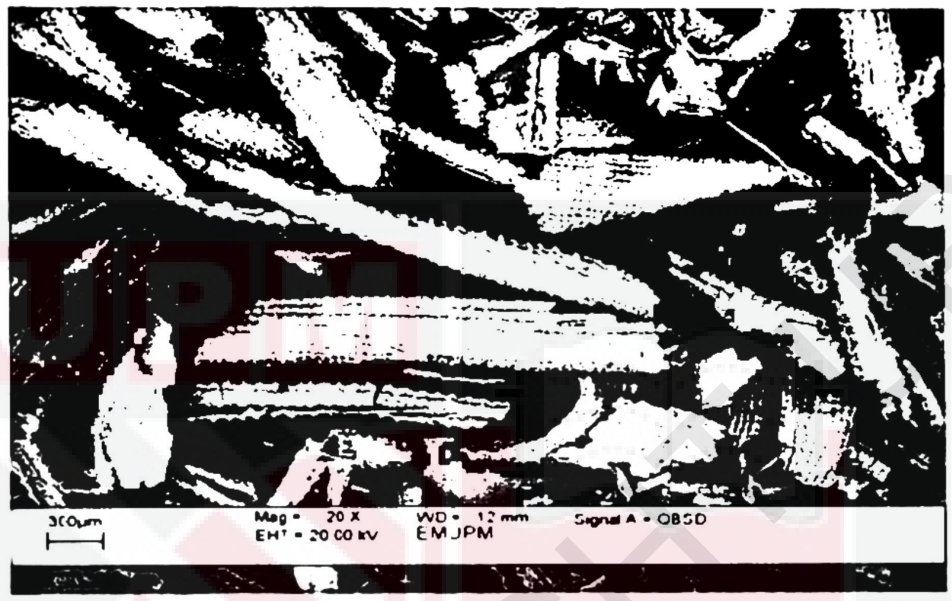

Figure 3. 4: SEM image of RHA structure before grinding (Mohd Basri, 2016)

Figure 3.5 shows the RHA structure after ground. The particles contain a higher concentration of silica in a solid-state in nature, with amorphous shapes similar to cristobalite and trace crystalline quartz (Shinohara & Kohyama, 2004).

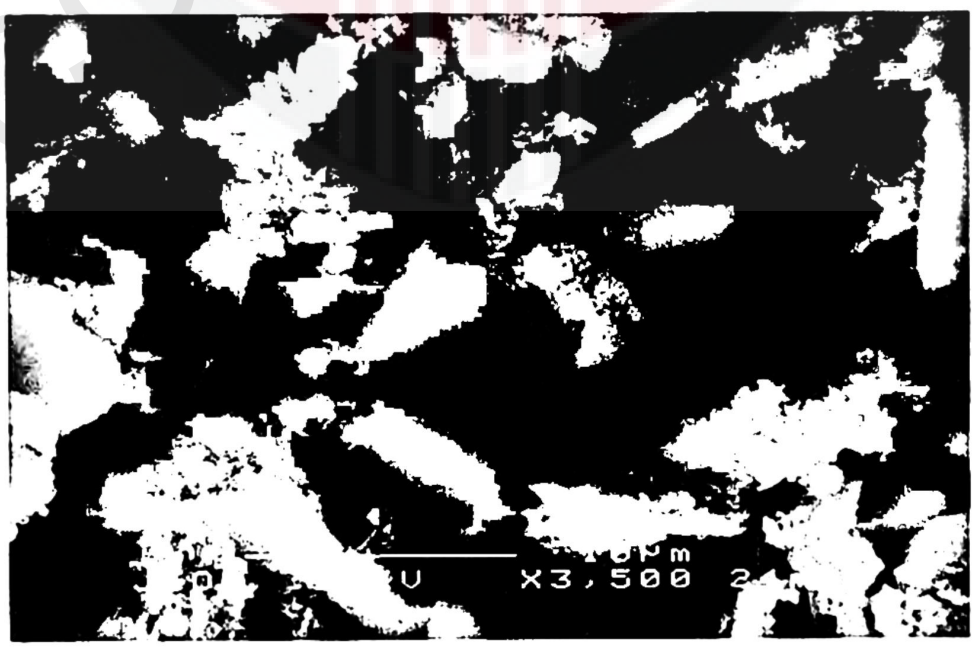

Figure 3. 5: SEM image of RHA structure after grinding

The RHA particles must be ground to very fine particle size to allow for their pozzolanic activity. The condition for burning RH is vital in the production of the highest silica RHA in an amorphous state. Conversely, silica derived from unchecked incineration (temperatures higher than 700°C - 800°C) is mostly cristobalite and tridymite, which are non - reactive silica minerals (Singh, 2018).

3.2.2 Activated alkaline solution

The activated alkaline solution consists of sodium silicate (Na_2SiO_3) solution and sodium hydroxide (NaOH). Wang *et al.* (2016) found that the geopolymer material can be quickly set and acquire high strength when an alkaline solution used with only NaOH. However, if only sodium silicate solution were used, the geopolymer material produced had good workability, but could hardly be set and possess low strength. Thus, a combined alkaline solution of sodium and sodium hydroxide is desired for the development of alkali-activated SiR-RHA-Ge composite paste with sufficient workability and strength.

The polymerization reaction of the geopolymer material could be accelerated with an optimal high alkaline concentration, which also improves the mechanical properties. It would, however, reduce the strength of the polymer if it was used at an excessive concentration. Table 3.2 shows the chemical properties of the alkaline solution (Yang, Chang et al., 2012).

Table 3. 2: Chemical composition of alkaline solutions (Yang *et al.*, 2012)

Elements	Sodium hydroxide	Sodium silicate
NaOH	98.2	-
$NaCO_3$	0.165	-
NaCl	0.0135	-
Fe	0.0004	< 0.02
SiO_2	-	29.2
Na_2O	-	8.19

3.2.3 Silicone rubber

The food-grade silicone rubber (SiR) has been used in this study. Food grade silicone is a non-toxic silicone that is not disposed of by harmful microbial agents or other contaminants. It is usually used for good grade gaskets and seals that can work for a long time without contamination or degradation. It is generally used at temperatures between -80°F and 450°F (Gallagher Fluid Seals, 2019). Figure 3.6 shows AB liquid food grade mold maker silicone with a pot life of 30 minutes. Silicone consists of parts A and B, where part A is the catalyzer and part B is the crosslinker. Both were mixed with a weight ratio of 1:1 and left for cure at room temperature between 3 and 8 hours. The process can be accelerated when higher curing temperatures are involved.

Figure 3. 6: AB liquid food-grade mold maker silicone

3.2.4 Mild steel plate

Mild steel or carbon steel is widely used in many applications such as in construction and industrial since it has high tensile strength, high compressive strength and a comparable density of 7.85 g/cm^3. An A36 standard carbon steel consists of carbon (0.26%), copper (0.20%), iron (99.0%), manganese (0.75%), phosphorous (<0.04%) and sulphur (<0.05%) (Matweb, 2015).

Mild steel plates used for the study have a thickness of 1±0.05mm with a dimension of 100mm in length and 100mm in width. The plate surface was cleaned using sandpaper to improve the surface roughness and washed with acetone to remove any unwanted oils or greases. Once the surface was dried at room temperature, the plates were placed in an oven at 45°C for further drying to remove excess water. The plates were then used as a substrate and coated with the SiR-RHA-Ge coating composite.

3.3 Sample preparation

Samples for fire retardant and moisture absorption tests were prepared, as shown in Figure 3.1. The samples were prepared in accordance with the experimental design of the FrFD and RSM, and the weight calculation is shown in Appendix A1. The SiR-RHA-Ge coating composite sample for the fire retardant test was prepared by dissolving the sodium hydroxide (NaOH) pellet in distilled water, followed by the addition of sodium silicate (Na_2SiO_3) into the NaOH solution at a ratio of 5.5. The mixture was designated as an AA solution. Then, RHA was added to the AA solution at a ratio of 0.25, which forms a dark grey slurry mixture, as shown in Figure 3.7.

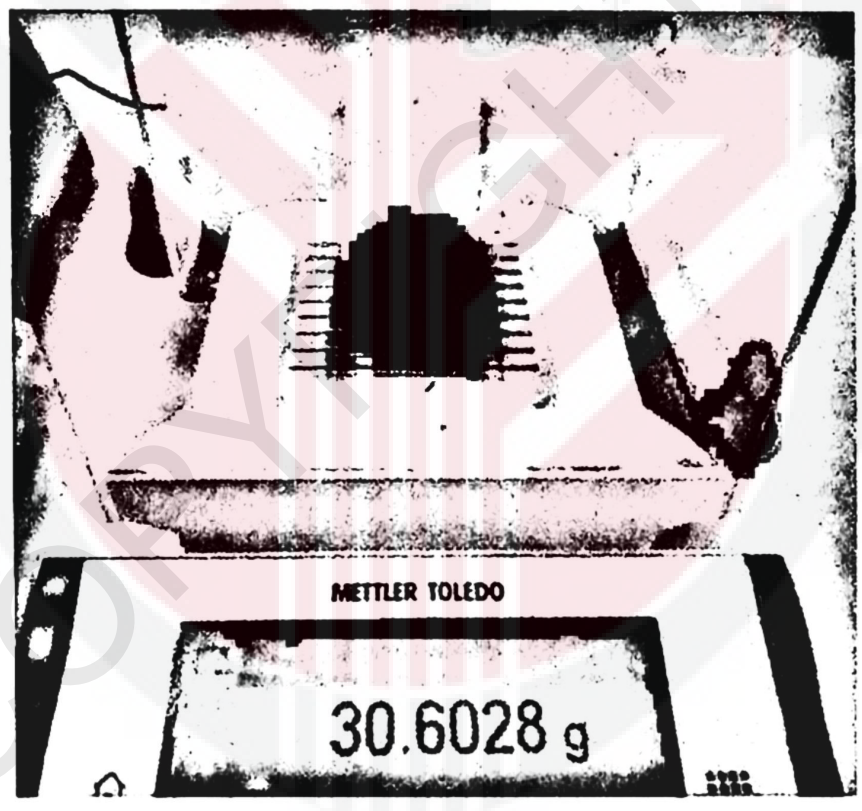

Figure 3. 7: Dark grey slurry mixture

Silicone rubber was added into the geopolymer mixture at the ratio of 0.85 and mechanically stirred (HS-300, WiseStir, Greece) at 500 rpm for 30 minutes. The mixture was coated onto the surface of the mild steel plate and evenly spread. The coated mild steel plate is shown in Figure 3.8.

Figure 3. 8: Coated mild steel plate

The coated plate was placed in the vacuum oven (Model 53, Binder, Germany) to reduce bubbles formation. The coated plate was then placed into the hot press machine (Gotech, Taiwan) for pre-drying at 70°C before being pressed to obtain a coating thickness of 1±0.3 mm.as shown in Figure 3.9.

Then, it is placed into the oven for 24 hours at 70°C to be cured. The plate was left at room temperature for six days for the complete curing process.

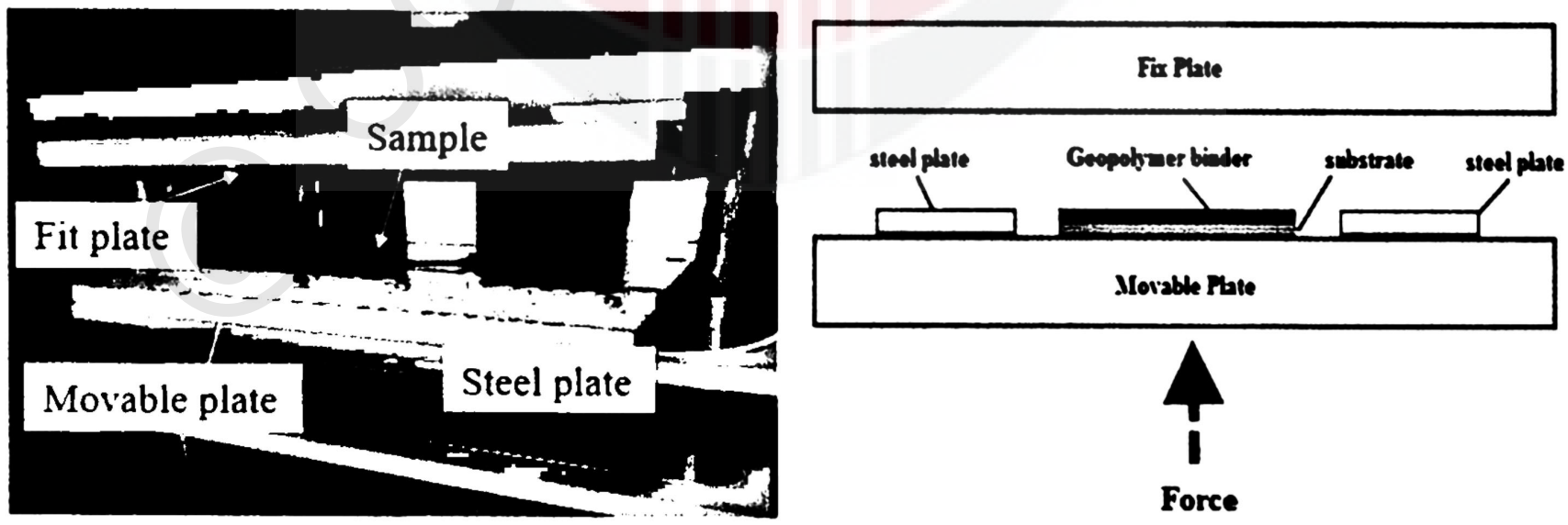

Figure 3. 9: Hot press machine

For the moisture absorption test, the dimension for the SiR-RHA-Ge composite sample was 3±0.05mm in thickness and 3mm in length and width, as shown in Figure 3.10. The sample mixing proportion is similar to that of the method used in the fire retardant test. When the mixture was ready, it was poured onto parchment paper, covered with other parchment paper, and pressed to a thickness of 3 mm using a hot press at 70°C for 3 minutes. The sample was then cured in the oven at 70 ° C for 24 hours before it was left to be fully cured at room temperature for six days. The sample was cut to the desired size.

Figure 3. 10:Samples for the moisture absorption test

3.4 Experiment procedure

3.4.1 Moisture absorption test

The moisture absorption test was carried out using a portable humidity chamber (PHC), as shown in Figure 3.11. The portable humidity chamber was designed to provide a controlled environment with consistent humidity and temperature. It is made using a

plastic container with a lid. At the top right of each side of the PHC, there was a temperature and humidity sensor and LCD. Three humidifier holes were created at the bottom of the PHC. For this study, humidifier 1 and 3 were closely sealed, while humidifier hole 2 was opened to enable the humidifier to spray fine mists into the chamber. Potassium sulfate was placed in the PHC to maintain the humidity inside the chamber at 98±1° (Quincot, Azenha, Barros, & Faria, 2011). Prior to testing, samples were placed in the PHC, and the lid was close tightly. The humidifier sprayed fine mist into the chamber via humidifier hole 2 for 1 minute. Then, the humidifier was removed, and the humidifier hole 2 was covered with adhesive tape. Temperature and humidity were recorded at a designated time interval. The chamber was able to test approximately 54 samples at a time.

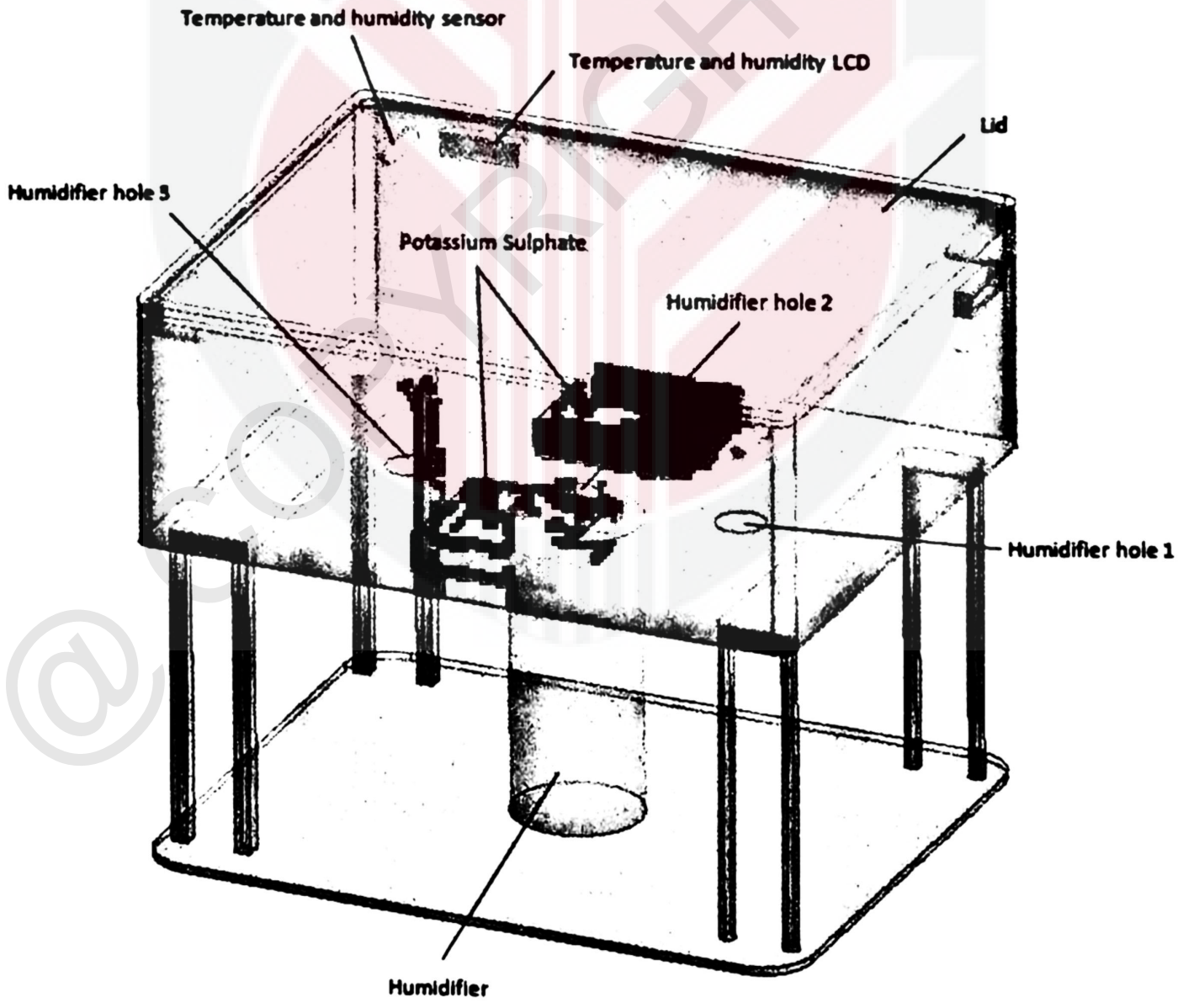

Figure 3. 11: Isometric design of a portable humidity chamber

The test was conducted according to the ASTM D5229-92 (ASTM standard, 2010). The percentage of relative humidity was controlled at 98±1% at room temperature. The initial weight of the sample was recorded before the test. During the moisture absorption test, the weight of the sample was recorded every two hours for 24 hours, four hours for the next 24 hours, six hours for the next 24 hours, and 24 hours for the next 48 hours. The maximum time required for the sample to reach equilibrium was 5 days. The percentage of moisture absorption was calculated based on Equation 4, where w_i is the weight of the sample at the current time, and w_b is the weight of the sample at baseline time.

$$\text{Moisture absorption, \%} = \left|\frac{w_i - w_b}{w_b}\right| \times 100\ \% \qquad \text{(Eq. 4)}$$

3.4.2 Fire retardant test

The test for fire retardant was set up, as shown Figure 3.12. The fire retardtant test was conducted by heating the samples with direct blow torch flame in accordance with UL-1709 standards (UL Standard, 2007). The coated samples were heated directly using a blow torch with flame temperatures around 900°C. The distance between the sample and the flame was 70mm. A thermocouple was placed at the back of the sample, where no coating is applied. The flame from the blow torch was fired directly to the centre of the sample. The thermocouple was connected to a computer that displayed and recorded the surface temperature at the back of the sample. A graph of temperature against time was generated automatically. The test was terminated once the temperature recorded achieve equilibrium.

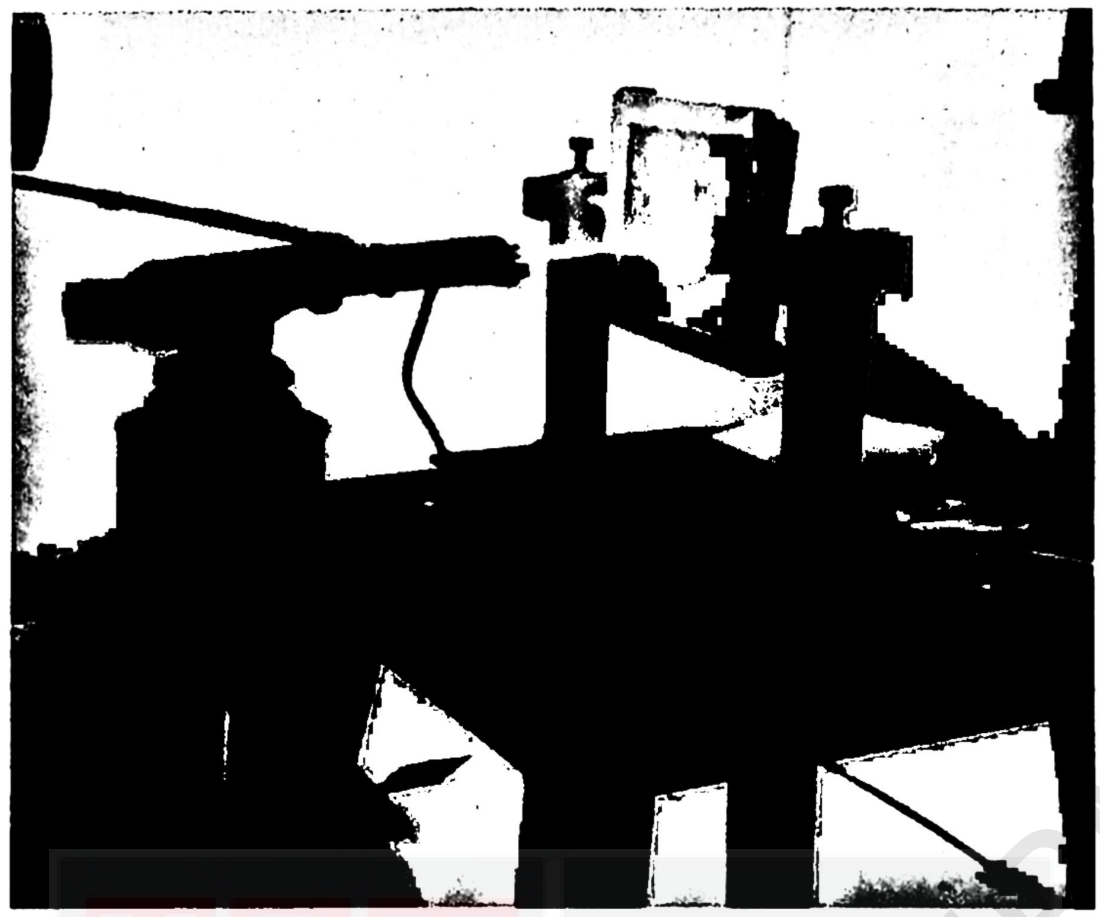

Figure 3. 12: Set up for fire retardant test

Two replication for each sample formulation was tested. The ambient temperature and humidity have also been recorded for each test. The bare mild steel plate was exposed directly to the blaze for 10 minutes as calibration and comparison purposes. Coatings without silicone rubber are tested for fire retardant and moisture properties to compare the result with the optimized sample.

3.5 Microstructure analysis

3.5.1 Scanning electron microscope

A scanning electron microscope (SEM) was used to analyze the microstructure of samples before and after testing. SEM was conducted using Hitachi S-3400N variable SEM as shown in Figure 3.13.

A total of nine samples, including before fire retardant test (3 samples), after fire retardant test (3 samples) and after moisture absorption test (3 samples), were first mounted with a conductive adhesive and sputter-coated with gold-palladium powder. The stub with sample specimens was inserted into the sample chamber of the SEM for viewing. The views of the sample surface were acquired at magnifications of 1000x and 5000x.

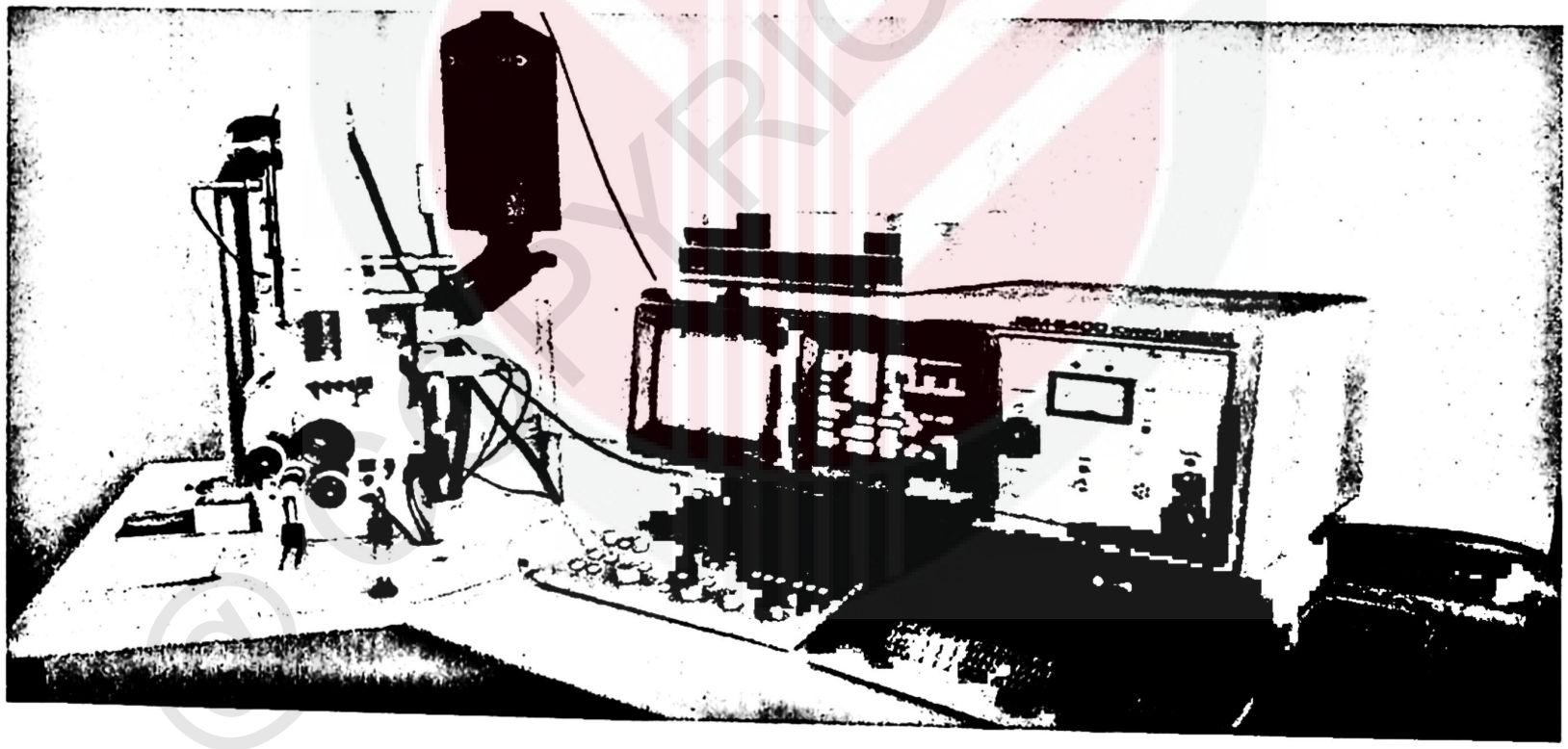

Figure 3. 13: Hitachi S-3400N

3.6 Experimental design and analysis

This study was carried out using a two-step experimental design, which was a fractional factorial design (FrFD) and a surface response methodology (RSM). The FrFD and RSM experiments were designed and analyzed using MINITAB software. FrFD was conducted to reduce the number of factors by identifying the significance of each factor and their interactions that affected the response (the temperature at equilibrium and moisture absorption percentage). Two factors from the FrFD analysis were selected based on the most significant value and interaction of a single factor. The factors were then used to design the RSM experiment used to perform the optimization process.

3.6.1 Fractional factorial design

Three factors were analyzed, including the NaOH concentration, the RHA / AA (Ge) ratio and the SiR / Ge ratio. The half fraction was selected in a fractional factorial design, and the experiment was based on two levels and three replications. The total number of the experimental run was 12. The experiment was conducted in two phases, with 6 samples per phase.

MINITAB, a statistical software, was used to design the experiments and analyze data obtained. Results were analyzed, and the ANOVA table was tabulated. Only second orders terms, in which the main factors and its second-degree interactions, were sufficient for the study. Pareto charts were generated and used to identify the significance of each factor and their interaction. The level choosen in FrFD and RSM were based on preliminary studies conducted by previous researchers and with minor modification

considering the workability of the sample during fabrication process. Table 3.3 shows the low and high level for each factor considered in the study using fractional factorial design.

Table 3. 3: Low and high level for each factor used in FrFD

Factors	Low	High
Concentration of NaOH	6 M	14 M
RHA/AA (Ge) ratio	0.25	0.85
SiR/Ge ratio	0.25	0.85

3.6.2 Response surface methodology

Two factors identified using fractional factorial design were used in designing the experiment using RSM. Full design with 13 runs, 5 levels and 2 replications were chosen with the total number of 24 experimental runs. The experiment was conducted in two phases (12 samples per phase), and the results analyzed using the MINITAB software were shown in the ANOVA table. The contour plots were used to indicate the relationship between factors and their effects on the responses. The optimization process was carried out using a response optimiser to predict the optimum composition of the SiR-RHA geopolymer binder. Using the predicted value of the optimization process, the validation was carried out using an experimental method to verify the accuracy of the prediction made by MINITAB software.

CHAPTER 4

RESULTS AND DISCUSSION

4.1 Fractional factorial design (FrFD)

FrFD aimed to determine the factors that have the most significant effect on the fire resistance and moisture absorption properties of SiR-RHA-based geopolymer composite coating. The statistical software package (MINITAB Release 16.2) was used to analyze the experimental design. The uncoded (actual value) design matrix for the factors and responses involving 12 experimental runs, which are fire retardant and moisture absorption tests, are given in Appendix B1. Results for the responses were statistically analyzed, and the mathematical models were developed based on the ANOVA table consisting of main factors and interaction which have confidence levels of more than 95.00 percent (p-value lower than 0.05).

4.1.1 Statistical analysis

A reduced linear regression model was fitted with the experimental data using the least square technique. Table 4.1 showed the standardized effect, P of the effects and model coefficients for the temperature at equilibrium (TAE), whereas the moisture absorption is shown in Table 4.2. Details for the statistical analysis of this study are shown in Appendix C1. The p-value in the ANOVA tables represented the significance level for each term (factor and their interactions) on the responses. The term was statistically significant when the p-value is less than 0.050 at the confidence level of 95.00 percent. Interactions which have not been significant are excluded from the ANOVA table, and the analysis of the remaining terms is repeated

All individual factors, as shown in Table 1 were found to be significant, and all interactions which were not significant and have been removed from the ANOVA table. The RHA/AA ratio (V_1) was significant with the p-value of 0.009, while the NaOH concentration (V_2) was found to have a very strong effect on the temperature at equilibrium (p-value of 0.000). The value for $R^{2,}$ which is 0.9495 and R^2 (adjusted) of 0.9306, was considered very high, which indicates that 94.95 percent of the results that can be explained and the experiment conducted yield an accurate result.

Table 4. 1: Estimated effects and coefficient for TAE

Term	Notation	Net Effect	Coeff.	Std. error of coefficient	Standardized Effect	p-value
Constant			305.25	8.010	38.11	0.000
RHA/AA ratio	V_1	55.10	27.55	8.010	3.44	0.009
NaOH concentration	V_2	-181.77	-90.88	8.010	-11.35	0.000
SiR/Ge ratio	V_3	-50.50	-25.25	8.010	-3.15	0.014
R^2 = 94.95 percent	R^2(adj) = 93.06 percent					

In Table 4.2, all factors were highly significant ($P \leq 0.000$) at 95.00 percent confidence level. Based on the coefficient value, the RHA/AA ratio (V_1) was the most significant factor, followed by SiR/Ge ratio (V_3) and NaOH concentration (V_2). The value for R^2 and R^2 (adjusted) was very high at 0.9851 and 0.9795, respectively.

Table 4. 2: Estimated effects and coefficient for moisture absorption

Term	Notation	Net Effect	Coeff.	Std. error of coefficient	Standardized Effect	p-value
Constant			24.658	0.4159	59.29	0.000
RHA/AA ratio	V_1	-13.667	-6.833	0.4159	-16.43	0.000
NaOH concentration	V_2	5.577	2.788	0.4159	6.70	0.000
SiR/Ge ratio	V_3	-12.153	-6.077	0.4159	-14.61	0.000
R^2 = 98.51 percent	R^2(adj) = 97.95 percent					

4.1.2 Regression model

Using coefficient and the terms from Table 4.1 and Table 4.2, the regression models can be formulated as shown in Equation 4.1 and 4.2 where Y_{TAE} is the temperature at equilibrium, Y_{MA} is the moisture absorption, V_1 is the RHA/AA ratio, V_2 is NaOH concentration, and V_3 is SiR/Ge ratio.

$$Y_{TAE} = 305.25 + 27.55\,(V_1) - 90.88\,(V_2) - 25.25\,(V_3) \quad \text{(Eq. 4.1)}$$

$$Y_{MA} = 24.658 - 6.833\,(V_1) + 2.788\,(V_2) - 6.077\,(V_3) \quad \text{(Eq. 4.2)}$$

4.1.3 Pareto plot

Figure 4. 1 shows the Pareto plot on the effects of the main factors. From Figure 4. 1(a), NaOH concentration (V_2) was found to be the most significant factor since it extended the most beyond the reference line. In contrast, V_2 was found to have the least effect on moisture absorption. Figure 4. 1(b) shows the Pareto chart for moisture absorption. The RHA/AA ratio (V_1) was found to be highly significant, followed by SiR/Ge ratio (V_3). Based on both Pareto charts, the RHA/AA ratio (V_1) was chosen to be used in response surface methodology (RSM) for optimization purposes. Between V_2 and V_3, V_3 was chosen based on two criteria. First, the study on the SiR/Ge ratio is of higher interest as compared to that of the NaOH concentration. Second, the optimization of silicon rubber in the mixture of geopolymer is very important to reduce overall material cost. Thus, the SiR/Ge ratio was chosen to be used in RSM.

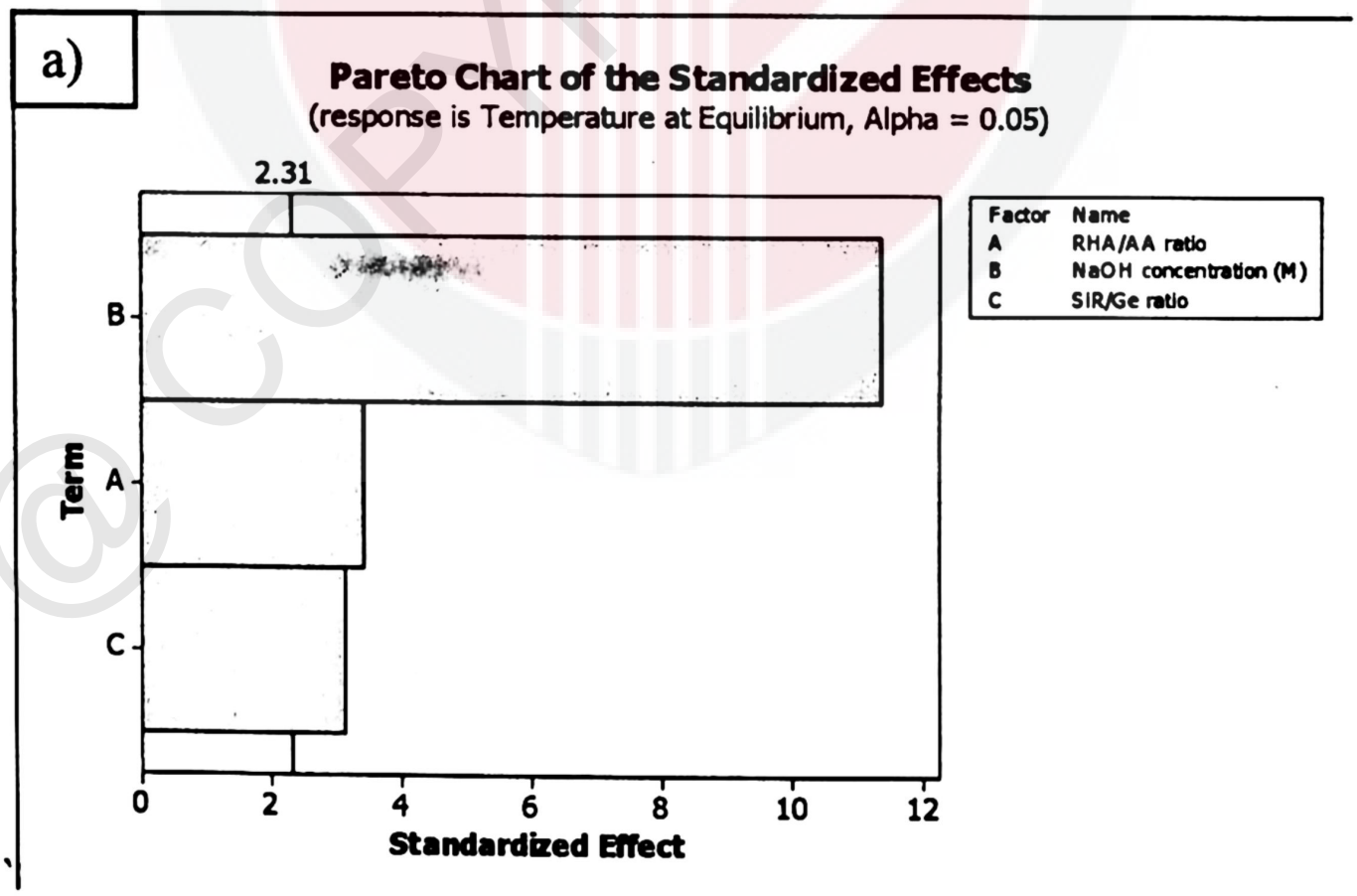

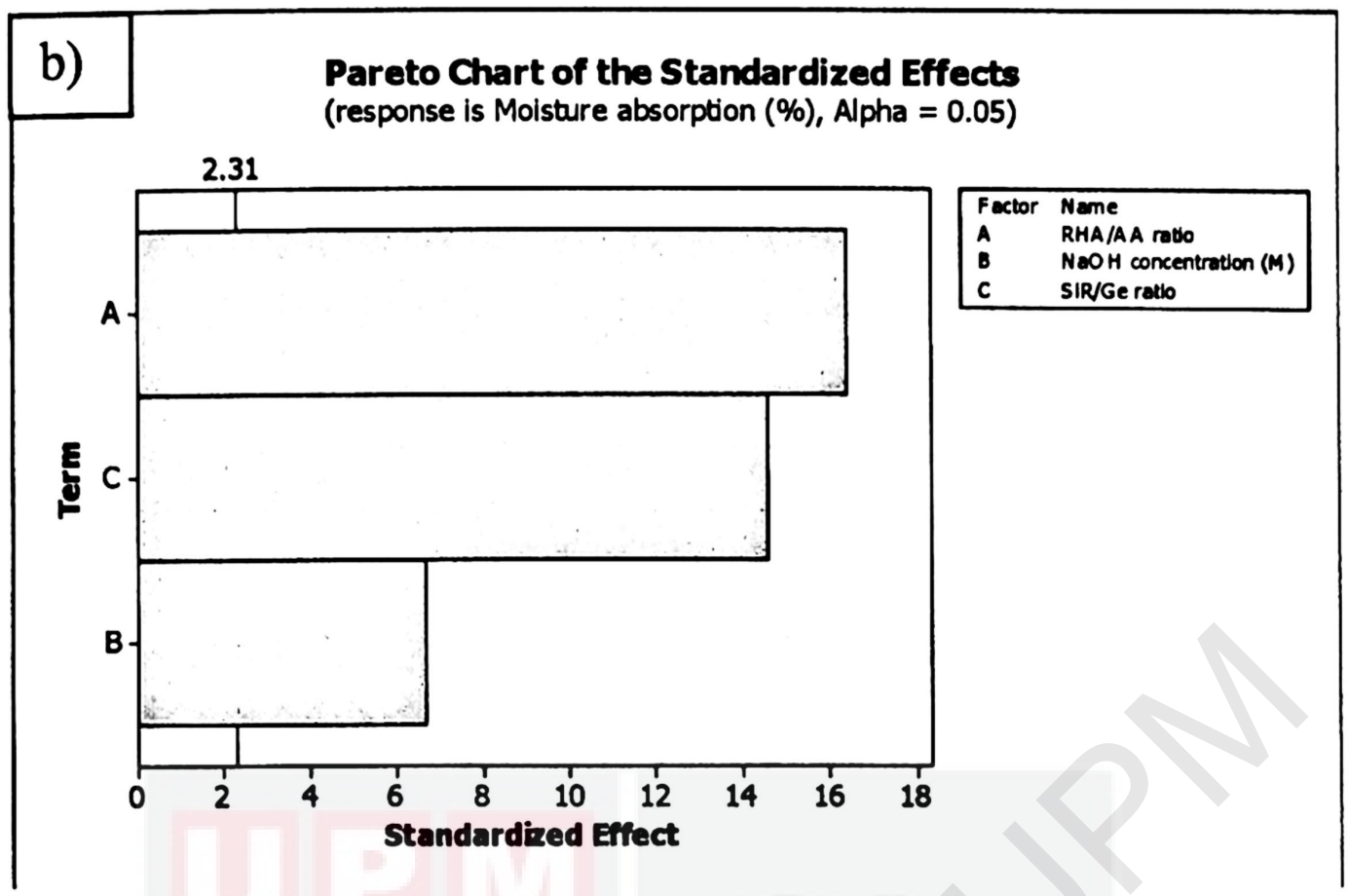

Figure 4. 1: Pareto plot of the standardized effects of (a) temperature at equilibrium, and (b) moisture absorption.

4.1.4 Main effect plot

It can be seen from Figure 4.2(a) that NaOH concentration (V_2) has the strongest negative effect on the temperature at equilibrium. In contrast, RHA/AA ratio (V_1) has the strongest negative effect on the moisture absorption, as shown in Figure 4.2(b) and indicated by a larger angle of inclination to the horizontal. Other factors showed smaller changes, and most of the factors have negative effects on the response. The result is parallel with the Pareto charts showed in Figure 4. 1.

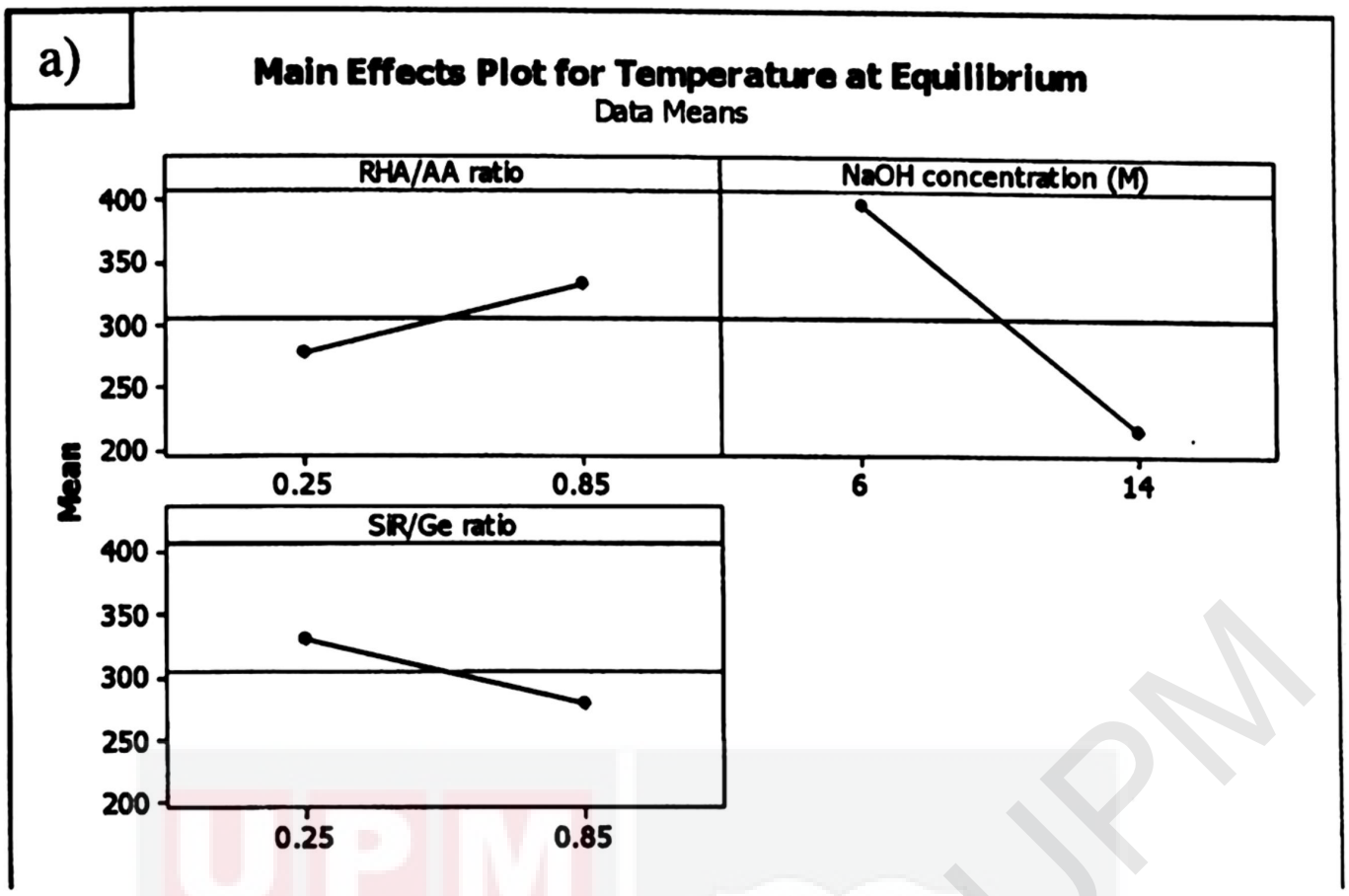

Figure 4. 2: Main effect plot for (a) temperature at equilibrium and (b) moisture absorption

4.1.5 Interaction plot

Contour plots were used to analyze the effect of various factors on the responses, which are the temperature at equilibrium (TAE) and moisture absorption, by providing a better illustration. Figure 4. 3 and Figure 4.4 show the effect of RHA/AA ratio (V_1) and NaOH concentration (V_2) on the responses. Figure 4. 3 shows the temperature at equilibrium below 180°C with low values of V_1 (below 0.4) and a high value of V_2 (above 13 M). Low temperature at equilibrium indicates excellent fire retardant properties. Inversely, the high value of V_1 (above 0.45) and low value of V_2 (below 7M) resulted in coating with poor fire retardant properties, which indicates by the high temperature at equilibrium of above 360°C. At a constant value of V_1, the temperature at equilibrium is decreased when the V_2 increased.

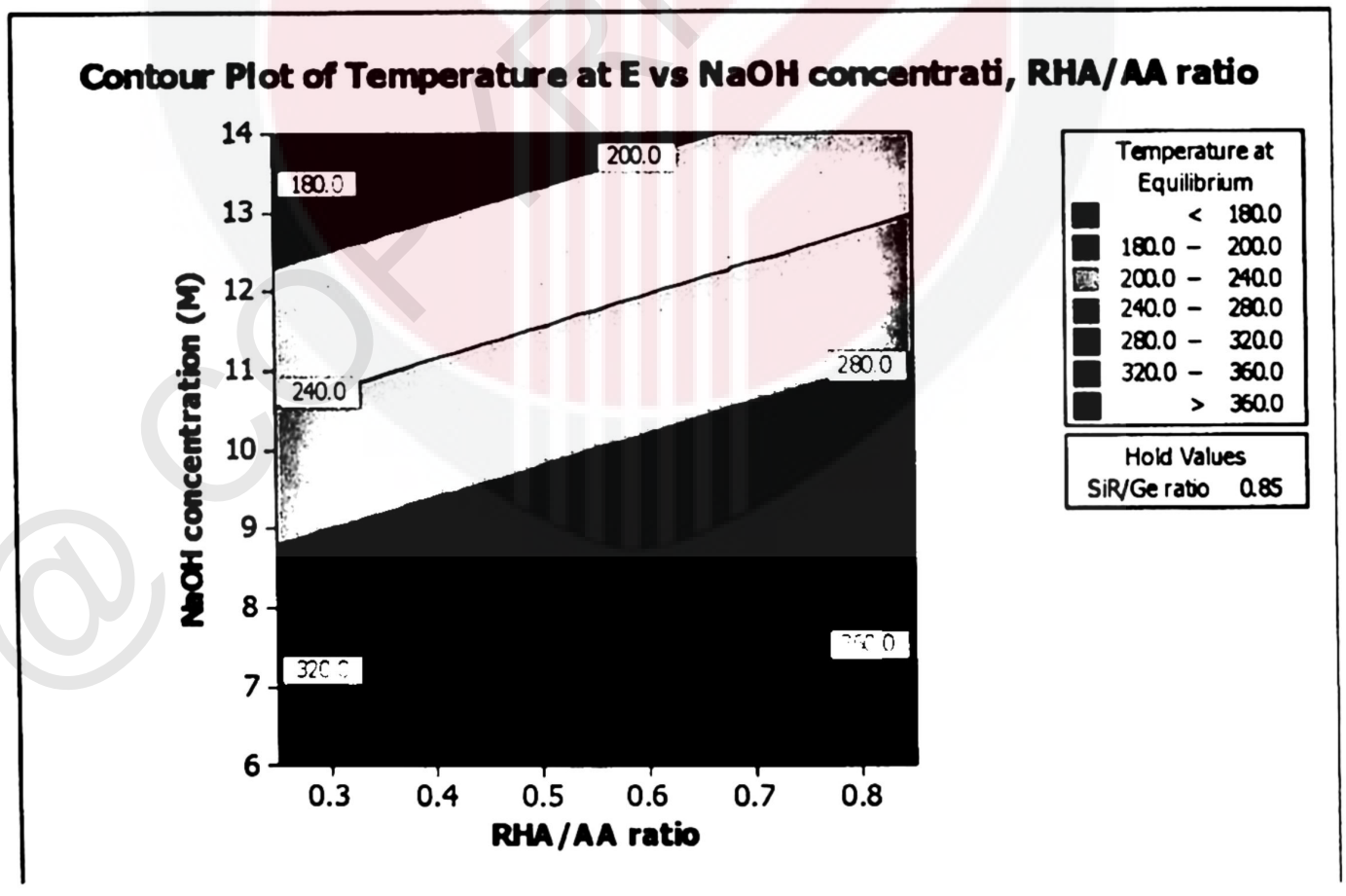

Figure 4. 3: Contour plot for the effect of RHA/AA ratio and NaOH concentration on the temperature at equilibrium

According to Huseien *et al.* (2016), the geopolymerization mechanism and microstructure composition of coatings can be enhanced by increasing the NaOH concentration and obtain a high strength property of coatings (Huseien *et al.*, 2016). Other research found that the soluble silicate and aluminate from pozzolanic material are strongly influencing the degree of polymerization, and the dissolution of RHA is affected by the concentration of an alkaline solution. A high concentration of NaOH resulted in a greater dissolution of the initial solid materials (RHA). The geopolymer strength increased by an improvement in the geopolymerization reaction (Kupaei, Alengaram, & Jumaat, 2014). It further suggested that, with high alkaline hydroxide concentration in AA solutions, a high compressive sample strength could be achieved (Yang et al., 2012).

Based on Figure 4.4, the moisture absorption of coating is less than 12 percent when the concentration of NaOH is between 6 and 10 mol, whereas the RHA/AA ratio is high as 0.8 because of the geopolymerization. According to Ibrahim *et al.*, the results revealed that the absorption of moisture decreased with an increase in the NaOH concentration from 6 to 12 mol. However, when 14 mol of NaOH concentration was used, an increase in the absorption of moisture occurred. It is due to the lower density of the geopolymer with the excess concentration used (Ibrahim, Hussin, Abdullah, Kadir, & Deraman, 2017). It may satisfy the result shown in Figure 4.4, that the absorption of moisture increases with an increase in the concentration of NaOH. There are many factors to consider, except for the concentration of NaOH used.

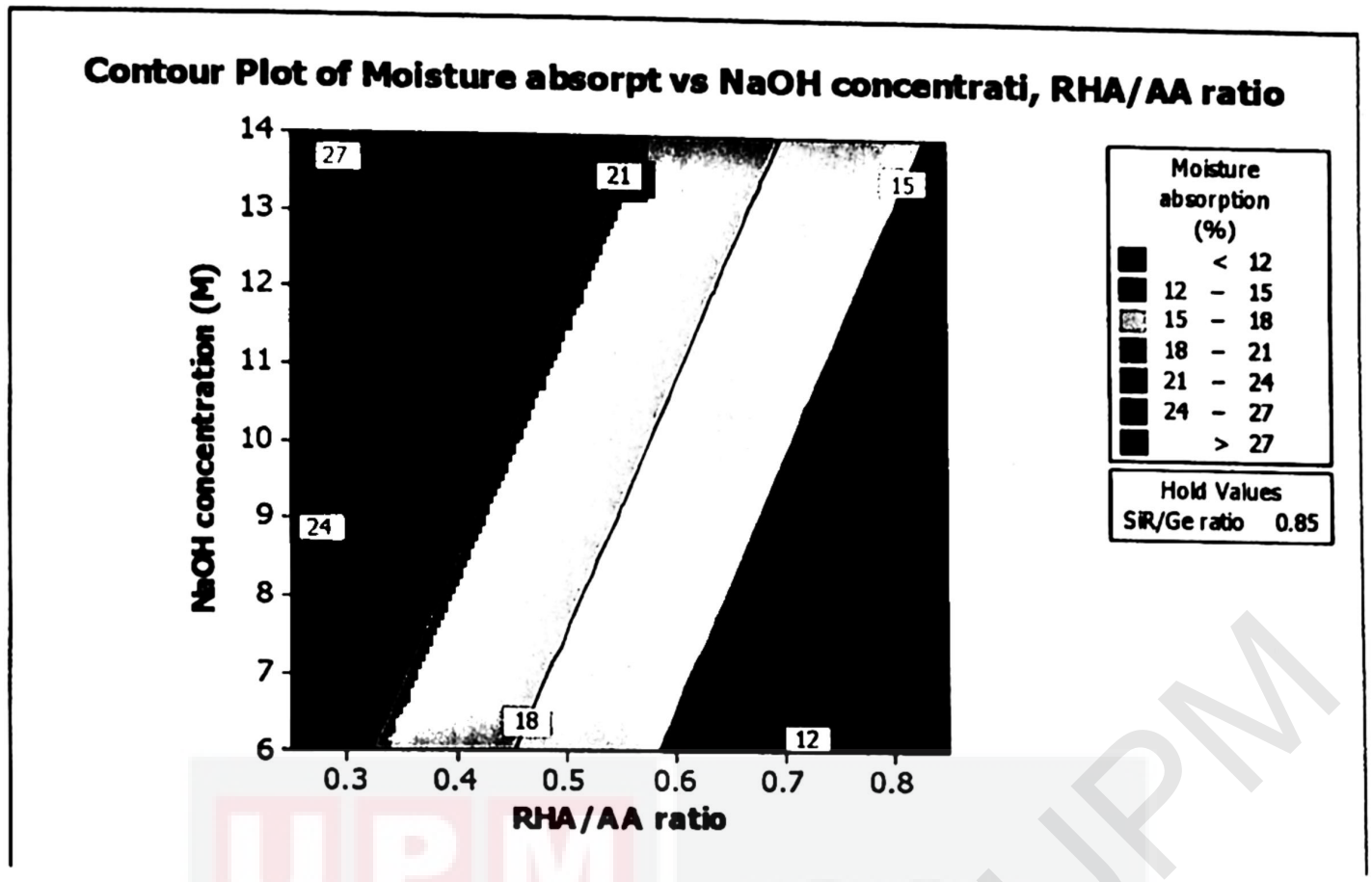

Figure 4. 4: Contour plot for the effect of RHA/AA ratio and NaOH concentration on the moisture absorption test.

The contour plot in Figure 4.4 showed an increase in moisture absorption when the RHA/AA ratio decreased. Low RHA/AA ratio indicates high sodium silicate used in the sample, which caused severe disruption of the crosslink reaction in geopolymer, water evaporation and the geopolymer structure. In addition, the presence of a high amount of sodium silicate tends to produce large pore size geopolymers. Thus, it causes more water absorbed to fill the pore between the particles. (Nurul Reffa et al., 2018).

As a result, the higher NaOH concentration can significantly enhance the fire resistance, whereas the moisture absorption is most influenced by RHA/AA ratio probably.

4.1.6 Optimization of the response

Figure 4.5 shows the optimization plot and the effect of the different combinations of factors on the response. Based on the optimization results, 14 mol sodium hydroxide was chosen as a fixed value in the surface response methodology.

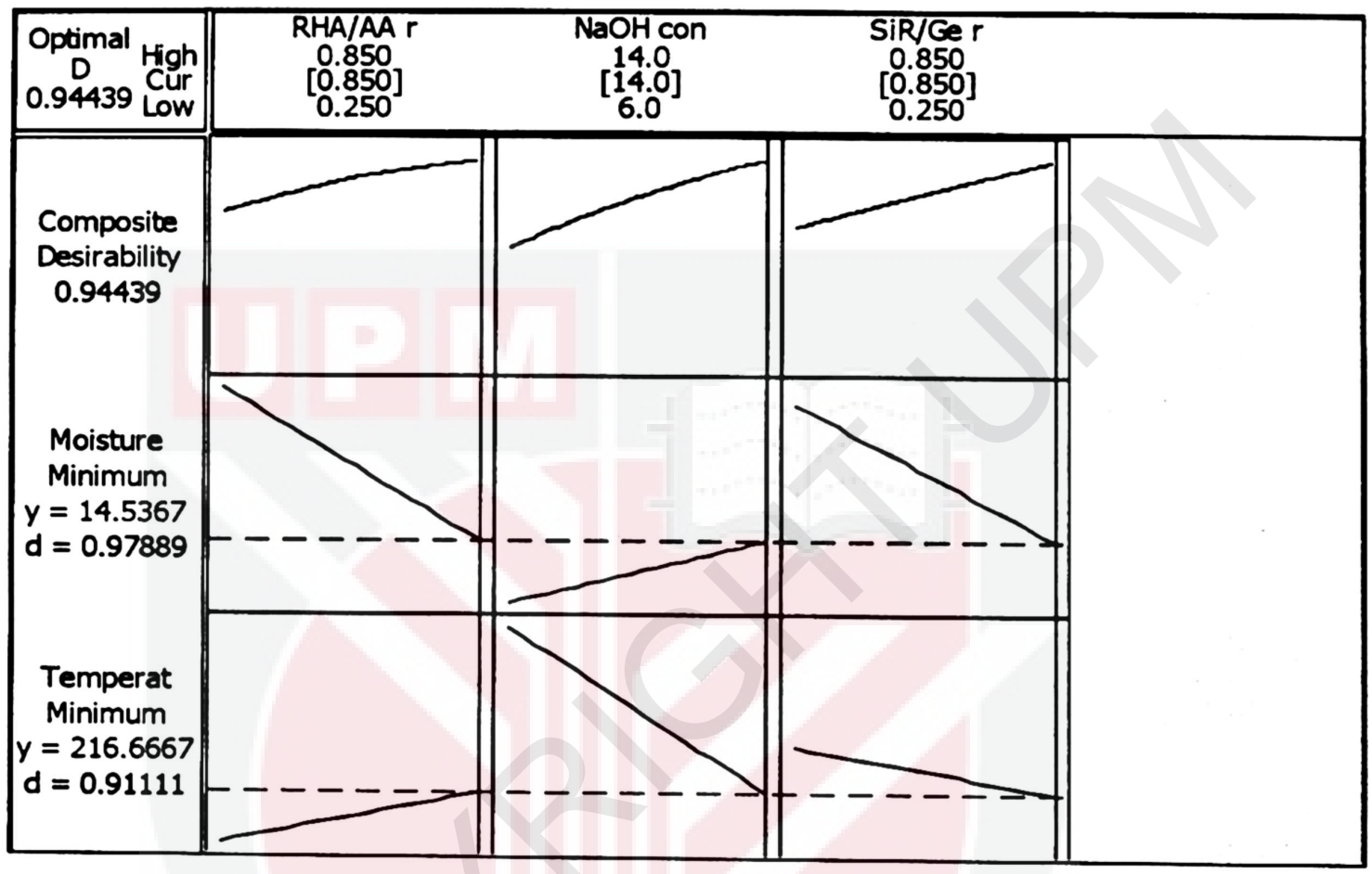

Figure 4. 5: Optimization plot for the formulation of SiR-RHA-based geopolymer composite coating.

The target values, which are to be reached by optimizing the moisture absorption formulation of the coating, are approximately 14.54 percent and 216.67°C for the temperature of the coated steel plate. The optimum formulation of SiR-RHA-based geopolymer composite coating can be achieved with the combination of RHA/AA ratio = 0.85, NaOH concentration = 14M, and SiR/Ge ratio = 0.85. The optimization desirability was calculated as 0.94439, indicating that all parameters were within the target to obtain the desired coating properties.

4.2 Response surface methodology (RSM)

The objective of this study is to determine the significance of each factor and their interaction, in particular: to elucidate the relationship between the factors and response under the condition of fire, and with 99 percent humidity; to provide an optimum value of temperature at equilibrium (TAE) and also moisture absorption of SiR-RHA-based geopolymer composite coating through optimal factor interaction and to elucidate the material behaviour of SiR-RHA-based geopolymer composite coating. Only the design matrix and response values for the fire resistance test samples S17, S18 and S21, were shown in Table 4.3 as the three samples were further discussed in the material characterization and microstructure analysis section. Whereas, the three samples of moisture absorption test showed in Table 4.4 would be discussed further in material characterization, and microstructure analysis section was S1, S14 and S21. Complete design matrix and response values are given in Appendix B2, and data were analyzed using MINITAB software.

Table 4. 3: Design matrix and response values for sample S17, S18 and S21 of fire resistance test.

Run	Sample	Coded factor		Uncoded factor		Response
		RHA/AA ratio (V_1)	SiR/Ge ratio (V_3)	RHA/AA ratio (V_1)	SiR/Ge ratio (V_3)	Temperature at Equilibrium (TAE)
17	S17	0	2	0.65	0.85	208
18	S18	1	1	0.75	0.70	243
21	S21	-1	-1	0.55	0.40	285

Table 4. 4: Design matrix and response values for sample S1, S14 and S21 of moisture absorption test.

Run	Sample	Coded factor		Uncoded factor		Response
		RHA/AA ratio (V_1)	SiR/Ge ratio (V_3)	RHA/AA ratio (V_1)	SiR/Ge ratio (V_3)	Moisture absorption
1	S1	2	0	0.85	0.55	16.8
14	S14	0	0	0.65	0.55	19.2
21	S21	-1	-1	0.55	0.40	25.2

4.2.1 Statistical analysis of fire retardant and moisture absorption properties

A linear regression model was fitted to the experimental data using the least square technique. There several main parameters that were considered in evaluating the statistical results, namely the coefficients of regression, the standardized error of coefficient, and the P of the effects of factors and its interaction for both responses, which are TAE and moisture absorption test. Complete statistical results for this study are shown in Appendix C2. Results in Table 4.5 indicated that most of the factors and interaction effects were highly significant ($P < 0.000$) except for V_1 with $P < 0.001$. However, for V_1*V_3, which showed insignificant values ($P > 0.050$) and had no effect on the responses. Values for $R^2 = 0.8467$ and R^2 (adjusted) = 0.8041 were considered to be high, indicating that 84.67 percent of the sample variation in the response was attributed to the factors.

Table 4. 5: Estimated effects and coefficient for TAE in fire retardant test.

Term	Notation	Coefficient	Std. error of coefficient	P
Constant		273.146	3.460	0.000
RHA/AA ratio	V_1	-8.958	2.188	0.001
SiR/Ge ratio	V_3	-10.792	2.188	0.000
RHA/AA ratio* RHA/AA ratio	V_1*V_1	-10.500	1.641	0.000
SiR/Ge ratio* SiR/Ge ratio	V_3*V_3	-9.313	1.641	0.000
RHA/AA ratio* SiR/Ge ratio	V_1*V_3	6.875	3.790	0.086
R^2 = 84.67 percent	R^2(adj) = 80.41 percent			

For the moisture absorption test, the P of the factors and their interactions were also considered significant when it was below the confidence level, which set to be 95 percent (P of 0.050). But, for interactions among them was considered insignificant where P > 0.050. The results shown in Table 4.6 indicated that all factors and interaction effects were significant, whereas V_1*V_3 was insignificant due to P is much greater than 0.050. The P of individual factors were highly significant (P < 0.000) except for V_1*V_1 with P < 0.008 and for V_3*V_3 with P < 0.001. Value for R^2 = 0.9459 and R^2 (adjusted) = 0.9309 were considered very high, which indicated that 98.45 percent of the sample variation in the response was attributed to the independent variables.

Table 4. 6: Estimated effects and coefficient for moisture absorption test.

Term	Notation	Coefficient	Std. error of coefficient	P
Constant		19.0313	0.2577	0.000
RHA/AA ratio	V_1	-1.9250	0.1630	0.000
SiR/Ge ratio	V_3	-2.0333	0.1630	0.000
RHA/AA ratio* RHA/AA ratio	V_1*V_1	0.3656	0.1222	0.008
SiR/Ge ratio* SiR/Ge ratio	V_3*V_3	0.4656	0.1222	0.001
RHA/AA ratio* SiR/Ge ratio	V_1*V_3	0.3750	0.2823	0.201

$R^2 = 94.59$ percent $R^2(adj) = 93.09$ percent

Equation 4.3 and 4.4 represent the regression models for the fire retardant test and moisture absorption test, respectively.

$$Y_{FT} = 273.146 - 8.958\,(V_1) - 10.792\,(V_3) - 10.500\,(V_1^2) - 9.313\,(V_3^2) + 6.875\,(V_1*V_3) \quad \text{(Eq. 4.3)}$$

$$Y_{MA} = 19.0313 - 1.9250\,(V_1) - 2.0333\,(V_3) + 0.3656\,(V_1^2) + 0.4656\,(V_3^2) + 0.3750\,(V_1*V_3) \quad \text{(Eq. 4.4)}$$

where Y_{FT} and Y_{MA} represent the responses which are TAE in fire retardant test and moisture absorption, respectively. The V_1 and V_3 are the decoded values of the RHA/AA ratio and SiR/Ge ratio, respectively. The regression models can be used to calculate and analyze the effect of factors on fire resistance performance of SiR-RHA-based geopolymer composite coating.

4.2.2 Effect of factors on fire resistance and moisture absorption properties

ANOVA and the regression models were used to analyze the effect of various factors on the fire resistance and moisture absorption properties. Contour plots were used for better illustration. Figure 4.6 and Figure 4.7 illustrate the effect of the RHA/AA ratio (V_1) and SiR/Ge ratio (V_3) on the responses. Both figures show that higher V_1 and V_3 resulted in lower TAE below 200 ° C and lower moisture absorption below 16 percent.

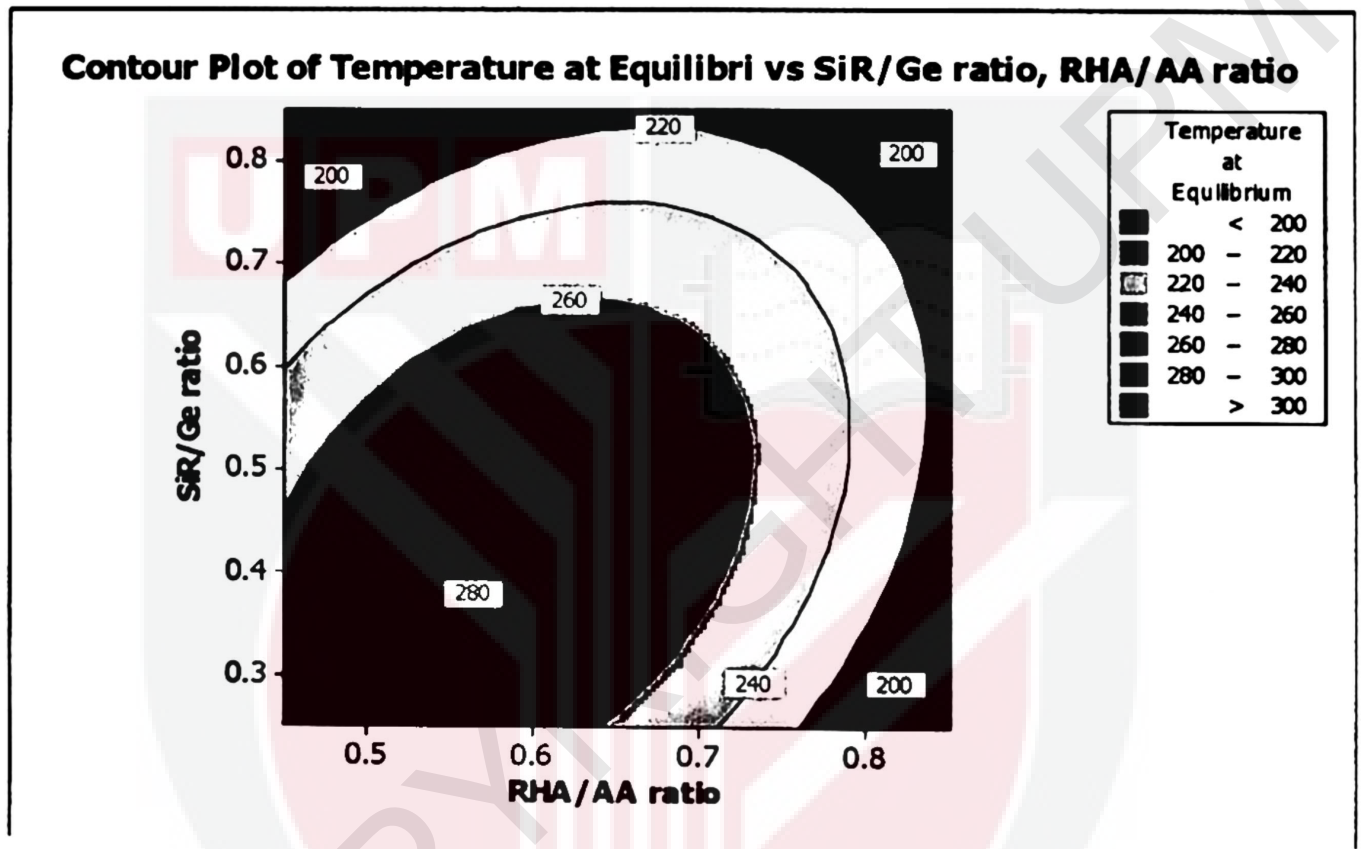

Figure 4. 6: Contour plot for the effect of RHA/AA ratio and SiR/Ge ratio on the TAE in fire retardant test.

Nasruddin et al. (2018) indicated that the bonding structure of the geopolymer becomes more compact and less porous as the high RHA/AA ratio is used, whereby the more RHA content and AA solution is constant. High ratio of SiO_2/Al_2O_3 was found to produce better thermal stability of the RHA geopolymer coating as well (Yong, Ming, Al Bakri Abdullah, & Hussin, 2015). It is due to high amorphous silica and low aluminium oxide content in RHA after a calcination process.

Besides, RHA is a porous material and has a high surface area, which causes significant absorption of moisture even though it has good fire retardant and mechanical properties. Increased sodium silicate content in the RHA / AA ratio increases the absorption of water due to an increase in the pore size of the geopolymer. Figure 4.7 shows the moisture absorption is decreased with an increase in the RHA/AA ratio.

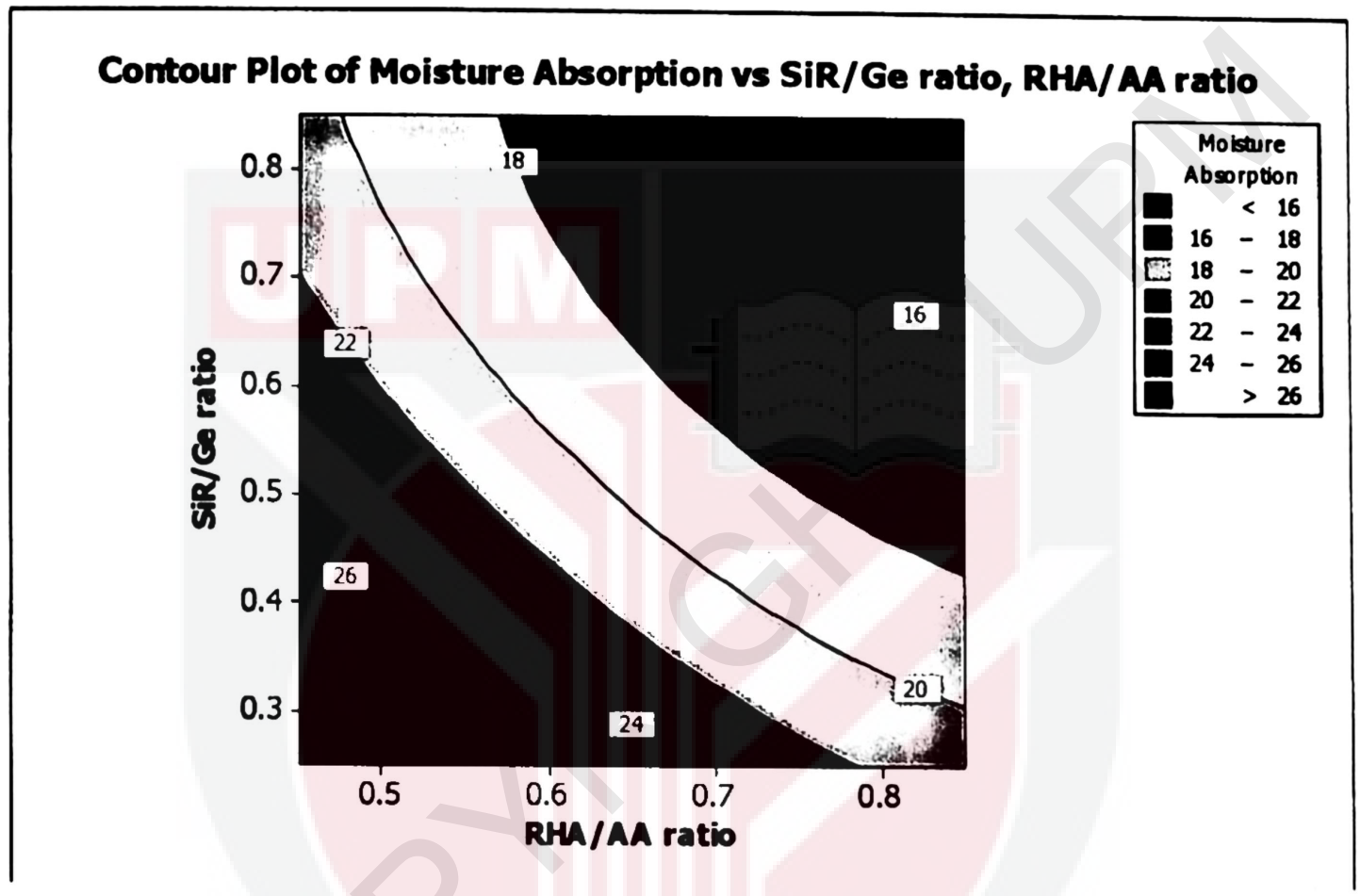

Figure 4. 7: Contour plot for the effect of RHA/AA ratio and SiR/Ge on the moisture absorption test.

Figure 4.6 and Figure 4.7 show that the use of high volume silicone rubber can significantly improve the fire retardant and moisture-resistant properties of geopolymer coatings, which then achieved a lower value of temperature at equilibrium and moisture absorption. It is because silicone rubber mostly contains methyl functionality with a few mol percent of vinyl, which can improve high temperature stability and low temperature flexibility (Timpe & Jr., 2007). According to Khan et al. (2017), the incorporation of silicone rubber and nano-SiO_2 particles may increase the temperature of degradation,

resulting in thermal stability. The interactions between nanoparticles and silicone rubber and the increase in physical and chemical crosslinking points are likely to contribute to the improvement of thermal stability (Kong, Mariatti, & Busfield, 2011). The stability in terms of water absorption is attributed to good binding interaction between silicone rubber and mineral fillers such as SiO_2 and $CaSiO_3$ for SiR based composites (Kamarudin *et al.*, 2020). In addition, silicone rubber can improve the resistance to moisture due to its good hydrophobicity, unlike silica, which is hydrophilic.

4.2.3 Optimization of the response

Figure 4.8 shows the optimization plot and the effect of the different combinations of factor settings on the response. The optimization was performed under designated parameters. Since the objective was to minimize the temperature at equilibrium (TAE), the upper values, which is the maximum acceptable value, was set at 298°C. The target values, which is the goal to be achieved (the lowest temperature at equilibrium), was set at 206°C. Based on Appendix B2, the maximum value was set as the highest value of TAE, and the target value was close to the lowest value of TAE.

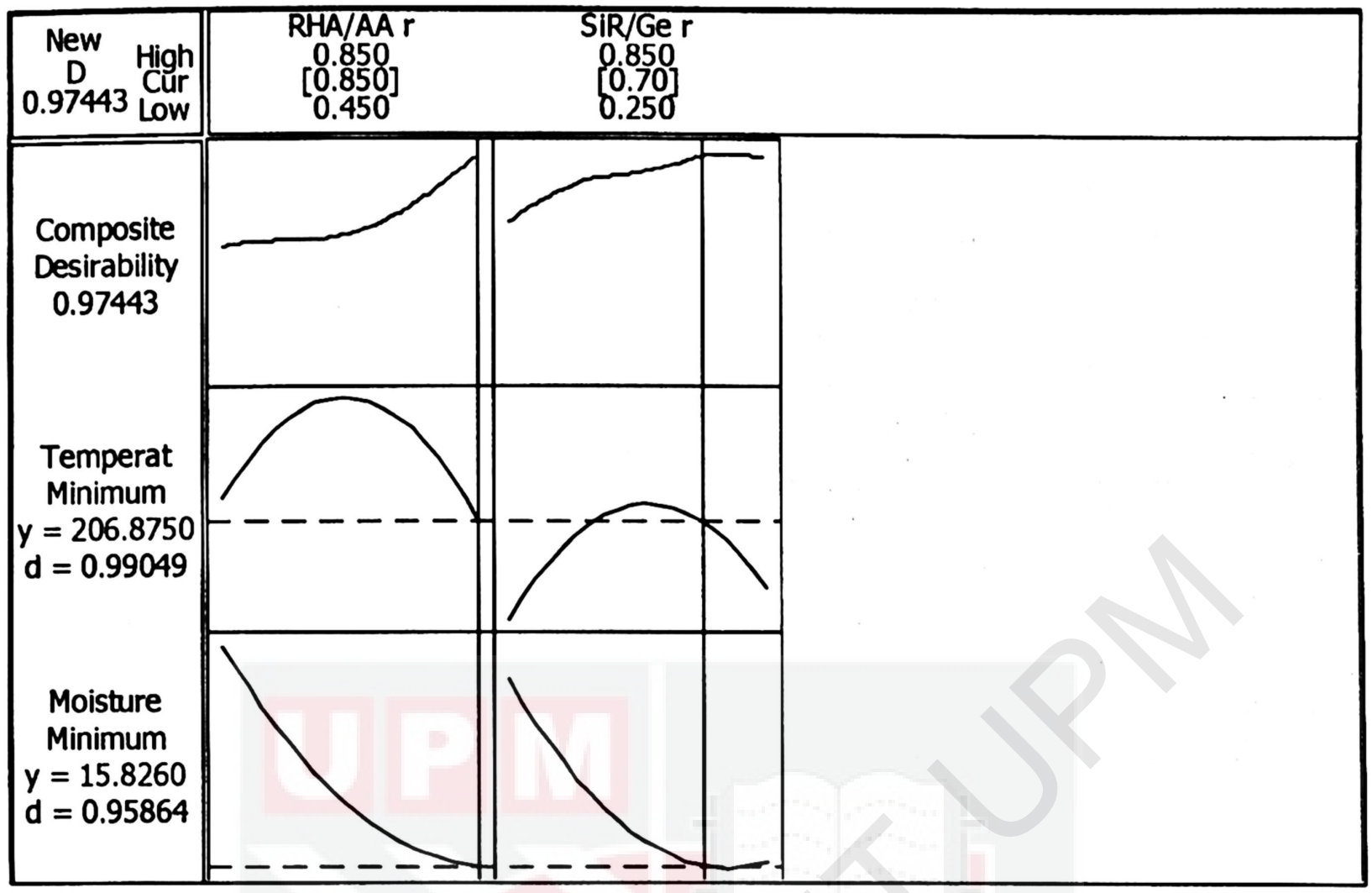

Figure 4. 8: Optimization plot in fire retardant and moisture absorption test.

For moisture absorption properties, higher values, which are the minimum acceptable, were set at 25.7 percent as the objective was to minimize the moisture absorption of SiR-RHA-based geopolymer composite coating. The target value for moisture absorption properties was set at 15.4 percent. The optimum TAE and moisture absorption values of 206.9°C and 15.8 percent, respectively, can be achieved with the combination of RHA/AA ratio (V_1) = 0.85 and SiR/Ge ratio (V_3) = 0.70. The desirability of optimization was calculated as 0.97443, indicating that all parameters were within the target, which was to obtain the maximum fire resistance properties while minimum moisture absorption properties.

4.2.4 Experimental validation

From Table 4.7, it was found that the average error for the TAE and moisture absorption were well below 15 percent at 12.13 percent and 1.31 percent, respectively. It was concluded that the developed regression model established using this method was able to optimize value for the responses accurately.

Table 4. 7: Experimental validation for the fire retardant and moisture absorption properties

Sample no.	TAE (°C)			Moisture absorption (percent)		
	Experimental value	Predicted value	Error (percent)	Experimental value	Predicted value	Error (percent)
SV1	248	206.9	19.86	15.73	15.8	0.44
SV2	211	206.9	1.98	15.43	15.8	2.34
SV3	237	206.9	14.55	15.62	15.8	1.14
	$\bar{x}$ Error		**12.13**	$\bar{x}$ Error		**1.31**

Based on Table 4.7, several factors affect the accuracy of the validation results in fire retardant properties. First is the coating thickness, where a small difference in coating thickness resulted in a high difference in the outcome. It is because the fire resistance properties of the material are very sensitive to the coating thickness. Therefore the variation in temperature was recorded. Second is the surrounding temperature and humidity, which might influence the temperature recorded during the experiment. For example, cold weather or high humidity cause decreases in temperature. The third is the input flame temperature where it may provide a small difference in the temperature

measured because the input flame temperature from blow torch is difficult to control. However, it does not significantly affect the outcome.

As compared to the control sample without the addition of silicone rubber, the control sample recorded higher temperature at equilibrium and higher moisture absorption at 350°C and 22.0%, respectively. These results are in agreement with other studies which obtained higher temperature at equilibrium was more than 350°C (Mohd Basri, 2016) and higher moisture absorption was about 30% (Parida, Bastia, & Kar, 2017) for a similar sample without the addition of silicone rubber. Figure 4.9 shows the surface structure of control and optimized samples after the fire retardant test.

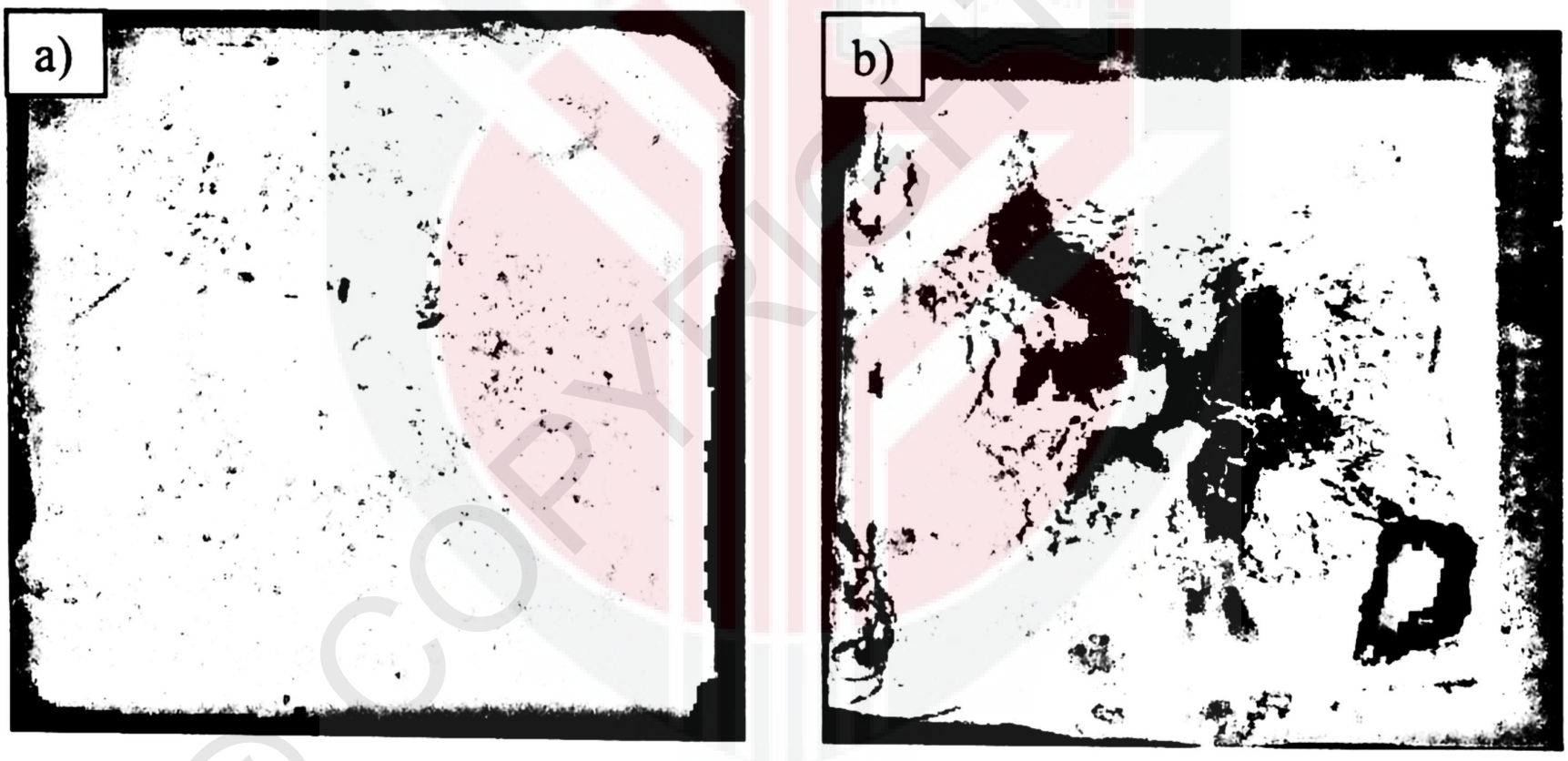

Figure 4. 9: (a) control sample and (b) optimized sample after fire retardant test

4.3 Microstructure analysis

Nine samples were selected to determine the microstructural properties of the SiR-RHA-based geopolymer composite coating. Three samples were selected for the pre- and post-fire retardant tests and three samples for the moisture absorption test. They were differentiated based on their fire retardant or moisture absorption performance, either good, moderate, or poor. Good, moderate, and poor samples were based on the value of the responses (temperature at equilibrium and moisture absorption) and were compared within the population from the experimental design for FrFD and RSM. Comparing with previous literature is not valid since the nature and method of the experiment were different. In addition, there is extremely limited literature on RHA-SiR geopolymer composite. The samples were analyzed using a scanning electron microscope (SEM). Table 4.8 shows the sample number and their performance.

Table 4. 8. Sample number and performance.

Performance	Pre-fire retardant test	Post-fire retardant test	Moisture absorption test
Good	S17 (0.65*,0.85**)	S17 (0.65*,0.85**)	S1 (0.85*,0.55**)
Moderate	S18 (0.75*,0.70**)	S18 (0.75*,0.70**)	S14 (0.65*,0.55**)
Poor	S21 (0.55*,0.40**)	S21 (0.55*,0.40**)	S21 (0.55*, 0.40**)

*RHA/AA ratio, **SiR/Ge ratio

Figure 4.10 illustrates the SEM micrographs of SiR-RHA-based geopolymer composite coating before fire retardant test at 1000x and 5000x magnifications. As shown in Figure 4.10(a) at 1000x magnification, sample S17, which possesses good fire retardant

properties, shows a relative corrugated wrinkled surface developed on the surface of the coating. It may due probably to the improper pressing process during fabrication and curing. At higher magnification, sample S17 which contained the highest amount of silicone rubber (SiR/Ge ratio of 0.85) showed a very smooth surface. The surface is an excess silicone rubber (SiR) which is not able to be mixed with the geopolymer matrix. It is evident from the SEM micrograph of the sample after fire retardant test. Thus, the SiR formed a thin layer and covered the layer of the composite coating matrix underneath.

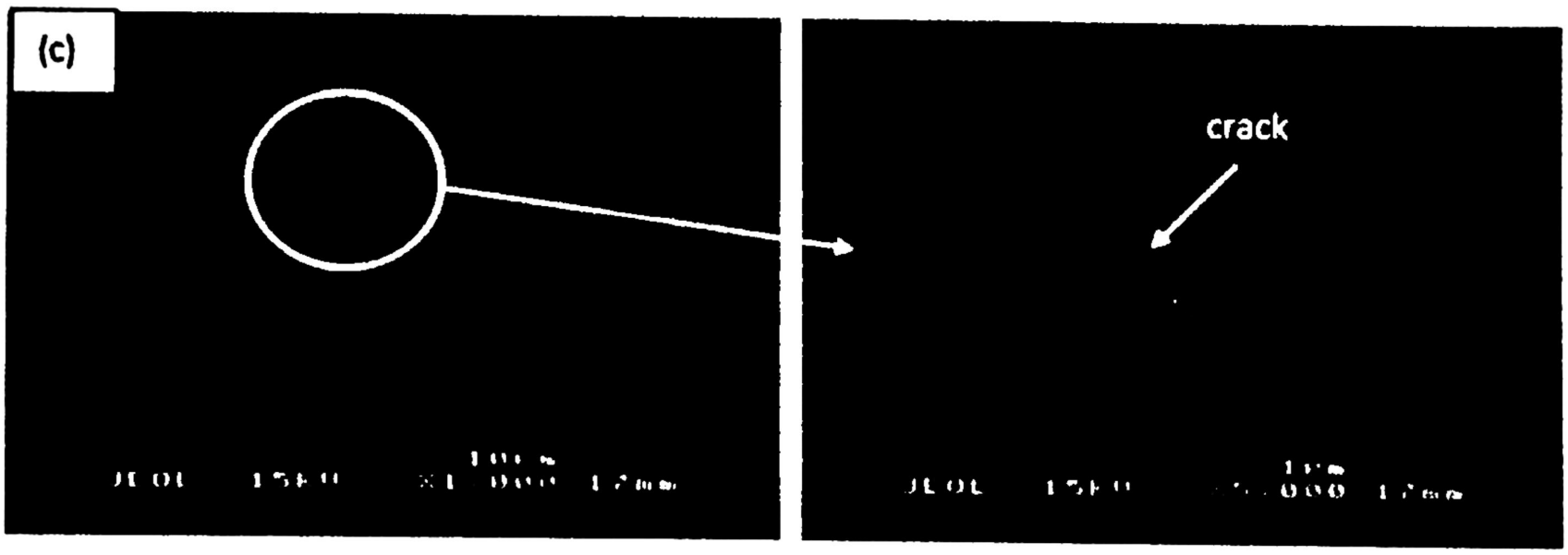

Figure 4. 10: SEM micrographs of SiR-RHA-based geopolymer composite coating before fire retardant test with (a) good (sample S17), (b) moderate (sample S18), and (c) poor fire retardant properties (sample S21) at 1000x and 5000x magnification

In comparison to sample S17, sample S18 in Figure 4.10(b) showed the rice husk ash (RHA) particles on the surface of the sample. Since S18 contained the highest amount of RHA (RHA/AA ratio of 0.75) and relatively high amount of silicone rubber at SiR/Ge ratio of 0.70, a small amount of unreacted RHA is mixed with the silicone rubber within the geopolymer composite matrix itself, resulted in excess RHA particles immerged on the coating surface.

Figure 4.10(c) shows sample S21 which contained the lowest content of RHA (RHA/AA ratio of 0.55) and silicone rubber (SiR/Ge ratio of 0.40) as compared to that of sample S17 and S18. The silicone rubber is well incorporated into the geopolymer composite matrix. However, due to the dominant geopolymer composite matrix and high water content (as compared to sample S17 and S18), cracks and corrugated wrinkled were developed during curing and hot pressing process. The effect of water content on crack formation was proved by Wei et al. (2020), which concluded that higher amount of water

in the geopolymer matrix resulted in sudden shrinkage during curing process thus formed cracks. The formation of cracks was consequently provided opening which allows heat to travel faster into the layers of coating and lower the fire retardant properties of the sample.

Figure 4.11 shows the SEM micrographs of SiR-RHA-based geopolymer composite coating of the residues obtained from fire retardant tests. As shown in Figure 4.11(a), the char residue of the geopolymer composite coating, which is a layer of excess silicone rubber, is porous and continuous. Although there are small holes located in the residue due to the permeating of gases resulting from the decomposition of silicone rubber, the structure is compact which provide shielding effect for the layer of geopolymer composite matrix underneath. The result was in agreement with Zhu et al. (2015). Since the coating has two layers which are the excess silicone rubber as the first layer and geopolymer composite matrix as the second layer, heat transferred through the small holes was shielded by the second layer.

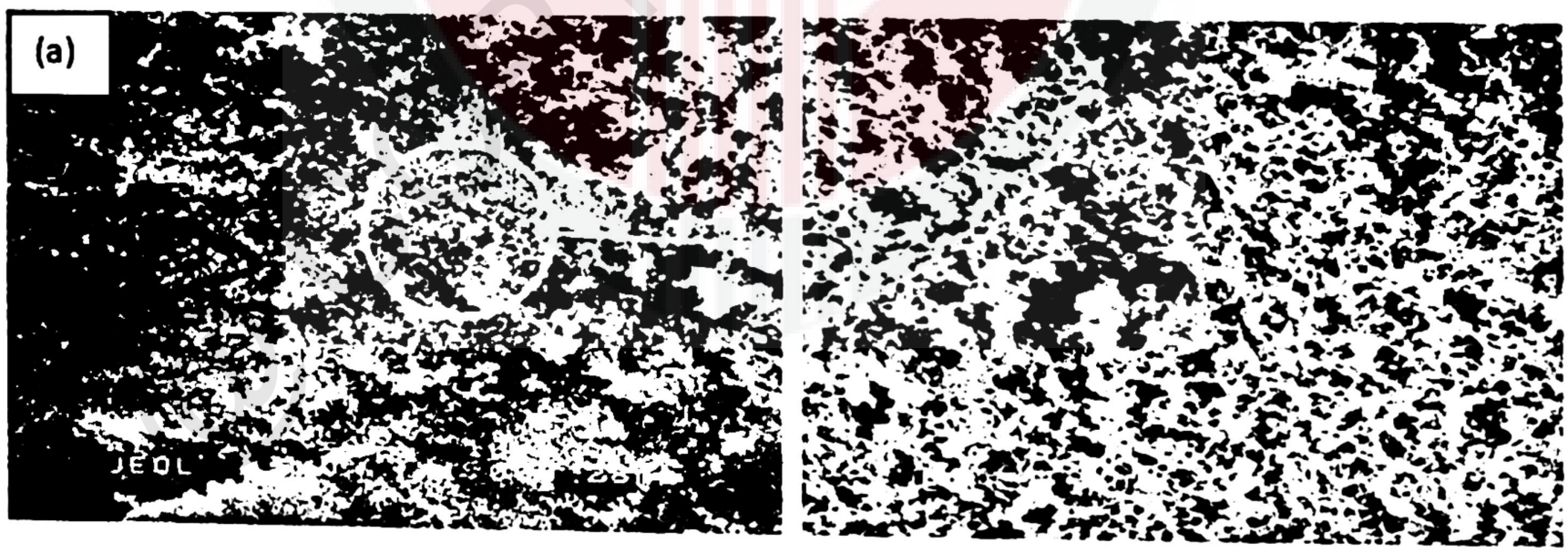

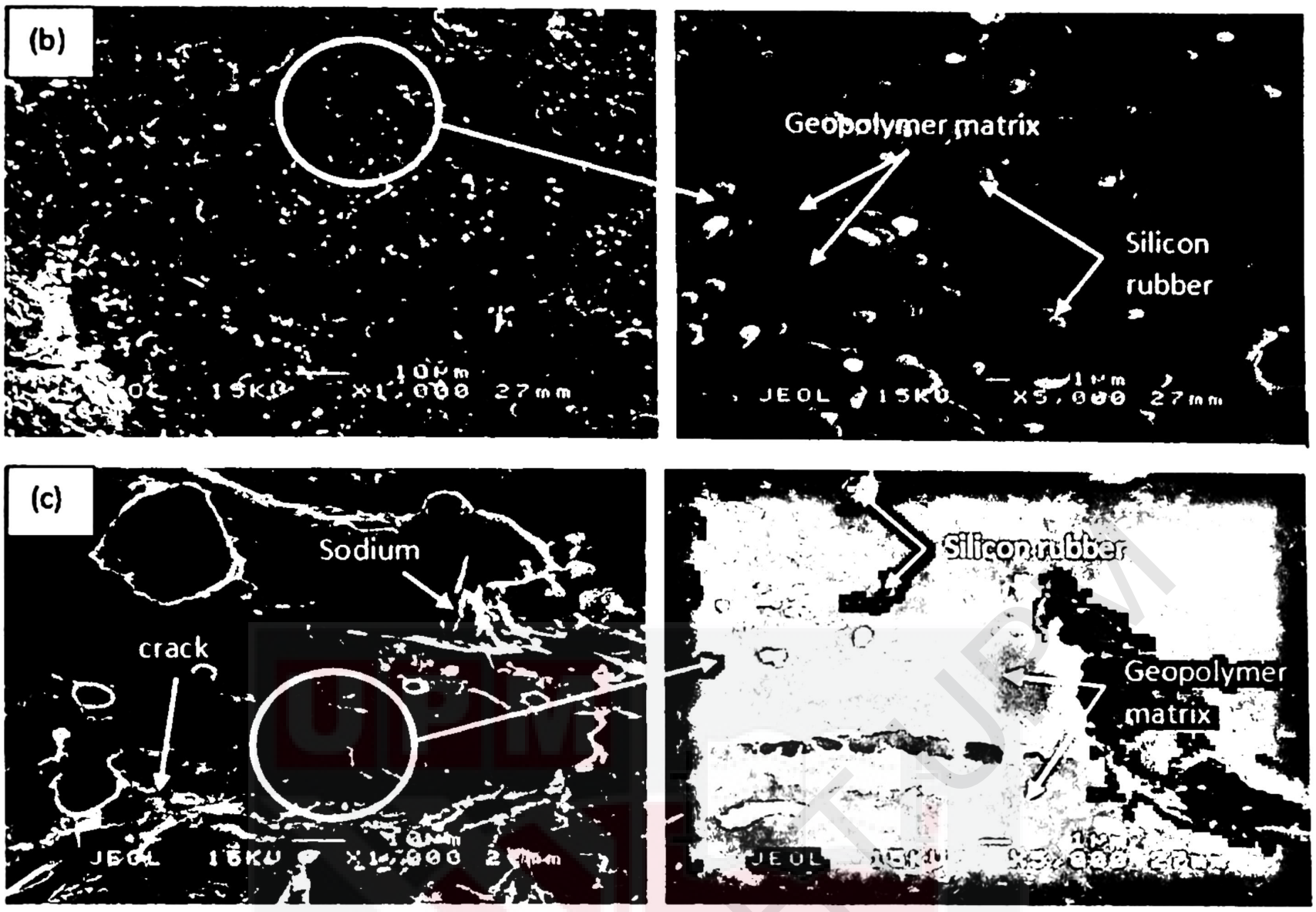

Figure 4. 11: SEM micrographs of SiR-RHA-based geopolymer composite coating of the residues obtained from fire retardant tests with (a) good (sample S17), (b) moderate (sample S18), and (c) poor fire retardant properties (sample S21) at 1000x and 5000x magnification

The residue char showed in Figure 4.11(b) is a mixture of silicone rubber and geopolymer composite matrix with a small amount of unreacted RHA. The geopolymer composite matrix is dense with small and large holes scattered in the residue char. The dense structure may be due to densification of the geopolymer as the binder, and viscous flow fills most of the voids present in the material (Vickers, Riessen, & Rickard, 2015). Simultaneously, silicone rubber solidified exothermally by a heat release during the crosslinking reaction (Ou, Sahli, Barriere, & Gelin, 2016). The silicone rubber also provides good adhesion to the crack faces, provide some crack bridging effect and keep

the cracked pieces together (Lv, Schlangen, & Xing, 2017). The small and large holes allow heat to penetrate through the holes and travelled directly to the substrate. According to Li et al. (2019), the dense structure may contribute by the formation of a ceramic skeleton which subsequently considered the coating had been substantially porcelainized.

Figure 4.11(c) shows the sample S21, which exhibited poor fire retardant properties. It shows the formation of long and wide cracks in the residual char. Large cracks were initiated and expanded out of a small crack. As the coating was heated, the water and air inside the coating swelled and expanded the cracks. Excess sodium from sodium hydroxide appeared as a long needle in some part of the coating's surface. Due to the insufficient amount of silicone rubber in the polymer matrix, it does not significantly help in providing additional protection for the substrate.

Figure 4.12 shows the SEM micrographs of the geopolymer composite coating based on SiR-RHA prior to the moisture absorption test. Figure 4.12(a) reveals that the silicone rubber formed as the outer layer of the sample S1 without any cracks formation. A highly viscous geopolymer composite matrix formed this layer with an RHA/AA ratio of 0.85. Since the content of RHA is higher than that of the sample S14 and S21, only a small amount of silicone rubber can be blended with the geopolymer composite matrix, and the unreacted SiR formed a thin layer beneath the geopolymer composite matrix. Since silicone rubber is hydrophobic, it retains only 1 percent of moisture even after prolonged exposure to water and acts as a barrier against moisture (Shit & Shah, 2013).

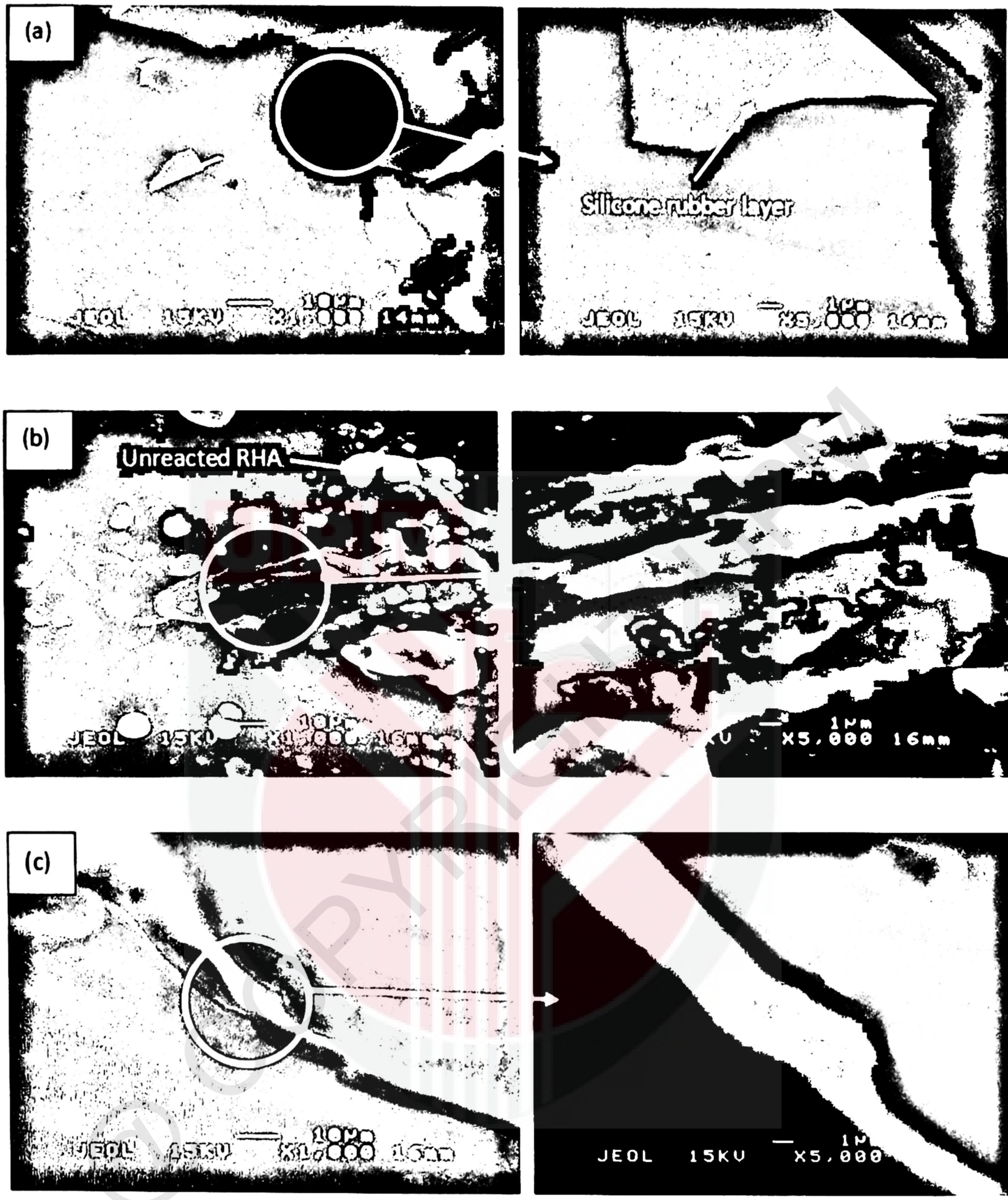

Figure 4. 12: SEM micrographs of SiR-RHA-based geopolymer composite coating prior to the moisture absorption test with (a) good (sample S1), (b) moderate (sample S14), and (c) poor moisture absorption properties (sample S21) at 1000x and 5000x magnification

The unreacted and agglomerated rice husk ash (RHA) can be seen on the surface of the coating, as shown in Figure 4.12(b). The silicone rubber is completely incorporated into the geopolymer composite matrix, some of which covered the RHA. Unreacted RHA is directly in contact with moisture and thus increases the rate and percentage of moisture absorption. The agglomerated RHA developed microvoids and gaps between the RHA particles and the geopolymer composite matrix, which resulted in the high percentage of moisture absorption.

Figure 4.12(c) shows the S21 sample, which had poor moisture absorption properties due to crack development on the surface of the coating. As reported by Wang et al. (2018), cracks and holes formed due to non-uniform mixing during hot pressing and consequently increased water absorption rate. When the gap is filled with water, the water flows into the adjacent matrix by capillary action and forms fractured process zones. In this damage zones, the water was absorbed quicker than in the undamaged material around the crack surface (Zhang et al., 2014).

CHAPTER 5

CONCLUSIONS AND RECOMMENDATION

5.1 Conclusion

The significant effect of different factors on the moisture and fire retardant properties of SiR-RHA-Ge coating composite and the optimum composition were identified using MINITAB software for screening process using fractional factorial design (FrFD) and optimization process using response surface method (RSM). The result from FrFD showed the most significant factor on fire retardant property was NaOH concentration. However, the most significant factor on moisture absorption property was RHA/AA ratio. For the optimization process, a pair of RHA/AA and SiR/Ge ratio was chosen instead of a pair of RHA/AA ratio and NaOH concentration, due the SiR/Ge ratio was more focused as compared to NaOH concentration in this study.

The best moisture resistance and fire retardant properties could be obtained when the values of RHA/AA ratio is 0.85, and SiR/Ge ratio is 0.70 at 14 M of NaOH concentration. The average validation result for both TAE and moisture absorption were about 232°C and 15.6%, respectively. While the average error form the validation test for the TAE and moisture absorption was well below 15 percent at 12.13 percent and 1.31 percent, respectively. Several factors that would affect the accuracy of the validation results on fire retardant properties are coating thickness, surrounding temperature and humidity, and input flame temperature.

The control sample recorded high temperature at equilibrium and moisture absorption at 350°C and 22.0%, respectively. As compared to the control sample without the addition of silicone rubber, the SiR-RHA-based geopolymer composite coating is well performed in the fire retardant test and moisture absorption test, where the temperature at equilibrium and moisture absorption obtained were below 350°C and 30%, respectively.

The SEM micrographs of SiR-RHA-based geopolymer composite coating with fire retardant properties showed a very smooth surface because of excess silicone rubber had formed a thin layer to cover the layer of the composite coating matrix underneath. The excess silicone rubber was then formed a compact structure which provided shielding effect for the layer of geopolymer composite matrix underneath when fire attacked. For the structure of geopolymer coating with good moisture resistance properties, the unreacted SiR would form a thin layer beneath the geopolymer composite matrix and act as a moisture barrier since only a small amount of SiR is blended with the geopolymer composite matrix.

5.2 Recommendation for future research

Several potential improvements were identified in this research that may improve on SiR-RHA-based geopolymer composite coating development. The followings are recommended for future investigate:

1) Perform thermogravimetric analysis (TGA) and differential scanning calorimetric (DSC) to study the thermal stability of the coating.
2) To use other substrates besides mild steel such as wood, tiles, glass to widen the potential application of geopolymer coating.
3) To reduce the viscosity of the coating so that it can be used as a spray coating method.
4) Conduct the flexural, compressive, adhesion test to investigate the strength of SiR-RHA-based geopolymer composite coating.
5) Reduce the particle size of rice husk ash in which smaller than this study to enhance the moisture and fire retardant properties.
6) Conduct the Energy dispersive X-ray (EDX) to identify the element composition of SiR-RHA-based geopolymer composite coating.

REFERENCES

A.N, S. N., & Ravi.S, R. (2017). Indian Rice Husk Ash – Improving the Mechanical Properties of Concrete: A Review. *International Journal of Engineering Research and Applications*. https://doi.org/10.9790/9622-0701017679

Amin, M., Akbar, M., & Amin, S. (2007). Hydrophobicity of silicone rubber used for outdoor insulation (An overview). *Reviews on Advanced Materials Science.*

Antoy, J. (2014). *Design of Experiments for Engineers and Scientists: Second Edition. Design of Experiments for Engineers and Scientists: Second Edition.* https://doi.org/10.1016/C2012-0-03558-2

ASTM standard. (2010). - ASTM D 5229– 92 – Standard Test Method for Moisture Absorption Properties and Equilibrium Conditioning of Polymer Matrix Composite Materials. *Annual Book of ASTM Standards*. https://doi.org/10.1520/D5229

Azrem Azmi, A., Mustafa Al Bakri Abdullah, M., Mohd Ruzaidi Ghazali, C., Ahmad, R., Musa, L., & Sheau Rou, L. (2019). The Effect of Different Crumb Rubber Loading on the Properties of Fly Ash-Based Geopolymer Concrete. *IOP Conference Series: Materials Science and Engineering*. https://doi.org/10.1088/1757-899x/551/1/012079

Ba, D., & Boyaci, I. H. (2007). Modeling and optimization i: Usability of response surface methodology. *Journal of Food Engineering*. https://doi.org/10.1016/j.jfoodeng.2005.11.024

Błaszczyński, T. Z., & Król, M. R. (2017). Alkaline Activator Impact on the Geopolymer Binders. In *IOP Conference Series: Materials Science and Engineering*. https://doi.org/10.1088/1757-899X/245/2/022036

Bleszynski, M., & Kumosa, M. (2018). Aging resistant TiO2/silicone rubber composites. *Composites Science and Technology*, *164*, 74–81. https://doi.org/10.1016/j.compscitech.2018.05.035

Chaipanit, N., Rattanakhongviput, C., & Sundararajan, R. (2001). Accelerated multistress aging of polymeric insulators under San Francisco coastal environment. In *Conference on Electrical Insulation and Dielectric Phenomena (CEIDP), Annual Report*. https://doi.org/10.1109/ceidp.2001.963624

Chuayjuljit, S., Eiumnoh, S., & Potiyaraj, P. (2001). Using Silica from Rice Husk as a Reinforcing Filler in Natural Rubber. *J. Sci. Res. Chula. Univ.*

Das, A. K., & Dewanjee, S. (2018). Optimization of Extraction Using Mathematical Models and Computation. In *Computational Phytochemistry*. https://doi.org/10.1016/b978-0-12-812364-5.00003-1

Duan, P., Yan, C., Luo, W., & Zhou, W. (2016). A novel surface waterproof geopolymer derived from metakaolin by hydrophobic modification. *Materials Letters*. https://doi.org/10.1016/j.matlet.2015.11.006

Eco-Efficient Masonry Bricks and Blocks. (2015). *Eco-Efficient Masonry Bricks and Blocks*. https://doi.org/10.1016/c2014-0-02158-2

Gallagher Fluid Seals, I. (2019). Why Use Food Grade Silicone? *הנוטע עלון*, *66*, 37–39.

Givi, A. N., Abdul Rashid, S., Abdul Aziz, F. N. & Mohd Salleh, M. a. (2010). Contribution of Rice Husk Ash to the Properties of Mortar and Concrete : A Review. *Journal of American Science*.

Givi, A. N., Rashid, S. A., Aziz, F. N. A., & Salleh, M. A. M. (2010). Assessment of the effects of rice husk ash particle size on strength, water permeability and workability of binary blended concrete. *Construction and Building Materials*. https://doi.org/10.1016/j.conbuildmat.2010.04.045

Gong, B., Tu, Y., Zhou, Y., Li, R., Zhang, F., Xu, Z., & Liang, D. (2013). Moisture absorption characteristics of silicone rubber and its effect on dielectric properties. In *Annual Report - Conference on Electrical Insulation and Dielectric Phenomena, CEIDP*. https://doi.org/10.1109/CEIDP.2013.6748283

Gupta, A. I., & Wayal, A. S. (2015). Use of rice husk ash in concrete. *IOSR Journal of Mechanical and Civil Engineering*. https://doi.org/10.9790/1684-12412931

Hallett, J., & Turner, R. (n.d.). Silicone Rubber Solutions for Transport Applications.

Hayashida, K., Tsuge, S., & Ohtani, H. (2003). Flame retardant mechanism of polydimethylsiloxane material containing platinum compound studied by analytical pyrolysis techniques and alkaline hydrolysis gas chromatography. *Polymer*. https://doi.org/10.1016/S0032-3861(03)00622-0

Hoc Thang, N., Kien, P. T., & Abdullah, M. M. A. B. (2017). Lightweight Heat Resistant Geopolymer-based Materials Synthesized from Red Mud and Rice Husk Ash Using Sodium Silicate Solution as Alkaline Activator. In *MATEC Web of Conferences*. https://doi.org/10.1051/matecconf/20179701119

Hu, Y., & Liu, K. (2017). Devices and technology for monitoring transmission lines. In *Inspection and Monitoring Technologies of Transmission Lines with Remote Sensing*. https://doi.org/10.1016/b978-0-12-812644-8.00005-9

Huhtamäki, T., Tian, X., Korhonen, J. T., & Ras, R. H. A. (2018). Surface-wetting characterization using contact-angle measurements. *Nature Protocols*. https://doi.org/10.1038/s41596-018-0003-z

Huseien, G. F., Mirza, J., Ismail, M., Hussin, M. W., Arrifin, M. A. M., & Hussein, A. A. (2016). The Effect of Sodium Hydroxide Molarity and Other Parameters on Water Absorption of Geopolymer Mortars. *Indian Journal of Science and Technology*. https://doi.org/10.17485/ijst/2016/v9i48/109629

Ibrahim, W. M. W., Hussin, K., Abdullah, M. M. A., Kadir, A. A., & Deraman, L. M. (2017). Effects of sodium hydroxide (NaOH) solution concentration on fly ash-based lightweight geopolymer. In *AIP Conference Proceedings*. https://doi.org/10.1063/1.5002205

Imiela, M., Anyszka, R., Bieliński, D. M., Pędzich, Z., Zarzecka-Napierała, M., & Szumera, M. (2016). Effect of carbon fibers on thermal properties and mechanical strength of ceramizable composites based on silicone rubber. *Journal of Thermal Analysis and Calorimetry*. https://doi.org/10.1007/s10973-015-5115-x

Kaloari, R. M., Syamsidar, Sulfiana, Haris, A., & Subaer. (2016). Synthesis of geopolymer paste as coating material based on kaolinite and rice husk ash. In *Materials Science Forum*. https://doi.org/10.4028/www.scientific.net/MSF.841.79

Kamarudin, N., Razak, J. A., Norddin, N., Mohamad, N., Tee, L. K., Chew, T., & Mohd Saad, N. (2020). Hardness and Water Absorption Properties of Silicone Rubber Based Composites for High Voltage Insulator Applications. https://doi.org/10.1007/978-981-13-9539-0_34

Khan, H., Amin, M., Ali, M., Iqbal, M., & Yasin, M. (2017). Effect of micro/nano-SiO2 on mechanical, thermal, and electrical properties of silicone rubber, epoxy, and EPDM composites for outdoor electrical insulations. *Turkish Journal of Electrical Engineering and Computer Sciences*. https://doi.org/10.3906/elk-1603-20

Khan, K. A., Raut, A., Chandrudu, C. R., & Sashidhar, C. (2019). MECHANICAL AND WATER TRANSPORT PERFORMANCE OF SUSTAINABLE GEOPOLYMER COMPOSITE USING BINARY BLENDS OF POZZOLANIC MATERIALS. *Jurnal Teknologi*. https://doi.org/10.11113/jt.v81.13530

Kim, Y. Y., Lee, B. J., Saraswathy, V., & Kwon, S. J. (2014). Strength and durability performance of alkali-activated rice husk ash geopolymer mortar. *Scientific World Journal*. https://doi.org/10.1155/2014/209584

Kong, S. M., Mariatti, M., & Busfield, J. J. C. (2011). Effects of types of fillers and filler loading on the properties of silicone rubber composites. *Journal of Reinforced Plastics and Composites*. https://doi.org/10.1177/0731684411416267

Kopylov, V. M., Kovyazin, V. A., Kostyleva, E. I., Fedorov, A. Y., & Kovyazin, A. V. (2016). The thermal stabilisation and ceramifying of silicone rubbers. *International Polymer Science and Technology*, *43*(4), T33–T40. https://doi.org/10.1177/0307174x1604300408

Kumar, S., Sangwan, P., V, D. R. M., & Bidra, S. (2013). Utilization of Rice Husk and Their Ash : A Review. *Journal of Chemical and Environmental Sciences*.

Kupaei, R. H., Alengaram, U. J., & Jumaat, M. Z. (2014). The effect of different parameters on the development of compressive strength of oil palm shell geopolymer concrete. *Scientific World Journal*. https://doi.org/10.1155/2014/898536

Li, Z., Liang, W., Shan, Y., Wang, X., Yang, K., & Cui, Y. (2019). Study of flame-retarded silicone rubber with ceramifiable property. *Fire and Materials*. https://doi.org/10.1002/fam.2802

Lv, L., Schlangen, E., & Xing, F. (2017). Self-sealing cementitious materials by using water-swelling rubber particles. *Materials*. https://doi.org/10.3390/ma10080979

Matweb. (2015). MatWeb-ASTM A36 Steel, bar. *MatWeb*, 1–2. Retrieved from http://www.matweb.com/search/datasheet.aspx?MatGUID=ff6d4e6d529e4b3d97c77d6538b29693

Maulana, A. I., Wardani, N. K., Syamsidar, D., Ariani, Nurfadilla, & Subaer. (2017). Development of Hybrid Composite Rice Husk Ash (RHA)-Geopolymer for Bricks Bearing Buildings. In *MATEC Web of Conferences*. https://doi.org/10.1051/matecconf/20179701009

Mohammed, B. S., Liew, M. S., S Alaloul, W., Al-Fakih, A., Ibrahim, W., & Adamu, M. (2018). Development of rubberized geopolymer interlocking bricks. *Case Studies in Construction Materials*. https://doi.org/10.1016/j.cscm.2018.03.007

Mohd Basri, M. S. (2016). Development of Rice Husk Ash-based Geopolymer Binder for Fire Resistant Caoting, (June).

Mohd Basri, M. S., Mustapha, F., Mazlan, N., & Ishak, M. R. (2016). Fire retardant performance of rice husk ash-based geopolymer coated mild steel - A factorial design and microstructure analysis. In *Materials Science Forum*. https://doi.org/10.4028/www.scientific.net/MSF.841.48

Moradi, M., Fazlzadehdavil, M., Pirsaheb, M., Mansouri, Y., Khosravi, T., & Sharafi, K. (2016). Response surface methodology (RSM) and its application for optimization of ammonium ions removal from aqueous solutions by pumice as a natural and low cost adsorbent. *Archives of Environmental Protection*. https://doi.org/10.1515/aep-2016-0018

Muthadhi, A., & Kothandaraman, S. (2013). Experimental investigations of performance characteristics of rice husk ash-blended concrete. *Journal of Materials in Civil Engineering*. https://doi.org/10.1061/(ASCE)MT.1943-5533.0000656

Nagrale, S. D., Hajare, H., & Modak, P. R. (2012). Utilization Of Rice Husk Ash. *International Journal of Engineering Research and Applications (IJERA)*.

Nasruddin, N. R. A., Mazlan, N., Mohd Basri, M. S., Mohamed Ariff, A. H., & Mohd Nasir, N. A. (2018). Thermogravimetric analysis on rice husk ashes-based geopolymer paste. In *IOP Conference Series: Materials Science and Engineering*. https://doi.org/10.1088/1757-899X/405/1/012014

Nurul Reffa, A. N., Norkhairunnisa, M., Azmah Hanim, M. A., & Nasir, N. A. M. (2018). Investigation on water absorption capability for different molarity of rice husk ash based pozzolan binder. *Journal of Engineering Science and Technology*.

Ofoegbu, S., Ofoegbu, P., Neife, S., & Okorie, B. (2011). Corrosion Behaviour of Steels in Nigerian Food Processing Environments. *Journal of Applied Sciences and Environmental Management*, *15*(1). https://doi.org/10.4314/jasem.v15i1.65690

Ou, H., Sahli, M., Barriere, T., & Gelin, J. C. (2016). Determination of the activation energy of silicone rubbers using different kinetic analysis methods. In *MATEC Web of Conferences*. https://doi.org/10.1051/matecconf/20168016007

Parida, U., Bastia, T. K., & Kar, B. B. (2017). A Study on the Water Absorption Efficiency of Porous Silica Gel Prepared from Rice Husk Ash. *Asian Journal of Water, Environment and Pollution*, *14*(1), 83–86. https://doi.org/10.3233/AJW-170010

Pathak, D., Satwani, M., Patel, M., & Patel, C. (2009). The development of silicone rubber composite insulators in power system. In *2009 International Conference on Control Automation, Communication and Energy Conservation, INCACEC 2009*.

Pędzich, Z., Bukańska, A., Bieliński, D., Anyszka, R., Dul, J., & Parys, G. (2012). Microstructure evolution of silicone rubber-based composites during ceramization in different conditions. *Composites Theory and Practice*, *R. 12*, *nr*(December 2014), 251–255.

Phonphuak, N., & Chindaprasirt, P. (2014). Types of waste, properties, and durability of pore-forming waste-based fired masonry bricks. In *Eco-efficient Masonry Bricks and Blocks: Design, Properties and Durability*. https://doi.org/10.1016/B978-1-78242-305-8.00006-1

Pike, D. J., Box, G. E. P., & Draper, N. R. (1988). Empirical Model-Building and Response Surfaces. *Journal of the Royal Statistical Society. Series A (Statistics in Society)*. https://doi.org/10.2307/2982196

Quincot, G., Azenha, M., Barros, J., & Faria, R. (2011). Use of salt solutions for assuring constant relative humidity conditions in contained environments. *Foundation for Science and Technology*, 33.

Rajamoorthy, Y., Rahim, K. b A., & Munusamy, S. (2015). Rice Industry in Malaysia: Challenges, Policies and Implications. *Procedia Economics and Finance*. https://doi.org/10.1016/s2212-5671(15)01183-1

Review on Current Geopolymer as a Coating Material. (2013). *Australian Journal of Basic and Applied Sciences*.

Ryan, D., & Chemist, P. (n.d.). Silicone Compounds for High-Voltage Insulators : Compounding Silicone Rubber.

Rybiński, P., Żukowski, W., & Bradło, D. (2016). Effect of cenospheric fillers on the flammability and fire hazard of silicone rubber composites. *Journal of Thermal Analysis and Calorimetry*. https://doi.org/10.1007/s10973-016-5741-y

Rybiński, Syrek, Żukowski, Bradło, Imiela, Anyszka, … Verbouwe. (2019). Impact of Basalt Filler on Thermal and Mechanical Properties, as Well as Fire Hazard, of Silicone Rubber Composites, Including Ceramizable Composites. *Materials*. https://doi.org/10.3390/ma12152432

Shaswat Kumar Das, Jyotirmoy Mishra, S. M. M. (2018). Rice Husk Ash as a Potential Source Material for Geopolymer Concrete: A Review . *International Journal of Applied Engineering Research* , *13*(7), 81–84.

Shin Etsu Company. (2013). Characteristic properties of Silicone Rubber Compounds Meeting the increasingly diverse and sophisticated needs of industry with the unique properties of silicone rubbers. https://doi.org/10.1111/j.1571-9979.2006.00094.x

Shinohara, Y., & Kohyama, N. (2004). Quantitative Analysis of Tridymite and Cristobalite Crystallized in Rice Husk Ash by Heating. *Industrial Health*. https://doi.org/10.2486/indhealth.42.277

Shit, S. C., & Shah, P. (2013). A review on silicone rubber. *National Academy Science Letters*. https://doi.org/10.1007/s40009-013-0150-2

Singh, B. (2018). Rice husk ash. *Waste and Supplementary Cementitious Materials in Concrete*, 417–460. https://doi.org/10.1016/B978-0-08-102156-9.00013-4

Timpe, D. C., & Jr., D. C. T. (2007). Silicone Rubber Flame Resistance. *Rubber and Plastics News*, 1–6.

UL Standard. (2007). Rapid Rise Fire Tests of Protection Materials for Structural Steel, UL 1709. *Underwriters Laboratories Inc.*, (Third Edition).

Vickers, L., Riessen, A. van, & Rickard, W. (2015). *Fire-resistant Geopolymers: Role of Fibres and Fillers to Enhance Thermal Properties*. *SpringerBriefs in Materials*.

Wang, L., Guo, Y., Chen, Y., Chen, T., Zhu, S., Zhang, T., & Liu, S. (2018). Enhanced mechanical and water absorption properties of rice husk-derived nano-SiO2 reinforced PHBV composites. *Polymers*. https://doi.org/10.3390/polym10091022

Wei, X., Ming, F., Li, D., Chen, L., & Liu, Y. (2020). Influence of water content on mechanical strength and microstructure of alkali-activated Fly Ash/GGBFS mortars cured at cold and polar regions. *Materials*, *13*(1), 8–12. https://doi.org/10.3390/ma13010138

Yang, T. R., Chang, T. P., Chen, B. T., Shih, J. Y., & Lin, W. L. (2012). Effect of alkaline solutions on engineering properties of alkali-activated GGBFS paste. *Journal of Marine Science and Technology (Taiwan)*.

Yong, H. C., Ming, L. Y., Al Bakri Abdullah, M. M., & Hussin, K. (2015). Fire resistant properties of geopolymers: A review. In *Key Engineering Materials*. https://doi.org/10.4028/www.scientific.net/KEM.660.39

Zain, H., Abdullah, M. M. A. B., Hussin, K., Ariffin, N., & Bayuaji, R. (2017). Review on Various Types of Geopolymer Materials with the Environmental Impact Assessment. In *MATEC Web of Conferences*. https://doi.org/10.1051/matecconf/20179701021

Zhang, P., Wittmann, F. H., Haist, M., Müller, M. S., Vontobel, P., & Zhao, T. J. (2014). Water penetration into micro-cracks in reinforced concrete. *Restoration of Buildings and Monuments: An International Journal*. https://doi.org/10.12900/RBM14.20.2-0008

Zhu, C., Deng, C., Cao, J. Y., & Wang, Y. Z. (2015). An efficient flame retardant for silicone rubber: Preparation and application. *Polymer Degradation and Stability*. https://doi.org/10.1016/j.polymdegradstab.2015.08.008

APPENDICES

Appendix A1

Calculation of actual weight of AA solution, RHA and SiR used in sample,

Example:

- Molarity of NaOH = 6 M:

  Molecular weight of NaOH = 40 g/mol

  Total weight of NaOH pellet used to produce 6 M of NaOH

  = 6 mol/L × 40 g/mol

  = 240 g in 1 little of distilled water

- Ratio of AA solution is 5.5:

AA solution = NaOH + Na_2SiO_3

$$\frac{NaOH}{Na_2SiO_3} = 5.5$$

If 11 g of NaOH used,

Weight of Na_2SiO_3 used = $\frac{11\ g}{5.5}$

= 2 g

Total weight = 11 g + 2 g

= 13 g

Appendix A1 (cont.)

- Ratio of RHA and AA solution (Ge) is 0.25:

$$\frac{RHA}{AA\ solution} = 0.25$$

Weight of RHA used = 0.25 × 13 g

= 3.25 g

Total weight = 13 g + 3.25 g = 16.25 g

- Ratio of silicone rubber and Ge is 0.85:

$$\frac{SiR}{Ge} = 0.85$$

Weight of silicone rubber used = 0.85 × 16.25 g

= 13.81 g

- Total of SiR-RHA geopolymer coating composite

= 16.25 g + 13.81 g = 30.06 g

*Notes: All the materials used in gram.

*Others were calculated by using Microsoft Excel.

Appendix B1

Moisture Absorption & Fire Retardant Test – FrFD

Run Order	Sample	RHA/A A ratio	NaOH concentration (M)	SiR/Ge ratio	Moisture Absorption (%)	Temperature at Equilibrium (°C)
1	S1	0.25	14	0.25	42.21	191
2	S2	0.25	14	0.25	41.09	220
3	S3	0.25	6	0.85	23.29	300
4	S4	0.85	6	0.25	22.80	418
5	S5	0.85	6	0.25	20.27	448
6	S6	0.85	14	0.85	15.22	200
7	S7	0.85	6	0.25	20.27	482
8	S8	0.85	14	0.85	14.45	218
9	S9	0.85	14	0.85	13.94	233
10	S10	0.25	6	0.85	22.60	360
11	S11	0.25	14	0.25	37.77	225
12	S12	0.25	6	0.85	21.99	370

Appendix B2

Moisture Absorption & Fire Retardant Test – RSM

Run order	Sample	Coded factor		Uncoded factor		Moisture Absorption (%)	Temperature at Equilibrium (°C)
		RHA/A ratio (V_1)	SiR/Ge ratio (V_3)	RHA/A ratio (V_1)	SiR/Ge ratio (V_3)		
1	S1	2	0	0.85	0.55	16.8 (good)	214
2	S2	0	-2	0.65	0.25	24.6	243
3	S3	0	0	0.65	0.55	18.4	288
4	S4	1	-1	0.75	0.4	20.3	252
5	S5	0	0	0.65	0.55	18.5	283
6	S6	0	0	0.65	0.55	18.6	280
7	S7	0	0	0.65	0.55	18.8	270
8	S8	-2	0	0.45	0.55	24.7	247
9	S9	0	0	0.65	0.55	18.8	268
10	S10	0	-2	0.65	0.25	24.3	256
11	S11	0	0	0.65	0.55	19.1	264
12	S12	2	0	0.85	0.55	17.3	212
13	S13	-2	0	0.45	0.55	22.5	244
14	S14	0	0	0.65	0.55	19.2 (moderate)	260
15	S15	1	1	0.75	0.7	15.4	230
16	S16	-1	1	0.55	0.7	19.7	242
17	S17	0	2	0.65	0.85	17.0	208 (good)

Appendix B2 (cont.)

18	S18	1	1	0.75	0.7	16.0	243 (moderate)
19	S19	-1	1	0.55	0.7	20.2	246
20	S20	0	0	0.65	0.55	19.5	257
21	S21	-1	-1	0.55	0.4	25.2 (poor)	285 (poor)
22	S22	1	-1	0.75	0.4	19.1	261
23	S23	0	2	0.65	0.85	17.0	229
24	S24	-1	-1	0.55	0.4	25.7	298

Appendix C1

Temperature at Equilibrium (TAE) – FrFD

Factorial Fit: Temperature versus RHA/AA ratio, NaOH concent, ...

Estimated Effects and Coefficients for Temperature at Equilibrium (coded units)

Term	Effect	Coef	SE Coef	T	P
Constant		305.25	8.010	38.11	0.000
RHA/AA ratio	55.10	27.55	8.010	3.44	0.009
NaOH concentration (M)	-181.77	-90.88	8.010	-11.35	0.000
SiR/Ge ratio	-50.50	-25.25	8.010	-3.15	0.014

S = 27.7470 PRESS = 13858.1

R-Sq = 94.95% R-Sq(pred) = 88.64% R-Sq(adj) = 93.06%

Analysis of Variance for Temperature at Equilibrium (coded units)

Source	DF	Seq SS	Adj SS	Adj MS	F	P
Main Effects	3	115876	115876	38625.4	50.17	0.000
RHA/AA ratio	1	9108	9108	9108.0	11.83	0.009
NaOH concentration (M)	1	99117	99117	99117.4	128.74	0.000
SiR/Ge ratio	1	7651	7651	7650.8	9.94	0.014
Residual Error	8	6159	6159	769.9		
Pure Error	8	6159	6159	769.9		
Total	11	122035				

Appendix C1 (cont.)

Obs	StdOrder	Temperature at Equilibrium	Fit	SE Fit	Residual	St Resid
1	7	190.800	212.067	16.020	-21.267	-0.94
2	11	220.000	212.067	16.020	7.933	0.35
3	1	300.000	343.333	16.020	-43.333	-1.91
4	2	417.500	448.933	16.020	-31.433	-1.39
5	6	447.500	448.933	16.020	-1.433	-0.06
6	4	200.000	216.667	16.020	-16.667	-0.74
7	10	481.800	448.933	16.020	32.867	1.45
8	12	217.500	216.667	16.020	0.833	0.04
9	8	232.500	216.667	16.020	15.833	0.70
10	9	360.000	343.333	16.020	16.667	0.74
11	3	225.400	212.067	16.020	13.333	0.59
12	5	370.000	343.333	16.020	26.667	1.18

Moisture Absorption – FrFD

Factorial Fit: Moisture absorption (%), Temperature at Equilibrium

Factorial Fit: Moisture abs versus RHA/AA ratio, NaOH concent, ...

Estimated Effects and Coefficients for Moisture absorption (%) (coded units)

Term	Effect	Coef	SE Coef	T	P
Constant		24.658	0.4159	59.29	0.000
RHA/AA ratio	-13.667	-6.833	0.4159	-16.43	0.000
NaOH concentration (M)	5.577	2.788	0.4159	6.70	0.000
SiR/Ge ratio	-12.153	-6.077	0.4159	-14.61	0.000

S = 1.44080 PRESS = 37.3663

R-Sq = 98.51% R-Sq(pred) = 96.64% R-Sq(adj) = 97.95%

Appendix C1 (cont.)

Analysis of Variance for Moisture absorption (%) (coded units)

Source	DF	Seq SS	Adj SS	Adj MS	F	P
Main Effects	3	1096.74	1096.74	365.580	176.11	0.000
RHA/AA ratio	1	560.33	560.33	560.333	269.92	0.000
NaOH concentration (M)	1	93.30	93.30	93.298	44.94	0.000
SiR/Ge ratio	1	443.11	443.11	443.111	213.45	0.000
Residual Error	8	16.61	16.61	2.076		
Pure Error	8	16.61	16.61	2.076		
Total	11	1113.35				

Obs	StdOrder	Moisture absorption (%)	Fit	SE Fit	Residual	St Resid
1	7	42.2100	40.3567	0.8318	1.8533	1.58
2	11	41.0900	40.3567	0.8318	0.7333	0.62
3	1	23.2900	22.6267	0.8318	0.6633	0.56
4	2	22.8000	21.1133	0.8318	1.6867	1.43
5	6	20.2700	21.1133	0.8318	-0.8433	-0.72
6	4	15.2200	14.5367	0.8318	0.6833	0.58
7	10	20.2700	21.1133	0.8318	-0.8433	-0.72
8	12	14.4500	14.5367	0.8318	-0.0867	-0.07
9	8	13.9400	14.5367	0.8318	-0.5967	-0.51
10	9	22.6000	22.6267	0.8318	-0.0267	-0.02
11	3	37.7700	40.3567	0.8318	-2.5867	-2.20R
12	5	21.9900	22.6267	0.8318	-0.6367	-0.54

Appendix C2

Temperature at Equilibrium (TAE) – RSM

Response Surface Regression: Temperature at E versus RHA/AA ratio, SiR/Ge ratio

The analysis was done using coded units.

Estimated Regression Coefficients for Temperature at Equilibrium

Term	Coef	SE Coef	T	P
Constant	273.146	3.460	78.949	0.000
RHA/AA ratio	-8.958	2.188	-4.094	0.001
SiR/Ge ratio	-10.792	2.188	-4.932	0.000
RHA/AA ratio*RHA/AA ratio	-10.500	1.641	-6.398	0.000
SiR/Ge ratio*SiR/Ge ratio	-9.313	1.641	-5.674	0.000
RHA/AA ratio*SiR/Ge ratio	6.875	3.790	1.814	0.086

S = 10.7198 PRESS = 3669.31

R-Sq = 84.67% R-Sq(pred) = 72.81% R-Sq(adj) = 80.41%

Analysis of Variance for Temperature at Equilibrium

Source	DF	Seq SS	Adj SS	Adj MS	F	P
Regression	5	11424.9	11424.9	2284.98	19.88	0.000
Linear	2	4721.1	4721.1	2360.54	20.54	0.000
RHA/AA ratio	1	1926.0	1926.0	1926.04	16.76	0.001
SiR/Ge ratio	1	2795.0	2795.0	2795.04	24.32	0.000
Square	2	6325.7	6325.7	3162.84	27.52	0.000
RHA/AA ratio*RHA/AA ratio	1	2625.5	4704.0	4704.00	40.94	0.000
SiR/Ge ratio*SiR/Ge ratio	1	3700.2	3700.2	3700.17	32.20	0.000
Interaction	1	378.1	378.1	378.13	3.29	0.086
RHA/AA ratio*SiR/Ge ratio	1	378.1	378.1	378.13	3.29	0.086
Residual Error	18	2068.4	2068.4	114.91		

Appendix C2 (cont.)

Lack-of-Fit	3	649.9	649.9	216.65	2.29	0.120
Pure Error	15	1418.5	1418.5	94.57		
Total	23	13493.3				

Obs	StdOrder	Temperature at Equilibrium	Fit	SE Fit	Residual	St Resid
1	18	214.000	213.229	6.744	0.771	0.09
2	19	243.000	257.479	6.744	-14.479	-1.74
3	24	288.000	273.146	3.460	14.854	1.46
4	14	252.000	248.292	5.360	3.708	0.40
5	22	283.000	273.146	3.460	9.854	0.97
6	23	280.000	273.146	3.460	6.854	0.68
7	21	270.000	273.146	3.460	-3.146	-0.31
8	5	247.000	249.063	6.744	-2.063	-0.25
9	10	268.000	273.146	3.460	-5.146	-0.51
10	7	256.000	257.479	6.744	-1.479	-0.18
11	9	264.000	273.146	3.460	-9.146	-0.90
12	6	212.000	213.229	6.744	-1.229	-0.15
13	17	244.000	249.063	6.744	-5.063	-0.61
14	11	260.000	273.146	3.460	-13.146	-1.30
15	4	230.000	240.458	5.360	-10.458	-1.13
16	15	242.000	244.625	5.360	-2.625	-0.28
17	8	208.000	214.313	6.744	-6.313	-0.76
18	16	243.000	240.458	5.360	2.542	0.27
19	3	246.000	244.625	5.360	1.375	0.15
20	12	257.000	273.146	3.460	-16.146	-1.59
21	13	285.000	279.958	5.360	5.042	0.54
22	2	261.000	248.292	5.360	12.708	1.37
23	20	229.000	214.313	6.744	14.687	1.76
24	1	298.000	279.958	5.360	18.042	1.94

Appendix C2 (cont.)

Estimated Regression Coefficients for Temperature at Equilibrium using data in uncoded units

Term	Coef
Constant	-34.0278
RHA/AA ratio	1023.33
SiR/Ge ratio	85.4167
RHA/AA ratio*RHA/AA ratio	-1050.00
SiR/Ge ratio*SiR/Ge ratio	-413.889
RHA/AA ratio*SiR/Ge ratio	458.333

Predicted Response for New Design Points Using Model for Temperature at Equilibrium

Point	Fit	SE Fit	95% CI	95% PI
1	213.229	6.74437	(199.060, 227.399)	(186.621, 239.837)
2	257.479	6.74437	(243.310, 271.649)	(230.871, 284.087)
3	273.146	3.45979	(265.877, 280.415)	(249.481, 296.811)
4	248.292	5.35988	(237.031, 259.552)	(223.112, 273.471)
5	273.146	3.45979	(265.877, 280.415)	(249.481, 296.811)
6	273.146	3.45979	(265.877, 280.415)	(249.481, 296.811)
7	273.146	3.45979	(265.877, 280.415)	(249.481, 296.811)
8	249.063	6.74437	(234.893, 263.232)	(222.455, 275.670)
9	273.146	3.45979	(265.877, 280.415)	(249.481, 296.811)
10	257.479	6.74437	(243.310, 271.649)	(230.871, 284.087)
11	273.146	3.45979	(265.877, 280.415)	(249.481, 296.811)
12	213.229	6.74437	(199.060, 227.399)	(186.621, 239.837)
13	249.063	6.74437	(234.893, 263.232)	(222.455, 275.670)
14	273.146	3.45979	(265.877, 280.415)	(249.481, 296.811)
15	240.458	5.35988	(229.198, 251.719)	(215.279, 265.638)
16	244.625	5.35988	(233.364, 255.886)	(219.445, 269.805)
17	214.313	6.74437	(200.143, 228.482)	(187.705, 240.920)

18	240.458	5.35988	(229.198, 251.719)	(215.279, 265.638)
19	244.625	5.35988	(233.364, 255.886)	(219.445, 269.805)
20	273.146	3.45979	(265.877, 280.415)	(249.481, 296.811)
21	279.958	5.35988	(268.698, 291.219)	(254.779, 305.138)
22	248.292	5.35988	(237.031, 259.552)	(223.112, 273.471)
23	214.313	6.74437	(200.143, 228.482)	(187.705, 240.920)
24	279.958	5.35988	(268.698, 291.219)	(254.779, 305.138)

Moisture Absorption – RSM

Response Surface Regression: Moisture Absorpt versus RHA/AA ratio, SiR/Ge ratio

The analysis was done using coded units.

Estimated Regression Coefficients for Moisture Absorption

Term	Coef	SE Coef	T	P
Constant	19.0313	0.2577	73.855	0.000
RHA/AA ratio	-1.9250	0.1630	-11.812	0.000
SiR/Ge ratio	-2.0333	0.1630	-12.477	0.000
RHA/AA ratio*RHA/AA ratio	0.3656	0.1222	2.991	0.008
SiR/Ge ratio*SiR/Ge ratio	0.4656	0.1222	3.809	0.001
RHA/AA ratio*SiR/Ge ratio	0.3750	0.2823	1.328	0.201

S = 0.798400 PRESS = 24.1773

R-Sq = 94.59% R-Sq(pred) = 88.60% R-Sq(adj) = 93.09%

Analysis of Variance for Moisture Absorption

Source	DF	Seq SS	Adj SS	Adj MS	F	P
Regression	5	200.662	200.662	40.1325	62.96	0.000
Linear	2	188.162	188.162	94.0808	147.59	0.000

Appendix C2 (cont.)

RHA/AA ratio	1	88.935	88.935	88.9350	139.52	0.000
SiR/Ge ratio	1	99.227	99.227	99.2267	155.66	0.000
Square	2	11.376	11.376	5.6878	8.92	0.002
RHA/AA ratio*RHA/AA ratio	1	2.125	5.704	5.7038	8.95	0.008
SiR/Ge ratio*SiR/Ge ratio	1	9.250	9.250	9.2504	14.51	0.001
Interaction	1	1.125	1.125	1.1250	1.76	0.201
RHA/AA ratio*SiR/Ge ratio	1	1.125	1.125	1.1250	1.76	0.201
Residual Error	18	11.474	11.474	0.6374		
Lack-of-Fit	3	6.735	6.735	2.2451	7.11	0.003
Pure Error	15	4.739	4.739	0.3159		
Total	23	212.136				

Obs	StdOrder	Moisture Absorption	Fit	SE Fit	Residual	St Resid	
1	18	16.800	16.644	0.502	0.156	0.25	
2	19	24.600	24.960	0.502	-0.360	-0.58	
3	24	18.400	19.031	0.258	-0.631	-0.84	
4	14	20.300	19.596	0.399	0.704	1.02	
5	22	18.500	19.031	0.258	-0.531	-0.70	
6	23	18.600	19.031	0.258	-0.431	-0.57	
7	21	18.800	19.031	0.258	-0.231	-0.31	
8	5	24.700	24.344	0.502	0.356	0.57	
9	10	18.800	19.031	0.258	-0.231	-0.31	
10	7	24.300	24.960	0.502	-0.660	-1.06	
11	9	19.100	19.031	0.258	0.069	0.09	
12	6	17.300	16.644	0.502	0.656	1.06	
13	17	22.500	24.344	0.502	-1.844	-2.97	R
14	11	19.200	19.031	0.258	0.169	0.22	
15	4	15.400	16.279	0.399	-0.879	-1.27	
16	15	19.700	19.379	0.399	0.321	0.46	

Appendix C2 (cont.)

17	8	17.000	16.827	0.502	0.173	0.28
18	16	16.000	16.279	0.399	-0.279	-0.40
19	3	20.200	19.379	0.399	0.821	1.19
20	12	19.500	19.031	0.258	0.469	0.62
21	13	25.200	24.196	0.399	1.004	1.45
22	2	19.100	19.596	0.399	-0.496	-0.72
23	20	17.000	16.827	0.502	0.173	0.28
24	1	25.700	24.196	0.399	1.504	2.18 R

R denotes an observation with a large standardized residual.

Estimated Regression Coefficients for Moisture Absorption using data in uncoded units

Term	Coef
Constant	69.6445
RHA/AA ratio	-80.5313
SiR/Ge ratio	-52.5694
RHA/AA ratio*RHA/AA ratio	36.5625
SiR/Ge ratio*SiR/Ge ratio	20.6944
RHA/AA ratio*SiR/Ge ratio	25.0000

Predicted Response for New Design Points Using Model for Moisture Absorption

Point	Fit	SE Fit	95% CI	95% PI
1	16.6438	0.502315	(15.5884, 17.6991)	(14.6620, 18.6255)
2	24.9604	0.502315	(23.9051, 26.0157)	(22.9787, 26.9422)
3	19.0313	0.257682	(18.4899, 19.5726)	(17.2687, 20.7938)
4	19.5958	0.399200	(18.7571, 20.4345)	(17.7205, 21.4712)
5	19.0313	0.257682	(18.4899, 19.5726)	(17.2687, 20.7938)
6	19.0313	0.257682	(18.4899, 19.5726)	(17.2687, 20.7938)
7	19.0313	0.257682	(18.4899, 19.5726)	(17.2687, 20.7938)
8	24.3438	0.502315	(23.2884, 25.3991)	(22.3620, 26.3255)

Appendix C2 (Cont.)

9	19.0313	0.257682	(18.4899, 19.5726)	(17.2687, 20.7938)
10	24.9604	0.502315	(23.9051, 26.0157)	(22.9787, 26.9422)
11	19.0313	0.257682	(18.4899, 19.5726)	(17.2687, 20.7938)
12	16.6438	0.502315	(15.5884, 17.6991)	(14.6620, 18.6255)
13	24.3438	0.502315	(23.2884, 25.3991)	(22.3620, 26.3255)
14	19.0313	0.257682	(18.4899, 19.5726)	(17.2687, 20.7938)
15	16.2792	0.399200	(15.4405, 17.1179)	(14.4038, 18.1545)
16	19.3792	0.399200	(18.5405, 20.2179)	(17.5038, 21.2545)
17	16.8271	0.502315	(15.7718, 17.8824)	(14.8453, 18.8088)
18	16.2792	0.399200	(15.4405, 17.1179)	(14.4038, 18.1545)
19	19.3792	0.399200	(18.5405, 20.2179)	(17.5038, 21.2545)
20	19.0313	0.257682	(18.4899, 19.5726)	(17.2687, 20.7938)
21	24.1958	0.399200	(23.3571, 25.0345)	(22.3205, 26.0712)
22	19.5958	0.399200	(18.7571, 20.4345)	(17.7205, 21.4712)
23	16.8271	0.502315	(15.7718, 17.8824)	(14.8453, 18.8088)
24	24.1958	0.399200	(23.3571, 25.0345)	(22.3205, 26.0712)